2021

ENTRY AND REPLICATION OF NEGATIVE-STRAND RNA VIRUSES

Kerri Boggs
University of Kentucky, kboggs475@gmail.com
Digital Object Identifier: https://doi.org/10.13023/etd.2021.017

STUDENT AGREEMENT:

I represent that my thesis or dissertation and abstract are my original work. Proper attribution has been given to all outside sources. I understand that I am solely responsible for obtaining any needed copyright permissions. I have obtained needed written permission statement(s) from the owner(s) of each third-party copyrighted matter to be included in my work, allowing electronic distribution (if such use is not permitted by the fair use doctrine) which will be submitted to UKnowledge as Additional File.

I hereby grant to The University of Kentucky and its agents the irrevocable, non-exclusive, and royalty-free license to archive and make accessible my work in whole or in part in all forms of media, now or hereafter known. I agree that the document mentioned above may be made available immediately for worldwide access unless an embargo applies.

I retain all other ownership rights to the copyright of my work. I also retain the right to use in future works (such as articles or books) all or part of my work. I understand that I am free to register the copyright to my work.

REVIEW, APPROVAL AND ACCEPTANCE

The document mentioned above has been reviewed and accepted by the student's advisor, on behalf of the advisory committee, and by the Director of Graduate Studies (DGS), on behalf of the program; we verify that this is the final, approved version of the student's thesis including all changes required by the advisory committee. The undersigned agree to abide by the statements above.

Kerri Boggs, Student

Dr. Rebecca Dutch, Major Professor

Dr. Trevor Creamer, Director of Graduate Studies

ENTRY AND REPLICATION OF NEGATIVE-STRAND RNA VIRUSES

DISSERTATION

A dissertation submitted in partial fulfillment of the
requirements for the degree of Doctor of Philosophy in the
College of Medicine
at the University of Kentucky

By
Kerri Beth Boggs
Lexington, Kentucky
Director: Dr. Rebecca Dutch, Professor of Molecular and Cellular Biochemistry
Lexington, Kentucky
2021

ABSTRACT OF DISSERTATION

ENTRY AND REPLICATION OF NEGATIVE-STRAND RNA VIRUSES

Hendra virus (HeV) and human metapneumovirus (HMPV) are negative-sense, singled-stranded RNA viruses. The paramyxovirus HeV is classified as a biosafety level 4 pathogen due to its high fatality rate and the lack of a human vaccine or antiviral treatment. HMPV is a widespread pneumovirus that causes respiratory tract infections which are particularly dangerous for young children, immunocompromised individuals, and the elderly. Like HeV, no vaccines or therapies are available to combat HMPV infections. These viruses fuse their lipid envelopes with a cell to initiate infection. Blocking cell entry is a promising approach for antiviral development, and many vaccines are designed based on the envelope protein responsible for fusion. Following fusion, the coated genome and its associated proteins are released into the cytoplasm for replication and transcription. HMPV and other negative-strand viruses form membrane-less inclusion bodies (IBs) which act as viral factories to promote these processes. HMPV IBs represent another promising target for developing new antivirals since they house the replication machinery. Viral fusion and cytoplasmic replication are ubiquitous to most negative-strand viruses and are addressed in this work through analysis of HeV and HMPV.

HeV utilizes a trimeric fusion protein (F) within its lipid bilayer to mediate membrane merger with a cell for entry. Previous HeV F studies showed that transmembrane domain (TMD) interactions are important for stabilizing the prefusion conformation of the protein prior to triggering. Thus, the current model for HeV F fusion suggests that modulation of TMD interactions is critical for initiation and completion of conformational changes that drive membrane fusion. HeV F constructs (T483C/V484C, V484C/N485C, and N485C/P486C) were generated with double cysteine substitutions near the N-terminal region of the TMD to study the effect of altered flexibility in this region. Oligomeric analysis showed that the double cysteine substitutions successfully promoted intersubunit disulfide bond formation in HeV F. Subsequent fusion assays indicated that the introduction of disulfide bonds in the mutants prohibited fusion events, likely due to the limited flexibility in the TMD. Further testing confirmed that T483C/V484C and V484C/N485C were expressed at the cell surface at levels that would allow for fusion. Attempts to restore fusion with a reducing agent were unsuccessful, suggesting that the introduced disulfide bonds were likely buried in the membrane. Conformational analysis showed that T483C/V484C and V484C/N485C were able

to bind a prefusion conformation-specific antibody prior to cell disruption, indicating that the introduced disulfide bonds did not significantly affect protein folding. This study strengthens the current model for HeV fusion and provides important insight for understanding the basic mechanisms of membrane fusion for negative-strand RNA viruses.

HMPV IBs are dynamic structures required for efficient replication and transcription. The minimum components needed to form IB-like structures in cells are the nucleoprotein (N), which coats the RNA genome, and the tetrameric phosphoprotein (P), which acts as a cofactor to the polymerase. HMPV P binds to two versions of N protein in infected cells: C-terminal P residues interact with oligomeric, RNA-bound N (N-RNA), and N-terminal P residues interact with monomeric N (N^0) to maintain a pool of protein to encapsidate new RNA. Recent work on other negative-strand viruses has shown that IBs are liquid-like organelles formed via liquid-liquid phase separation (LLPS). Recombinant versions of HMPV N and P proteins were purified to analyze the interactions required to drive LLPS *in vitro*. Purified HMPV P was shown to form liquid droplets in the absence of other protein binding partners, suggesting that it functions as a scaffold to recruit client proteins to IBs. HMPV P recruited a monomeric N protein construct, N^0-P, to liquid droplets. In addition, HMPV P incorporated N-RNA into liquid droplets, though N-RNA formed aggregates independently. These findings support that HMPV P acts as a scaffold protein to mediate multivalent interactions with monomeric and oligomeric HMPV N to promote phase separation of IBs. Collectively, the work presented here provides important insight into the processes of viral entry, replication, and IB formation for negative-strand RNA viruses.

KEYWORDS: Paramyxovirus, Membrane Fusion, Phase Separation, Human Metapneumovirus, Viral Replication, Inclusion Body

Kerri Beth Boggs

(Name of Student)

12/02/2020

Date

ENTRY AND REPLICATION OF NEGATIVE-STRAND RNA VIRUSES

By
Kerri Beth Boggs

Dr. Rebecca Dutch
Director of Dissertation

Dr. Trevor Creamer
Director of Graduate Studies

12/02/2020
Date

ACKNOWLEDGEMENTS

The work presented here would not have been possible without the support of my outstanding mentors and fellow lab members. In 2015, I participated in the summer NSF-REU program through the biochemistry department at the University of Kentucky. I had an extremely rewarding experience working in Dr. Craig Vander Kooi's lab and interacting with the faculty and graduate students. I was excited to return to the department for my first-year rotations through the labs of Drs. Jessica Blackburn, Yvonne Fondufe-Mittendorf, and Becky Dutch in 2016-2017.

Dr. Dutch's lab became my home at the end of my first year. I am thankful that she gave me opportunities to grow as a scientist, writer, and teacher. She serves as a respected leader in many roles at UK and within the virology community, and the example she sets encourages her trainees to take on challenges outside of research. Dr. Dutch is also a gifted teacher, and she inspires me to think creatively about how I can tell an exciting story through science in the classroom. My dissertation committee, which includes Dr. Sidney Whiteheart, Dr. Haining Zhu, and Dr. Beth Garvy, has also helped me develop into a well-rounded scientist. They are excellent researchers, and I am grateful for the mentorship that they offered throughout my PhD training. In addition, I would like to thank my outside examiner, Dr. Christopher Norris, for his review of my dissertation.

I would like to thank Dr. Martin Chow and Dr. Vander Kooi for sharing their expertise on protein expression and purification. I would also like to thank Dr. Carole Moncmon for training me to use the microscopes in our department. Their assistance and expertise helped me acquire the skills I needed to complete my phase separation project.

The current graduate students in the biochemistry department are particularly lucky to have a fantastic Director of Graduate Studies. Dr. Trevor Creamer was the coordinator of my NSF-REU program, and he was influential in my decision to return to UK for graduate school. He prioritizes the needs of the

biochemistry graduate students, and I am thankful for his dedication over the last few years and especially during the shutdown this spring.

My experience in Dr. Dutch's lab has been memorable because of the community I built with my fellow lab members. I am grateful for the many conversations we shared during coffee time and at lunch. I would like to specifically thank Dr. Nicolás Cifuentes-Muñoz for the kindness that he showed to everyone in lab and his patience as a mentor during my first rotation. I would also like to thank the graduate students who have made this journey with me. Dr. Stacy Webb, Dr. Tyler Kinder, Chelsea Barrett, Jean Branttie, Rachel Thompson, and Hadley Neal have been wonderful friends and a source of endless encouragement along the way. In addition, Kearstin Edmonds has been a blessing for our lab to help us get organized and pursue more research projects.

Finally, I would like to end by thanking my family. To my husband Mason, thank you for cheering me on through long days in lab and job interviews. Thank you for the sacrifices you have made to help me achieve my goals. To my parents Chris and Angie, thank you for your love, prayers, advice, and encouragement. I am grateful for the opportunities you provided for me to study science at Milligan College. Additionally, my sister Shannon, brother-in-law David, and Mason's family have been an amazing support system over the past few years. To all my family and friends, thank you for your prayers and encouragement.

TABLE OF CONTENTS

LIST OF FIGURES

Chapter 1: Background and Introduction

The *Mononegavirales* order

The *Mononegavirales* order was created in 1991 to classify three families of viruses. As of 2018, the order now includes eight families: *Bornaviridae*, *Filoviridae*, *Mymonaviridae*, *Nyamiviridae*, *Paramyxoviridae*, *Pneumoviridae*, *Rhabdoviridae*, and *Sunviridae* (1). Four of these families are recognized for their role in human disease: *Filoviridae*, *Paramyxoviridae*, *Pneumoviridae*, and *Rhabdoviridae* (2). All viruses within these families possess a lipid bilayer envelope that is derived from the host cell. The envelope includes membrane glycoproteins that are responsible for binding to a cell and fusing the envelope with the target cell membrane. Fusion of the membranes allows for the release of the viral genome and its associated proteins into the cell cytoplasm. The *Mononegavirales* viruses possess nonsegmented genomes, meaning that the genetic material is included on one strand of nucleic acid. Additionally, the genomes are made of negative-sense RNA, so the viruses must deliver the genome with proteins needed for replication and transcription into the target cell to initiate infection (1). The genome is flanked by a 3' leader sequence and 5' trailer sequence that help regulate replication and transcription. Five to ten genes are encoded by the genome, and transcription of the genes generates viral mRNAs that are capped and polyadenylated. The viral mRNAs are translated and the genome is replicated so that new viral particles can be assembled and released, often through budding events at the cell plasma membrane. The results reported in later chapters of this dissertation describe viruses from the *Paramyxoviridae* and *Pneumoviridae* families. Specifically, this work focuses on fusion events related to viral entry and mechanisms involved in viral replication. Though this work analyzes two viruses to explore these life cycle steps, the findings are applicable to many viruses throughout the *Mononegavirales* order. Understanding basic mechanisms in the life cycle of negative-sense, single-stranded RNA viruses is critical for the development of vaccines and antivirals to combat human disease.

Paramyxoviruses

The *Paramyxoviridae* family contains numerous members, including several human pathogens of medical significance, such as measles virus (MeV), mumps virus (MuV), and the parainfluenza viruses (PIVs). The family also includes the zoonotic pathogens Hendra virus (HeV) and Nipah virus (NiV) which were discovered in 1994 and 1999, respectively, after spillovers occurred in humans (3). Members of the *Paramyxoviridae* family such as Sendai virus and Newcastle disease virus are known to infect other animal species (4). Viruses within this family transmit via a horizontal pathway, meaning that they spread between members of the same generation rather than from mother to offspring, and they typically utilize airborne routes (5).

Paramyxovirus particles are generally 150 to 500 nm in diameter, and they are pleomorphic, though most have a spherical shape (5). The viral lipid bilayer encloses the RNA genome which is coated in nucleoprotein (N) to form a helical nucleocapsid. Genomes for paramyxoviruses range from 15 to 19 kilobases. The genome codes for six to ten gene products, including two transmembrane glycoproteins found in the viral lipid bilayer. These transmembrane proteins allow the virus to attach and fuse with target cells to initiate the viral life cycle (4). Some paramyxoviruses also encode a third membrane protein known as the small hydrophobic protein (SH), but the function of this protein is less clear. The SH protein is reported to inhibit TNF-alpha signaling for two rubulaviruses within the *Paramyxoviridae* family (6). Once the virus fuses with a target cell, transcription of the genome occurs in the cytoplasm. The viral phosphoprotein (P) and RNA-dependent RNA polymerase use the N-encapsidated, negative-sense genome as a template to encode mRNAs that are translated by host cell machinery to produce viral proteins. Additionally, the negative-sense RNA genome is used as a template to produce positive-sense antigenome. In turn, the positive-sense antigenome is replicated to make negative-sense genomic copies that are coated in N protein and transported to the plasma membrane for assembly with other viral components, followed by budding of nascent virions (5).

Hendra virus

HeV was identified in 1994 after an outbreak in Brisbane, Australia that led to the death of 14 horses and one human (7, 8). Horses infected with HeV typically experience acute respiratory symptoms and high fevers (9). In humans, HeV causes flu-like respiratory symptoms that can progress to severe pneumonia, and infection is also associated with encephalitis, leading to symptoms such as confusion and headaches (7, 10). All human cases of HeV have been linked to close contact with infected horses (11). The initial outbreak and subsequent cases in Australia culminated in an 89 percent fatality rate in horses and a 57 percent fatality rate in humans (10). Since HeV is designated as a biosafety level 4 pathogen, work with live HeV is restricted to specialized biocontainment facilities (12). The life cycle of HeV initiates with an attachment and fusion event, in which the viral membrane merges with the target cell membrane (FIG 1.1). The coated genome is released into the target cell where it undergoes replication and transcription in the cytoplasm. The viral mRNAs are translated into protein and assembled with newly synthesized viral genome at the cell surface. The virus acquires its membrane, studded with viral proteins, from the host as it buds from the surface.

Further research into the causes of the HeV outbreak led to the identification of Australian flying fox fruit bats of the *Pteropus* genus as the natural reservoir for the zoonotic virus. These bats are nocturnal foragers, and they are abundant in urban areas within eastern Australia where they find reliable food sources (9). The four flying fox species of bats native to Australia are all seropositive for HeV antibodies (12). A model was proposed that horses were exposed to HeV by eating fruit contaminated with infected bat urine (10). Horse-to-horse transmission of infection has been observed in subsequent outbreaks (9). Horses have served as an intermediate host to amplify the virus and pass the infection to humans. Though a horse vaccine against HeV became available in 2012, there are currently no approved vaccines or treatments to protect humans (11).

HeV is closely related to the paramyxovirus NiV, which caused an outbreak of encephalitic disease in Malaysia in 1999. During the outbreak, 265 encephalitic cases were confirmed in patients, and 105 deaths were reported, leading to a fatality rate of approximately 40 percent (13). Since the zoonotic HeV and NiV showed many differences from other members of the *Paramyxoviridae* family, the *Henipavirus* genus was created in 2000 to categorize these pathogens (1). Research into the source of the NiV outbreak showed that the virus was transmitted from bats to pigs before spilling into humans (3). Deadly NiV outbreaks have also occurred in Bangladesh, Singapore, and India. Additionally, human-to-human transmission of NiV was observed in Bangladesh and India (14). Like HeV, there are no approved vaccines or therapies to combat future NiV disease outbreaks in humans.

Scientists have also discovered a non-pathogenic henipavirus, known as Cedar virus (CedPV), which was isolated from the urine of Australian fruit bats (15). Since studies of HeV and NiV are limited due to their biosafety classification, research on live CedPV will be beneficial for elucidating the infectious mechanisms of henipaviruses. The current COVID-19 pandemic highlights the importance of studying the life cycle of emergent respiratory pathogens like HeV and NiV. Severe acute respiratory syndrome coronavirus 2 (SARS-CoV-2), which causes COVID-19, is a positive-strand RNA virus with a genome of approximately 30 kilobases. Some coronavirus replication complexes have been shown to possess proofreading ability, which is important for controlling the mutation rate during replication of the large RNA genomes (16). When mutations do occur, they may increase the likelihood of spillover into a different species. Like HeV and NiV, SARS-CoV-2 is a zoonotic virus that is thought to have originated in bats before spilling into humans, and it primarily transmits via respiratory droplets (17). The high quantity of asymptomatic SARS-CoV-2 infections has contributed to the worldwide spread of disease. Although the henipaviruses and coronaviruses are categorized within different phylogenetic orders, similarities in their origin and transmission routes suggest that further research is needed to analyze the emergence of respiratory pathogens. Understanding the processes by which HeV

and NiV initiate infection, replicate, and spread may contribute to discoveries to prevent widespread outbreaks of newly emerged RNA viruses. Specifically, research into HeV fusion events is critical for the development of novel therapies and vaccines that may protect human populations from deadly infections.

Paramyxovirus surface glycoproteins

Paramyxoviruses possess attachment proteins (H, HN, or G) and fusion proteins (F) that are located on the surface of the virus. The attachment proteins are homotetrameric type II integral membrane proteins that bind to specific receptors on target cells (4). They consist of a globular receptor binding domain and a membrane proximal stalk. Paramyxoviruses with HN attachment proteins bind to sialic acid and possess a neuraminidase function (4). The morbilliviruses within the *Paramyxoviridae* family use the attachment protein H, which binds sialic acid but does not have neuraminidase activity. Interestingly, the G protein of henipaviruses is unable to bind or cleave sialic acid. Instead, it interacts with the protein receptor Ephrin B2 or Ephrin B3 to promote close contact between the viral and cellular membranes for fusion events (4). Along with mediating initial binding events with a cell, paramyxovirus attachment proteins are reported to have fusion-promoting functions, since co-expression of both the attachment and fusion protein is required for viral spread (4). Some studies have suggested that the attachment protein and F protein must physically interact to promote membrane fusion (18). However, the mechanisms that regulate this attachment protein-dependent triggering are not fully understood.

Paramyxoviruses express homotrimeric type I F proteins that undergo irreversible conformational changes to mediate membrane fusion events between the virus and a cell. Domains of the protein include a hydrophobic fusion peptide (FP), two heptad repeat regions (HRA and HRB), a single-pass transmembrane domain (TMD), and a C-terminal cytoplasmic tail (CT). The F protein is synthesized at the endoplasmic reticulum (ER) in an inactive precursor form (F_0). During translation, the protein inserts into the ER membrane and folds into its trimeric structure. Proper folding of the F protein is essential for its triggering function which

requires dynamic conformational changes. The newly synthesized F_0 must undergo proteolytic cleavage to generate the metastable prefusion form (F_1+F_2) that is capable of mediating fusion events once triggered. Proteolytic cleavage of F_0 yields the disulfide-linked heterodimer F_1+F_2 which helps to properly position the FP and may lower the energy barrier for F protein triggering (FIG 1.2) (4). The F protein must also undergo glycosylation. Though all paramyxovirus F proteins are glycosylated, the glycosylation sites vary depending on the virus. For HeV F, four glycosylation sites were shown to be required for proper folding and fusion. Two of these glycosylation sites are present in the F_2 subunit (N67 and N69) and two are present in the F_1 subunit (N414 and N464) (19).

Proteolytic cleavage of the F protein is an essential step for all paramyxoviruses. Without this step, the F protein is maintained in an inactive form that prohibits the virus from fusing with target cells to initiate infection. The pathways and proteases utilized to process F_0 to generate F_1+F_2 vary amongst the paramyxoviruses. Many paramyxovirus F proteins are processed by the protease furin as they are transported through the *trans*-Golgi network to reach the cell plasma membrane (20). The furin enzyme belongs to the subtilisin-like proprotein convertase family and is enriched in the Golgi apparatus. It recognizes the sequence R-X-K/R-R and cleaves proteins to generate their mature or active form. This F protein proteolytic cleavage pathway is used by paramyxoviruses such as PIV5 and MeV (21, 22). Neither HeV F nor NiV F contains the furin recognition sequence. Instead, these henipaviruses have been shown to utilize the cellular protease cathepsin L to generate the metastable F_1+F_2 heterodimer (23-25). Cathepsin L is an endosomal/lysosomal protease that is typically recognized for its role in destruction of intracellular and endocytosed proteins. Both HeV F and NiV F possess endocytosis motifs within their CTs and trafficking signals in their TMDs (26-28). After trafficking to the plasma membrane, the CT motifs signal for the F proteins to be endocytosed. The F proteins are processed by cathepsin L in a pH-dependent manner within recycling endosomes before being trafficked back to the cell surface where they can participate in fusion events (FIG 1.3).

To mediate fusion, the paramyxovirus F protein must overcome the energetically unfavorable process of merging two lipid bilayers. The F protein provides the energy required for this process by refolding from its metastable conformation into a stable, low energy, postfusion state. After the G protein binds to the target cell receptor, interactions between the F and G proteins are thought to trigger conformational changes in the F protein for fusion, and different models have been suggested for these interactions. The “clamp” model suggests that the F and G proteins form a complex that is trafficked to the cell surface, allowing the G protein to stabilize the F protein in its metastable state. Upon receptor binding, the F protein dissociates from the G protein to undergo refolding events. In the “association” model, the G protein is not required to stabilize the F protein prefusion state. Rather, the G protein binds to its receptor and then interacts with the F protein in a manner that destabilizes the prefusion form to promote fusion (18). Once triggered, the hydrophobic FP of the F protein is inserted into a target cell membrane. Further conformational changes irreversibly transform the F protein into a stable six-helix bundle while simultaneously generating a fusion pore through which the viral genome can be released into the target cell (4).

Work on the fusion proteins of different viruses, including influenza virus and human immunodeficiency virus, has shown that the TMD plays a significant role in promoting fusion (29-39). Our lab has explored various aspects of the HeV F TMD to better understand its role in protein folding, stability, and fusion promotion. The TMD region has been studied in isolation using sedimentation equilibrium analysis, an ultracentrifugation method for quantitating protein molecular masses and protein-protein interactions. Results showed that the HeV F TMD associated as a trimer in the absence of the rest of the protein (40). Peptides mimicking the HRB region were added to isolated TMDs and were found to disrupt TMD-TMD interactions. Though HRB peptides fail to associate in isolation, they form a trimeric coiled coil within the HeV F prefusion conformation. The HRB coiled coil acts as a stalk that is N-terminally connected to the globular head domain and C-terminally connected to the TMDs. Spacing between the HRB and TMD was shown to be important for protein stability but changes in the spacing

did not impact TMD interactions. Together, these results suggest that TMD interactions contribute to the stability of the HRB region (41).

C-terminal residues of the HeV F TMD were also analyzed to determine their role in TMD interactions. Mutation of the C-terminal TMD residues dramatically inhibited fusogenic activity, suggesting that the β-branched residues in this region promote TMD interactions required for fusion (41). The HeV F TMD also includes a heptad repeat leucine-isoleucine zipper, and these residues were shown to be important for HeV F prefusion stability. Overall, these findings highlight the importance of HeV F TMD interactions for maintaining the metastable prefusion conformation and for promoting fusion events. These results generated the hypothesis that the HeV F TMDs must dissociate to initiate refolding events. This idea is explored in the work described in Chapter 3, in which the HeV F TMDs were locked together with disulfide bonds to examine the effects on protein stability and fusion.

Pneumoviruses

Pneumoviridae is another family classified within the *Mononegavirales* order. This taxon was previously classified as a subfamily within *Paramyxoviridae* but was reclassified in 2016 (42). The pneumovirus genomes, which range from 13 to 15 kilobases, encode 9 to 11 proteins. Pneumovirus virions vary in size and shape, but they are often filamentous and up to 2 μm in length (42). Two pneumoviruses that cause disease in humans by infecting epithelial cells of the respiratory tract are the respiratory syncytial virus (RSV) and human metapneumovirus (HMPV). This family also includes avian metapneumovirus, which infects birds, and the murine and bovine orthopneumoviruses, which infect mice and cattle, respectively.

The pneumovirus life cycle begins with the virus fusing its membrane with a host cell membrane. Like the paramyxoviruses, this process is mediated by the F protein which is maintained in a metastable state until it is triggered to undergo

conformational changes that merge the host cell membrane with the viral lipid bilayer. In contrast to the paramyxoviruses, studies of RSV and HMPV suggest that the attachment protein G is dispensable for initiating infection (4). RSV and HMPV particles are first endocytosed, and fusion events occur within the endosome (43, 44). For HMPV, low pH has been shown to trigger the F protein for some strains (45, 46). Since viruses in the *Pneumoviridae* family possess a negative-sense RNA genome, the viral particle must also deliver proteins involved in transcription and replication of the genome, including the large polymerase protein (L), P protein, M2-1, M2-2, and the N protein, to the host cell. Like the paramyxovirus N protein, the pneumovirus N protein interacts with the RNA genome to form the nucleocapsid which protects the genetic material from host cell nucleases and acts as a template for transcription and replication (47). The P protein interacts with the N protein and recruits the polymerase and M2-1 to the viral nucleocapsid to form a replication complex (48). The matrix-2 proteins, M2-1 and M2-2, promote polymerase processivity and regulate the switch between viral replication and transcription, respectively (49, 50). The polymerase initiates transcription at the 3' terminus of the genome and sequentially produces transcripts for each gene. The genes are separated by non-transcribed intergenic regions, and each gene contains a short *gene start* and *gene end* signal. As the polymerase moves along, it scans the intergenic regions until it finds the next *gene start* sequence. Since the polymerase sometimes falls off during this process, transcripts for the genes closer to the 3' terminus are produced in greater abundance than those at the 5' terminus. The transcripts are capped and polyadenylated prior to translation by the host cell ribosome complex (48). Once the virus accumulates a pool of proteins, it switches from transcription to replication to produce full-length, positive-sense antigenomes. This switching mechanism is not fully understood, but it likely involves the M2-2 protein (51). M2-2 is also thought to play a role in virulence by inhibiting the innate immunity of the host (52). The polymerase then uses the antigenome as a template to produce negative-sense genomes that can be formed into ribonucleoproteins and packaged into new viral particles. Viral particle assembly is regulated by the matrix protein (M), which

mediates interactions between the host cell membrane and the ribonucleoprotein complex (53). Self-assembly of the viral proteins at the plasma membrane is followed by budding events in which the virus acquires a lipid bilayer.

Human metapneumovirus

HMPV is a member of the *Pneumoviridae* family that causes acute respiratory infections. Though HMPV was discovered in the Netherlands in 2001, research suggests that the virus circulated since at least the 1950s before it was identified. HMPV was likely not identified earlier due to similarities with the symptoms of RSV infections and due to difficulties associated with propagating the virus in cell culture. Respiratory illness linked to HMPV infection can be particularly dangerous for infants, children, immunocompromised individuals, and the elderly (49). HMPV consists of two genetic groups known as A and B, which are divided into the four subgroups A1, A2, B1, and B2 (54). The seasonal pattern for HMPV infections is similar to other respiratory pathogens, such as RSV and influenza, but HMPV tends to peak in later months (49). Hospitalization rates for children with HMPV infections are highest until they reach age one, but reinfections often occur throughout childhood (49). Nearly all people experience an HMPV infection by the age of five. However, immunity against the virus is typically weak, so HMPV infections reoccur in adulthood (55). Symptoms of HMPV infection are similar to other respiratory viruses and include sore throat, cough, fever, nasal congestion, and shortness of breath (49). Bronchiolitis and pneumonia are often diagnosed in conjunction with HMPV infection (49). Currently, there are no approved vaccines or antivirals to combat HMPV infections.

The HMPV genome is approximately 13,000 nucleotides and includes eight genes in the following order: 3’-N-P-M-F-M2-SH-G-L-5’. These eight genes encode nine proteins, since the matrix-2 gene sequence codes for two proteins, M2-1 and M2-2. With the RNA genome, these proteins form the HMPV particle which is surrounded by a lipid bilayer derived from the host (FIG 1.4). Unlike RSV, the HMPV genome does not include the non-structural proteins NS1 and NS2 which are thought to play a role in inhibiting the antiviral response. The F protein,

G protein, and SH protein are found within the viral membrane. The M protein lines the inner layer of the viral membrane and plays a role in assembly and budding. The membrane surrounds the helical nucleocapsid, which interacts with the P protein, polymerase, M2-1, and M2-2 (52). Delivery of the nucleocapsid into a target cell leads to the formation of viral factories, called inclusion bodies (IBs), in the cytoplasm to enhance replication and transcription (FIG 1.5) (56). These structures are particularly interesting because they represent a potential target for the development of antivirals to treat HMPV infections.

The role of inclusion bodies in pneumovirus infections

The pneumoviruses HMPV and RSV, along with other specific members of the *Mononegavirales* order, form spherical structures known as IBs in the cytoplasm of infected cells (57-65). Though IBs were once thought to serve as sites of accumulation for misfolded proteins, they have more recently been shown to serve as sites of viral replication and transcription for viruses such as HMPV, RSV, MeV, rabies virus (RABV), and Ebola virus (56, 57, 66-73). These findings suggest that IB formation is a common mechanism utilized by negative-strand RNA viruses to promote replication. Viral replication components, including the P protein, N protein, L protein, and viral RNA, concentrate within IBs to produce viral transcripts, antigenome, and genome (56, 67). Microscopic analysis of pneumovirus IB structures has shown that they form in the absence of membranes and often localize near the nucleus (56, 74). The minimum components required to reconstitute pneumovirus IB-like structures in cells are the P protein and N protein (65, 75).

For HMPV, IBs containing viral genomic and antigenomic RNA are easily detected by 24 hours post infection and were shown to form when smaller replicative spots coalesce into larger inclusions (56). As the infection progresses to later time points, IBs are maintained at low numbers within the cell (56). This is due in part to the fusion of IBs in a cytoskeleton-dependent manner. Though microtubule polymerization does not appear to be required for IB coalescence, actin polymerization is critical for forming these structures to promote efficient viral

replication and transcription (56). The compartments are highly dynamic and undergo fusion and fission. The dynamics are similar to the nature of cellular structures such as processing bodies (P-bodies) and stress granules, but HMPV IBs represent a distinct structure within the cytoplasm to enhance the viral life cycle (56). Additional studies have shown that HMPV primarily spreads through a direct cell-to-cell mechanism, in which infected cells form long, branched extensions that connect to uninfected cells (76). Viral RNA and structures resembling IBs were identified within extensions, suggesting that the dynamic nature of IBs may be important for spreading infectious materials to new target cells (76, 77).

RSV inclusions were first described in 1970 using electron microscopy techniques to study infected cells. The RSV IBs were dense and contained filamentous structures (64). More recent studies have shown that RSV IBs serve as a major site for viral RNA synthesis. Similar to HMPV, RSV IBs are not detected at early time points of infection, suggesting that these structures form as viral components accumulate in the cytoplasm and as smaller structures coalesce (67). Additionally, RSV IBs were shown to possess sub-compartments, called IB-associated granules (IBAGs), which concentrate nascent viral mRNA and the M2-1 protein (67). Interestingly, viral genomic RNA, N protein, P protein, and L protein were excluded from IBAGs within the IBs (67). These findings suggest that IBAGs function in sorting viral mRNA with the help of the M2-1 protein, which competes with the P protein to bind RNA (67). This is the first description of an additional role for IBs to serve as viral mRNA sorting sites. RSV IBs have also been implicated in sequestering the NF-κB subunit p65, suggesting that IBs help to antagonize the innate immune system response from the host (78). Like HMPV, RSV has been shown to induce the formation of intercellular extensions which may serve as a route for transporting viral IB components directly from cell-to-cell (79).

Liquid-liquid phase separation and inclusion body formation

The dynamic nature of viral IBs and the similarities they share with other membrane-less cell structures led to the hypothesis that IBs are liquid organelles formed via liquid-liquid phase separation (LLPS) within the cytoplasm (FIG 1.6A).

The biological cell is highly organized to bring specific components together to increase reaction kinetics. Membranes surrounding classic organelles, such as the ER and Golgi, provide a physical barrier to concentrate materials for a particular set of biochemical reactions (80). In addition to membrane-bound compartments, IBs and other membrane-less compartments concentrate proteins and nucleic acids in the absence of a physical barrier. Examples include nucleoli, Cajal bodies, P-bodies, and stress granules which house different varieties of reactions. LLPS, which is thought to drive the formation of many of these structures, allows for the concentration of materials to form condensed liquid droplets (81). The nucleolus, which was first described in the 1830s, was the first membrane-less compartment to be observed by microscopy (80, 82). Improvements in microscopes led to the discovery of many other membrane-less compartments within the nucleus, the cytoplasm, and at the plasma membrane (80). However, scientists have struggled to explain the properties that allow for the formation and maintenance of these structures. Analysis of P granules in *Caenorhabditis elegans* germ cells led to the first suggestion that these structures were liquid-like in nature (80). Though the membrane-less compartments found in cells have diverse functions and characteristics, scientists have now classified them together as biomolecular condensates since they generally form through the same process of phase separation (80).

The condensation reaction relies on the formation of weak, multivalent protein-protein and protein-nucleic acid interactions. This process is influenced by factors such as pH, protein concentration, charge, RNA-binding, and post-translational modifications (83). Additionally, protein features such as low sequence diversity, low-complexity regions, and blocks of oppositely charged residues often contribute to biomolecular condensate formation (84). Although LLPS has been implicated in liquid organelle formation for normal cellular functions, it also plays a role in neurodegenerative disease. In some diseases, such as amyotrophic lateral sclerosis and Alzheimer’s, mutated proteins in liquid droplets cause the condensates to undergo a liquid-to-solid transition or to nucleate aggregation, leading to pathological effects (83). Recent studies of some

RNA viruses have highlighted LLPS as the mechanism utilized within the cytoplasm of a host cell to promote processes such as viral replication, transcription, and assembly. Specifically, several negative-sense, single-stranded RNA viruses have been shown to form cytoplasmic IBs via LLPS which contain viral RNA and proteins (64, 83-86) (66, 85-88).

Characterization of proteins that phase separate under physiological conditions has revealed specific features that are common to these molecules. Condensates often consist of scaffold proteins, which drive phase separation, and client proteins, which partition into liquid droplets (83). One protein feature that promotes multivalent interactions between scaffold proteins, client proteins, and nucleic acids is intrinsically disordered regions (IDRs), which are dynamic in solution. IDRs often give proteins the ability to interact with a variety of partners and are associated with high rates of evolution (89). In addition, proteins with IDRs are frequently found in condensates that contain RNA (80). HMPV and other viruses within the *Mononegavirales* order possess a P protein that acts as a cofactor for the RNA-dependent RNA polymerase by stabilizing interactions with the RNA template during replication and transcription. The P proteins of paramyxo-, pneumo-, and rhabdoviruses have been shown to include long IDRs (84, 90, 91). Paramyxovirus and pneumovirus P proteins associate as homotetramers via a central oligomerization domain that is flanked on both sides by large IDRs. In contrast, the rhabdovirus P protein contains a central dimerization domain that is flanked by IDRs (90). The oligomeric and intrinsically disordered nature of these P proteins allows them to interact with multiple binding partners to form the viral replication complex.

Negative-sense, single-stranded RNA viruses also possess N proteins with features that may promote phase separation in cells. First, a cleft of positively charged amino acids gives the N protein the ability to strongly bind RNA. In addition to coating the RNA genome to form stable nucleocapsids, a pool of N protein is maintained in a monomeric state (N^0) so that it can be sequestered to the viral replication complex to bind newly synthesized RNA. Like viral P proteins, some

viral N proteins contain IDRs. However, the IDRs found in negative-strand virus N proteins are typically smaller than the IDRs in P proteins. For instance, in the paramyxovirus MeV, 30 percent of the N protein is disordered, compared to 75 percent of the P protein (91). Together, these viral protein characteristics suggest that the P protein and N protein are predisposed to participate in LLPS for the formation of inclusions to enhance viral replication.

HMPV phosphoprotein and nucleoprotein

Since the HMPV P and N proteins represent the minimum requirements for IB-like structure formation, further analysis of these proteins is needed to understand how they may regulate LLPS for IB formation during infection. The HMPV P protein plays various roles during the viral life cycle, particularly during replication and transcription. It is 294 amino acids in length and contains a stable, tetrameric coiled coil domain from residue 158 to 237. The hydrophobic amino acids that line the interior of the coiled coil are highly conserved within the *Pneumoviridae* family (84). Overall, the protein sequence includes approximately 35 percent lysine, arginine, glutamic acid, and aspartic acid residues which are often present in repetitive blocks (84). The tetramerization domain is surrounded by IDRs at the N- and C-termini (FIG 1.7). Specifically, the N-terminus includes four long IDRS, and the C-terminus includes four relatively shorter IDRs (47). HMPV P binds to the polymerase primarily through its central oligomerization domain and some regions in the C-terminus (92). The disordered regions of the N- and C-termini are available to interact with other proteins to tether them to the polymerase for replication and transcription activities (92). The disordered HMPV P N-terminus interacts with RNA-free N (N^0). This chaperoning role for the P protein is common among negative-strand viruses and is crucial so that N does not oligomerize or bind host nucleic acids (47, 93-96). The interaction is mediated by a molecular recognition element at the beginning of the N-terminal region of the P protein (82). This region of P binds to a hydrophobic groove within the C-terminal domain of HMPV N to block oligomerization (47, 92).

The C-terminus of HMPV P also plays a role as an adaptor for the N protein by binding to N-RNA to facilitate interactions with the polymerase (47). This portion of P is proposed to help remove the template RNA from the ribonucleoprotein complex to feed it into the polymerase tunnel (47, 92). Interestingly, recent cryo-electron microscopy findings for the HMPV P protein-polymerase complex suggest that the C-terminal regions of HMPV P occupy non-equivalent positions within the structure (92). Upon binding to the polymerase, portions of the HMPV P C-terminus undergo disorder-to-order transitions. This led to the development of a model in which three HMPV P C-terminal domains displace genomic RNA from the ribonucleoprotein, while the other P C-terminal domain plays a structural role at the polymerase tunnel (92). In addition to binding the N^0, N-RNA, and the polymerase, HMPV P is proposed to bind the processivity factor M2-1 via residues 136-161 based on studies of RSV (97-99). Together, these findings highlight the dynamic nature of the P protein as an adaptor for recruiting viral proteins to the polymerase.

The HMPV N protein, which consists of 394 amino acids, encapsidates the viral genome and protects it from host cell nucleases. The protein consists of two globular domains, the N-terminal domain (NTD) and C-terminal domain (CTD), which play a role in binding RNA within the positively charged groove located between the domains. In addition, the domains are attached to NTD and CTD arms that help the N protomers oligomerize. The N protein is found in two conformations, depending on whether it is bound to P protein or RNA. HMPV N and other negative-strand virus N proteins are known for their ability to readily bind nucleic acid and oligomerize into complex structures. Therefore, wild type (WT) HMPV N protein is generally purified in the form of decameric RNA-bound rings. In the crystallized N protein ring structure, the RNA is tightly bound between the NTD and CTD within a positively charged cleft of each N protomer (47). Each N protein interacts with seven RNA nucleotides. This is unique compared to the closely related paramyxoviruses which show six nucleotides bound to each N protomer within a ring structure (47). To form the oligomerized ring, the NTD arm and CTD arm of each N protein latches to the subsequent N protomer (47). When N^0 protein is

recruited to newly synthesized viral RNA, the P protein is displaced, and the N protein CTD arm is proposed to flip upward to accommodate the insertion of the viral RNA into the positively charged cleft (47). Understanding the complex interactions between HMPV N, P, and viral RNA is crucial for analyzing LLPS experiments *in vitro* and in cells.

Methods for analyzing LLPS

Investigations of biomolecular condensates led to the development of criteria to define the properties of liquid organelles in cells:

1. Liquid organelles undergo fusion and fission (FIG 1.6B).

2. The internal contents of liquid organelles diffuse rapidly.

3. Liquid organelles possess a round shape due to surface tension.

Virologists have used these criteria to study the formation and nature of IBs in cells. Tools including live cell imaging and fluorescence recovery after photobleaching (FRAP) have been important for generating qualitative and quantitative data regarding the dynamics of IBs. For FRAP, fluorescently-tagged viral proteins have been utilized to assess the diffusion of components within IB structures (FIG 1.8). FRAP analysis of MeV, RABV, VSV, and RSV IBs has shown that the contents of these structures possess diffusion rates that are similar to other known liquid organelles (64, 83, 84, 86) (66, 85, 86, 88). Live cell imaging has allowed for observation of the spherical shape of viral IBs over time, which is deformed during fusion and fission events and subsequently recovered.

In addition to cellular studies of IBs, purified protein systems are a powerful tool for understanding the basic LLPS mechanisms of viral proteins *in vitro*. The advantage of conducting experiments with purified proteins is that the simplistic system allows for the identification of specific components that are required for phase separation (83). LLPS of purified systems is generally analyzed using light microscopy, fluorescence microscopy, and turbidity assays. Phase separation of

the purified protein may be induced by modifying a factor such as ionic strength, pH, temperature, or by adding RNA or another protein binding partner. The protein solution can then be plated and imaged with microscope to look for the presence of liquid droplets.

Turbidity assays are used in conjunction with microscopy analysis to detect changes in absorbance as protein droplets form in solution. The assemblies scatter visible light as they form, which can be analyzed using optical density measurements, generally between wavelengths of 340 and 400 nm (83). However, turbidity measurements lack some sensitivity because they cannot differentiate the size or shape of assemblies in solution (83). For instance, a protein prone to aggregation may give high absorbance readings, even though it does not form liquid droplets. Thus, turbidity measurements must be considered along with microscopy results to more clearly determine if a protein phase separates. Centrifugation is also a useful tool for analyzing proteins that undergo LLPS *in vitro*. First, LLPS of a solution is induced by changing specific conditions. Then, the dense phase that forms is sedimented by centrifugation. The concentration of the light phase can then be measured spectroscopically (83).

Other *in vitro* methods provide crucial data for understanding the material properties of liquid droplets. Though FRAP has been important for analyzing IBs in cells, it can also be utilized to quantify the mobility of molecules within phase separated droplets *in vitro*. This technique has been particularly useful for understanding the effects of RNA on protein solutions (83). Additionally, fusion of liquid droplets can be quantitatively analyzed to determine the inverse capillary viscosity. The inverse capillary viscosity is the ratio of viscosity to surface tension. With other calculations, this analysis provides data regarding the chemical nature of the surface of liquid droplets (83). In combination, cellular and *in vitro* phase separation experiments provide insight into the mechanisms regulating viral IB formation for negative-strand viruses. Future efforts to analyze LLPS and viral replication must focus on bridging the gap between cellular and *in vitro* work. Together, these studies will open new doors to understanding how negative-strand

viruses utilize phase separation dynamics to efficiently replicate and infect new cells.

Dissertation overview

Cell entry and replication are critical aspects of the basic viral life cycle that must be understood to effectively combat pathogens which cause human disease. We are particularly interested in understanding how these processes occur for negative-strand RNA viruses, which are notable for their high mutation rates. High mutation rates contribute to viral evolution, which means that these viruses are excellent at finding new ways to evade the host immune system. Additionally, these mutations can lead to the emergence of novel infections within humans. Thus, work on these viruses is important for determining how we can protect populations against current and future threats. We study the basic mechanisms of cell entry and replication by analyzing the proteins of HeV and HMPV. Our work has identified similarities and differences among negative-strand viruses which may be crucial for learning how we can target these deadly pathogens.

For enveloped viruses, studies of cell entry focus on explaining the mechanisms that allow for the fusion of two membranes, an energetically unfavorable process. Years of research on class I fusion proteins have generated a model for membrane fusion. However, gaps still exist in the model and warrant further research. The high kinetic barrier associated with membrane merger is overcome by the fusion protein which sits within the viral membrane. Many copies of the fusion protein stud the surface of the virus, ready to be triggered to mediate fusion with a cell. The fusion protein must be held in a metastable prefusion state, a higher energy conformation, until it is triggered to undergo the irreversible refolding events which lead to the formation of the lower energy postfusion conformation. Our interest in viral fusion has focused on the interactions within the HeV F protein that maintain the stability of the prefusion conformation. In addition, we have explored changes in these interactions which occur upon triggering. Our work highlights the importance of the HeV F TMD, which is required for anchoring the protein and plays a role in proper folding, stability, trafficking, and fusogenic

activity. Studies of the basic mechanisms of HeV F are needed to build a complete picture of viral membrane fusion. Novel information that is discovered about paramyxovirus F proteins may also be beneficial for the development of new vaccines and therapeutics. In Chapter 3, we explore the hypothesis that HeV F TMD dissociation is required for subsequent conformational changes that drive fusion. We tested this idea by locking the TMDs together with disulfide bonds to see how HeV F stability and fusion would be impacted. Our results provide support for this hypothesis and show for the first time that blocking HeV F TMD dissociation abolishes fusogenic activity.

Once cell entry is accomplished, the virus must take on the next challenge of replicating its genetic material and producing proteins which will be packaged into new virions. Many negative-strand RNA viruses have evolved mechanisms to house replication and transcription within distinct cytoplasmic compartments, which we call IBs. The lack of a physical barrier around these structures creates challenges for analyzing and targeting the compartments. A combination of cellular and *in vitro* studies is important for describing the interactions that allow these dynamic structures to form. Cellular experiments have provided useful findings regarding the nature of viral IBs during different stages of infection. Since proteins and other materials can freely diffuse into IBs in cells, *in vitro* analysis of purified viral proteins provides an opportunity to study IB components in isolation. IB formation is a hallmark of HMPV and RSV infections. Until now, HMPV IBs have not been characterized as liquid organelles formed by LLPS. In Chapter 4, we analyze the basic components of HMPV IBs, the N and P proteins, in our *in vitro* system to explain the basic interactions that promote IB formation. The HMPV N and P proteins phase separate to form liquid droplets *in vitro*, supporting that LLPS is the mechanism which leads to HMPV IB formation. Additionally, we show that HMPV P acts as a scaffold protein to recruit oligomeric or monomeric N protein to liquid droplets, suggesting that the P protein is the driver of LLPS during HMPV infection.

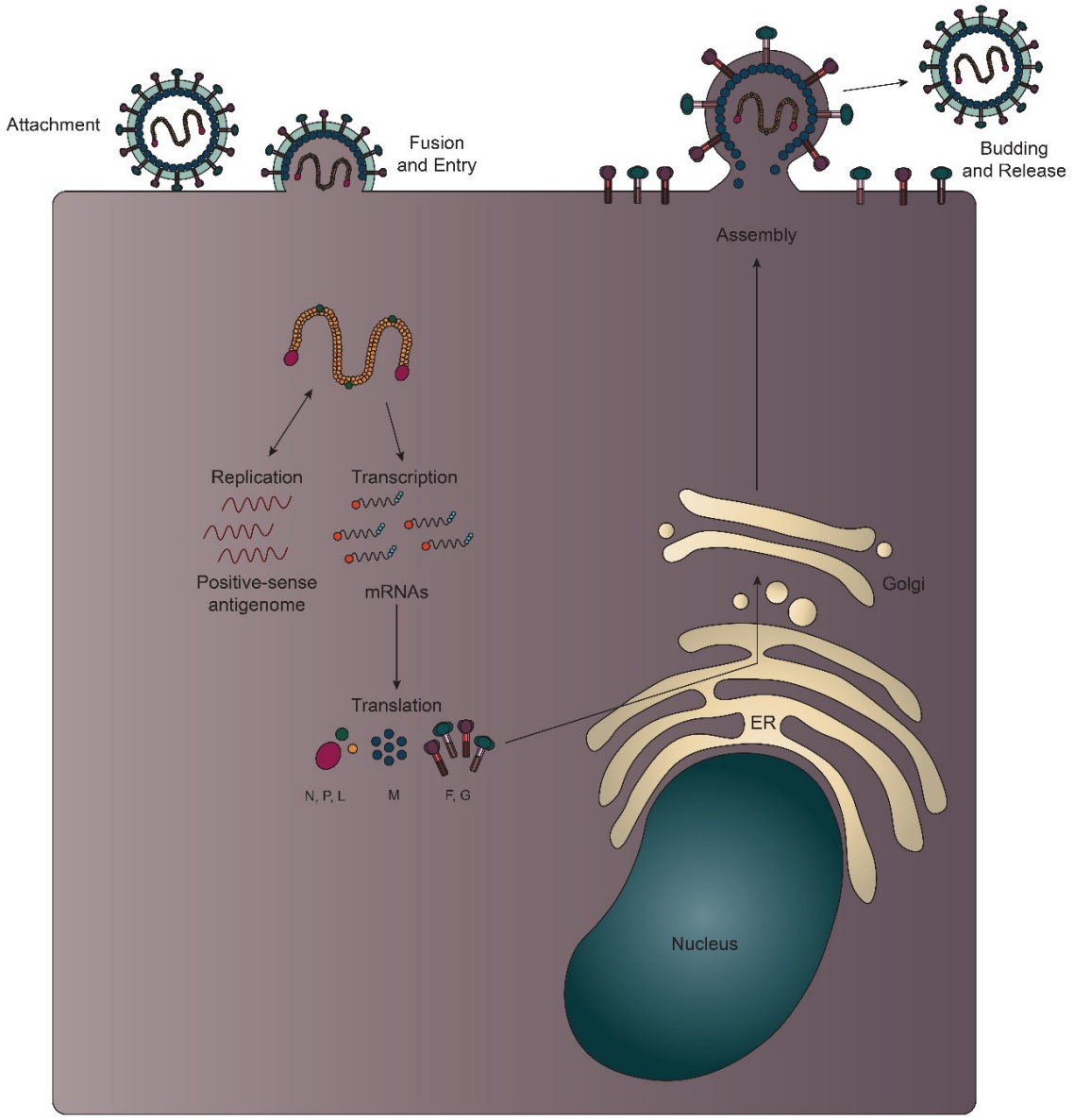

Figure 1.1 HeV life cycle. A HeV virion attaches to a target cell via an interaction between the G protein and the receptor Ephrin B2/B3. The F protein undergoes conformational changes to merge the viral membrane with the target cell membrane. The viral genome is released into the cytoplasm where it undergoes replication and transcription. Replication of the genome yields antigenome which is then used to generate new negative-sense RNA genome copies. Transcription of the genome produces viral mRNAs which are translated into viral proteins k and assembled at the cell surface into new virions. Nascent virions bud from the surface of the cell to continue the cycle of infection.

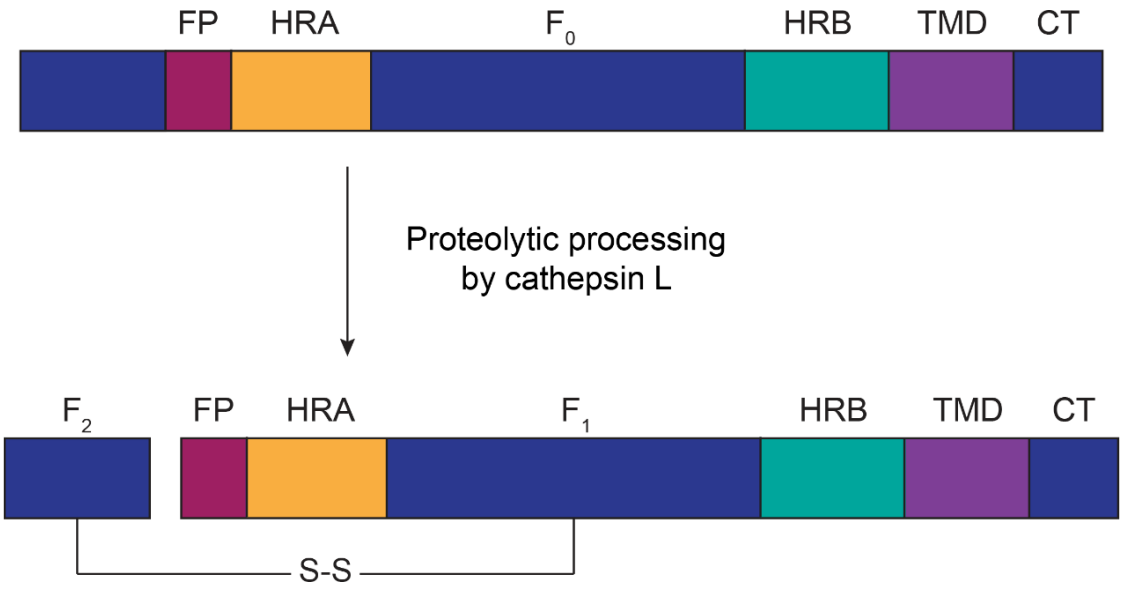

Figure 1.2. Cleavage of HeV F_0 to generate F_1+F_2. The HeV F protein includes a hydrophobic fusion peptide (FP, pink), heptad repeat A (HRA, yellow), heptad repeat B (HRB, teal), transmembrane domain (TMD, purple), and C-terminal cytoplasmic tail (CT, blue). After trafficking to the cell surface, the inactive form of HeV F (F_0) is endocytosed and proteolytically cleaved by cathepsin L into a disulfide-linked heterodimer (F_1+F_2). Then, HeV F is transported back to the cell surface where it can be triggered to promote fusion events.

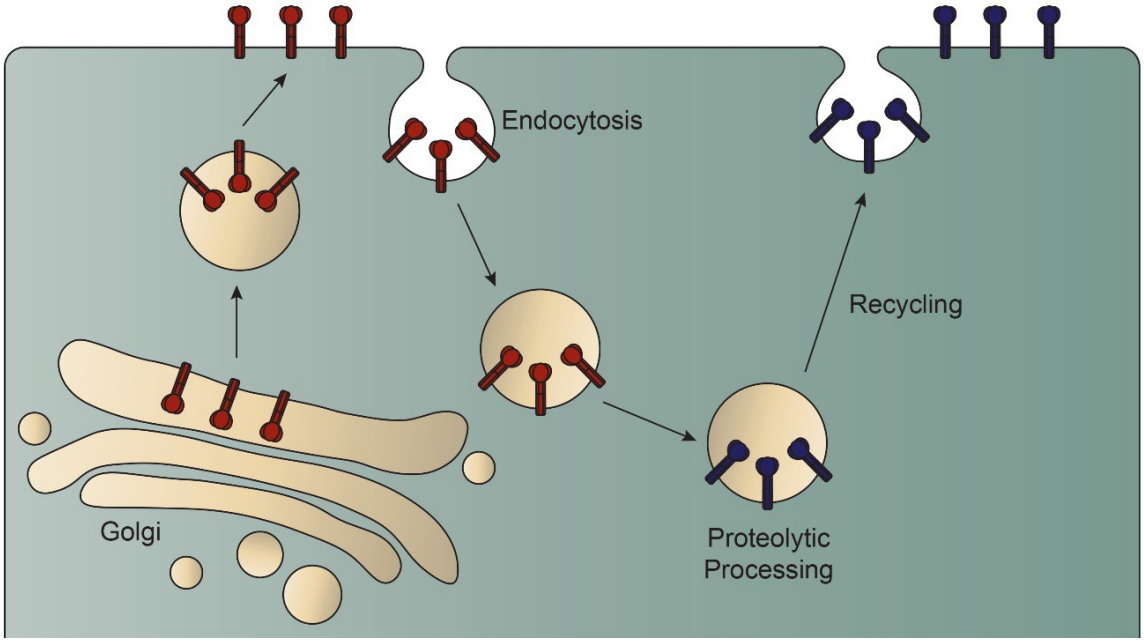

Figure 1.3. HeV F processing in the host cell. The precursor F_0 (red) is trafficked through the secretory pathway to reach the plasma membrane. F_0 is then endocytosed and cleaved by cathepsin L within the endosome to generate F_1+F_2 (blue). The proteolytically activated HeV F is then recycled back to the cell surface.

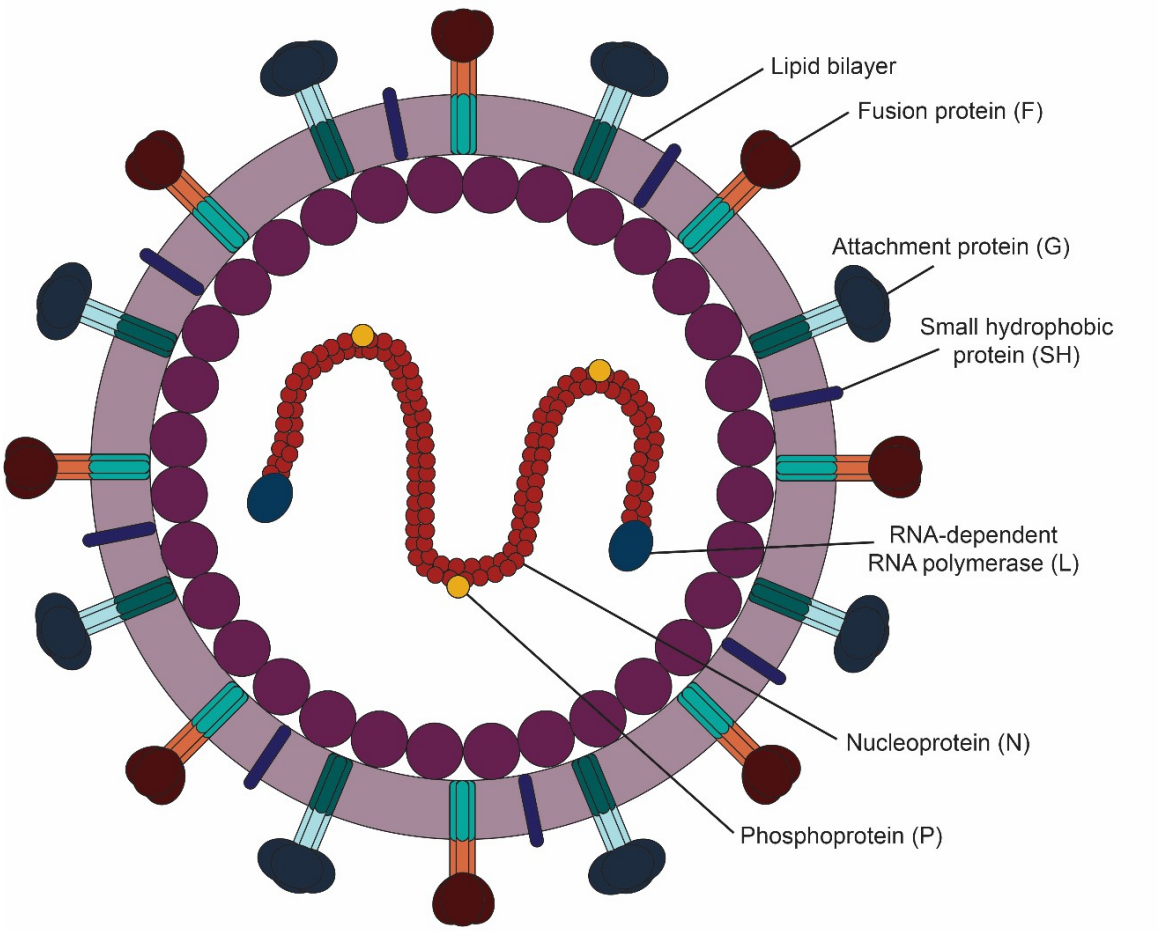

Figure 1.4. HMPV particle schematic. The HMPV virion contains a negative-sense, single-stranded RNA genome that is coated with N protein. The genome is enclosed within a lipid bilayer derived from the host cell. The M protein lines the inside of the viral membrane. The SH, F, and G proteins are transmembrane proteins within the bilayer. The F protein undergoes conformational changes to fuse the viral membrane with a target cell membrane. The coated genome can then be released with its associated proteins into the cytoplasm of the cell where it can be replicated and transcribed.

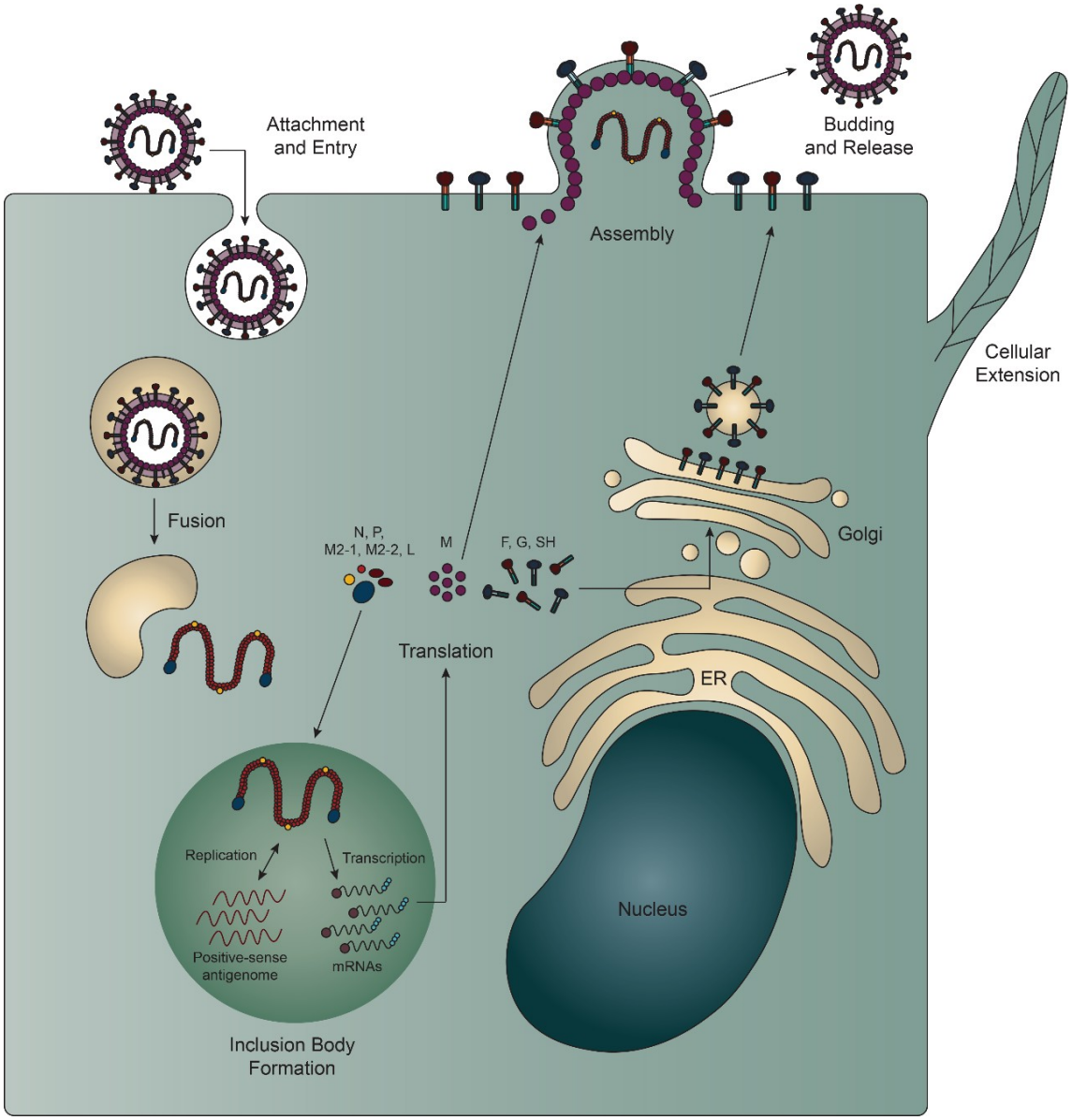

Figure 1.5. HMPV life cycle. An HMPV virion attaches to a target cell, leading to endocytosis of the particle. The viral particle fuses its membrane with the endosomal membrane to release the genome and its associated proteins. The genome is replicated and transcribed in the cell cytoplasm. As the infection progresses, membrane-less IBs form to house replication and transcription events. The mRNAs for viral membrane proteins (F, G, SH) are translated at the ER and trafficked to the cell surface. Viral proteins involved in replication and transcription are translated in the cytoplasm and then localized to IBs. New viral particles are assembled at the plasma membrane where they can bud from the surface. The

virus also induces the formation of cellular extensions for cell-to-cell spread of infection.

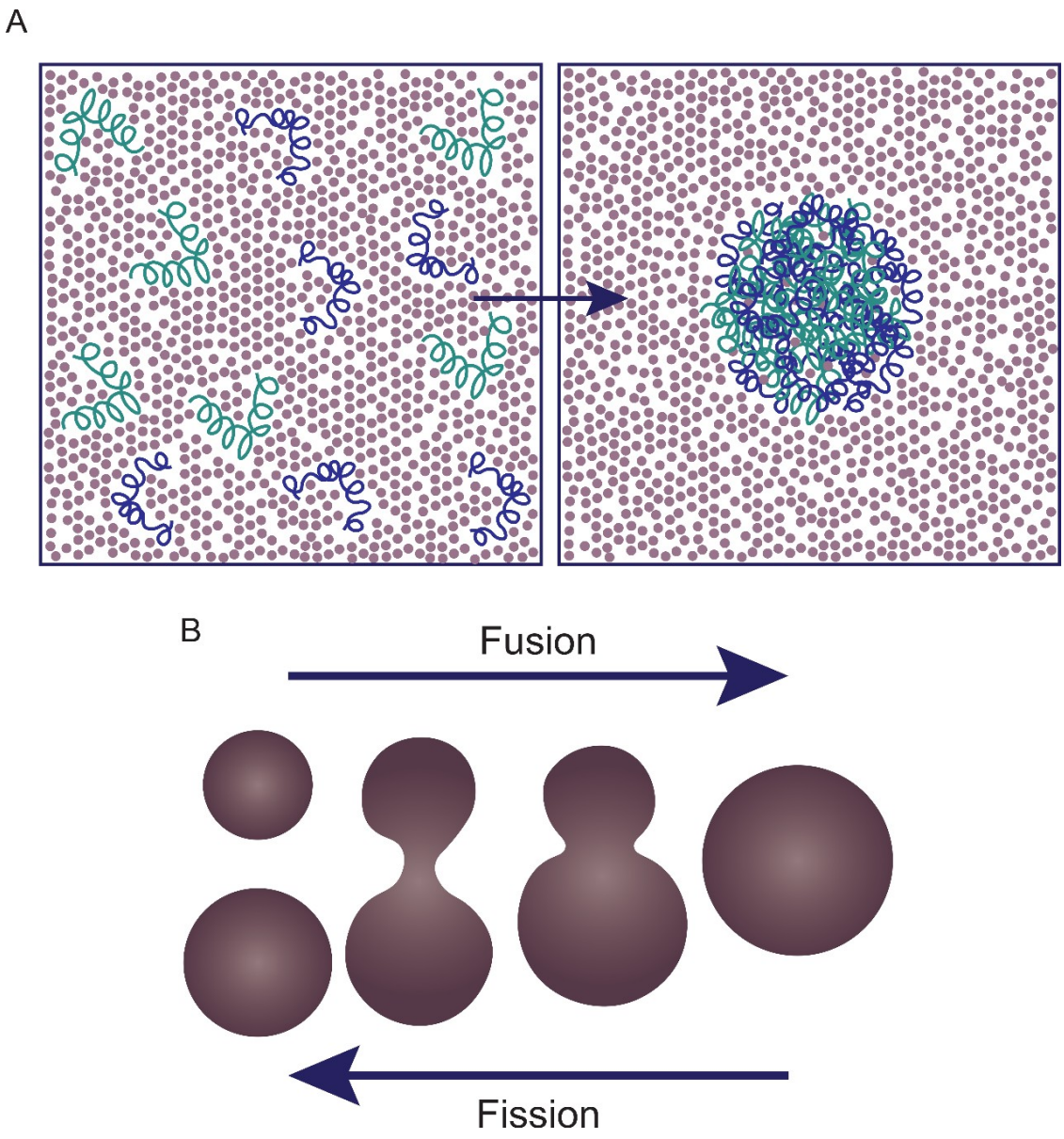

Figure 1.6. LLPS diagrams. (A) Molecules condense from a single phase to form a droplet phase. (B) Phase separated liquid droplets are dynamic structures which can undergo fusion and fission events and then relax into spherical shapes.

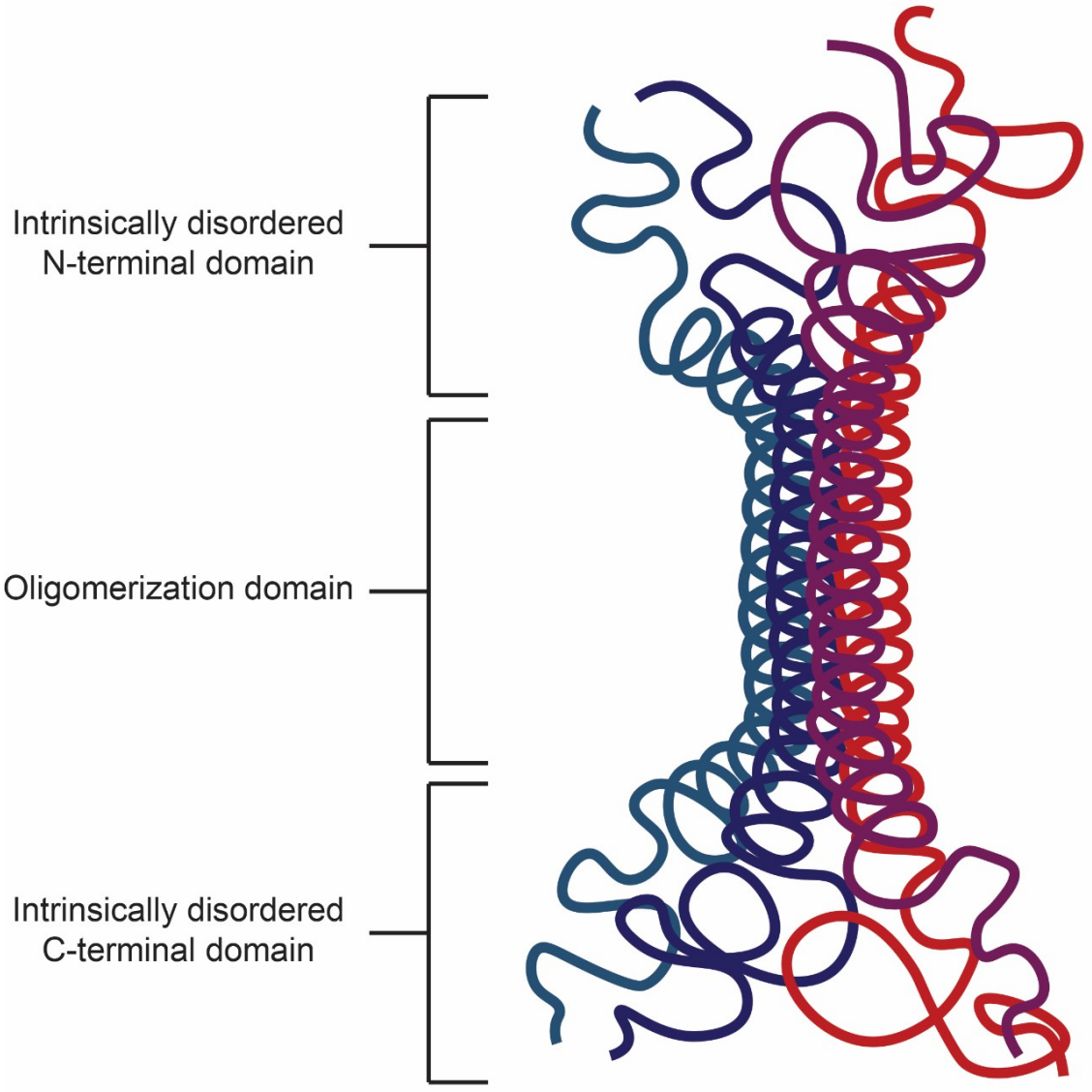

Figure 1.7. HMPV P schematic. HMPV P protomers associate via a central oligomerization domain to form a tetramer. The oligomerization domain is flanked by long IDRs that give the protein the ability to interact with a variety of binding partners.

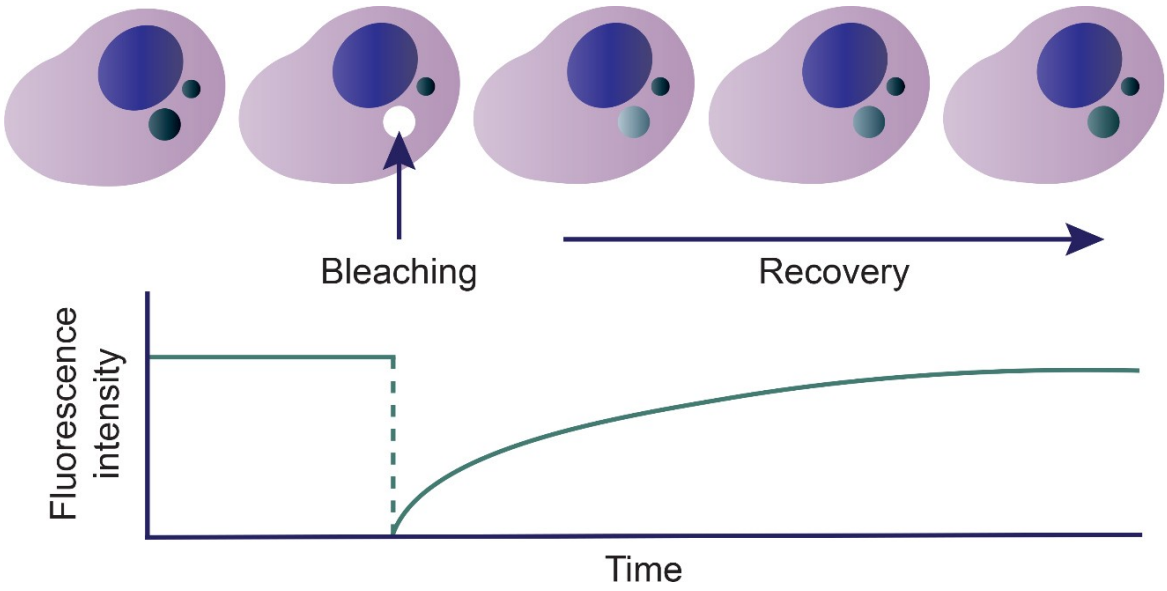

Figure 1.8. FRAP diagram. FRAP analysis of live cells requires the use of fluorescent labels which can be bleached by a laser. After a specific area of fluorescence is bleached, the fluorescence intensity is monitored over time. This data can be used to compare fluorescence recovery rates for different structures within the cell.

Chapter 2: Materials and Methods

HeV fusion project

Plasmids

Plasmids containing HeV F and G were kindly provided by Dr. Lin-Fa Wang from the Australian Animal Health Laboratory. The HeV F TMD mutants were generated in pGEM using the QuikChange Site-Directed Mutagenesis Kit from Stratagene and subcloned into pCAGGS using the forward primer 5' GCG ATT GAA TTC TAA GCA ATG GCT ACA CAA GAG 3' and reverse primer 5' CG GCG GCC ATG CAT ATT TTA TGT TCC AAT ATA ATA 3' for PCR amplification. The constructs were verified by sequencing.

Antibodies

Anti-peptide antibody to the HeV F cytoplasmic tail residues 527-539 (25) were used to pull down WT HeV F or the TMD mutant constructs. The prefusion conformation-specific antibody, mAb 5B3, generously provided by Dr. Christopher Broder (Uniformed Services University of the Health Sciences) was also used to detect HeV F (100).

Cell lines

Vero cells (ATCC) and BSR cells (provided by Karl-Klaus Conzelman, Pettenkofer Institut) were maintained in Dulbecco's modified Eagle's media (DMEM; Invitrogen) supplemented with 10% fetal bovine serum (Sigma). For the BSR cells, 0.5 mg/mL geneticin (Gibco) was added to the media with every third passage to select for T7 polymerase-expressing cells.

Syncytia assay

Vero cells in 6-well plates were transiently transfected using Lipofectamine 3000 (Invitrogen) per the manufacturer's protocol with pCAGGS-HeV F and pCAGGS-HeV G at a 1:3 ratio. At 48 hr post-transfection, the cells were imaged using a Zeiss Axiovert 100 microscope with a 10X objective.

Oligomeric analysis

Vero cells in 6-well plates were transiently transfected using Lipofectamine and Plus (Invitrogen) per the manufacturer's protocol with pCAGGS-HeV F or one of the TMD mutants. At 24 hr post-transfection, the cells were washed 2X with PBS and starved with DMEM lacking cysteine and methionine (Cys-/Met-) for 45 min. Then, the cells were labeled for 3 hr with Cys-/Met- DMEM containing Tran35S-label (100 µCi/mL; MP Biomedicals). The cells were washed 3X with PBS and lysed with 500 µL RIPA lysis buffer (100 mM TrisHCl (pH=7.4), 150 mM NaCl, 0.1% SDS, 1% Triton X-100, 1% deoxycholic acid, 1 mM phenylmethylsulfonyl fluoride (Sigma), 25 mM iodoacetamide (Sigma), 1:100 aprotinin (Calbiochem)). The sample lysate was centrifuged at 136,500 x g for 15 min at 4 ºC, and the supernatant was incubated for 3 hr with 4 µL anti-peptide antibody. Then, the sample was incubated with 30 µL protein A-sepharose beads (ThermoFisher) for 30 min at 4 ºC with rocking and washed 2X with RIPA buffer + 0.30 M NaCl, 2X with RIPA buffer + 0.15 M NaCl, and 2X with SDS wash II (150 mM NaCl, 50 mM Tris-HCl (pH=7.4), 2.5 mM EDTA). Depending on the experiment, the samples were resuspended with loading buffer lacking or containing dithiothreitol (DTT; Goldbio) for non-reducing or reducing conditions, respectively. Then, the samples were boiled and separated using 3.5% polyacrylamide gels for SDS-PAGE and visualized using the Typhoon imaging system (GE Healthcare). For the tris(2-carboxyethyl) (TCEP) (Calbiochem) treatment experiments, 1 mL of 6 mM TCEP in DMEM supplemented with 10% FBS was added to the cells following the metabolic label. The cells were incubated with the TCEP solution for 3 hr at 37 ºC before washing 2X with PBS and adding RIPA lysis buffer. Results were visualized using the Typhoon imaging system.

Reporter gene assay

Vero cells in 6-well plates were transiently transfected using Lipofectamine and Plus per the manufacturer's protocol with 0.8 µg luciferase under the control of the T7 promoter, 0.9 µg pCAGGS-HeV G, and 0.3 µg pCAGGS-HeV F or one of the TMD mutants. At 24 hr post-transfection, the Vero cells were washed 1X

with PBS and overlaid with BSR cells, previously lifted with trypsin (Invitrogen) and diluted in DMEM supplemented with 10% FBS, that stably express the T7 polymerase for 3 hr at 37 ºC. For specific experiments, 6 mM TCEP was added to the overlay media for the 3 hr incubation. Then, the cells were lysed with reporter lysis buffer (Promega) and analyzed for luciferase activity using the luciferase assay system (Promega) per the manufacturer's instructions. The Lmax luminometer (Molecular Devices; Sunnyvale, CA) was used with a 2 sec delay and a 5 sec integration time. Results were normalized to samples expressing WT HeV F and G.

Cell surface biotinylation

Vero cells in 60-mm dishes were transiently transfected using Lipofectamine and Plus reagent or Lipofectamine 3000 per the manufacturer's protocol with 4 µg pCAGGS-HeV F or one of the TMD mutants. At 24 hr post-transfection, the cells were washed 2X with PBS and starved with Cys-/Met-DMEM for 45 min. Then, the cells were radiolabeled for 4 hr in Cys-/Met- DMEM containing Tran35S-label. The cells were washed 2X with ice cold PBS (pH=8.0) and incubated with 1 mL of 1 mg/mL EZ-Link Sulfo-NHS-Biotin (Pierce) in PBS (pH=8.0) for 35 min at 4 ºC with rocking followed by 15 min at room temperature. Next, the cells were washed 3X with ice cold PBS (pH=8.0) and 500 µL RIPA lysis buffer was added. The sample lysate was centrifuged at 136,500 x g for 15 min at 4 ºC. The supernatant was transferred to 1.5 mL tubes and incubated with 8 µL of the anti-peptide HeV F antibody for 3 hr at 4 ºC with rocking. Next, each sample was incubated with 30 µL protein A-sepharose beads for 30 min at 4 ºC with rocking. The samples were washed 2X with RIPA buffer + 0.30 M NaCl, 2X with RIPA buffer + 0.15 M NaCl, and 2X with SDS wash II. Following the washes, 60 µL of 10% SDS was added, and the samples were boiled for 10 min, transferred to a new tube, and repeated with 40 µL of 10% SDS to give a total of 100 µL. Ten µL of each sample was separated and resuspended in 2X SDS loading buffer containing DTT for total protein expression analysis. The remaining 90 µL of sample was treated with 400 µL biotinylation dilution buffer (20 mM Tris (pH=8.0),

150 mM NaCl, 5 mM EDTA, 1% Triton X-100, 0.2% bovine serum albumin (US Biological Life Sciences)) and 30 µL streptavidin beads for 1 hr at 4 ºC with rocking. The washes described previously were repeated, and the samples were resuspended in 2X SDS loading buffer containing DTT. After boiling the samples, analysis of HeV F was conducted using 15% SDS-PAGE and visualized using the Typhoon imaging system. Quantifications from band densitometry using ImageQuant 5.2 were reported as relative expression (%), the sum of F_0 and F_1, normalized to WT HeV F.

Time course immunoprecipitation

Vero cells in 6-well plates were transiently transfected using Lipofectamine and Plus per the manufacturer's protocol with pCAGGS-HeV F or one of the TMD mutants. At 24 hr post-transfection, the cells were washed 2X with PBS, starved for 45 min, and metabolically labeled for 3 hr (described previously). Then, the cells were washed 3X with PBS and chased with DMEM + 10% FBS. At different time points, the cells were washed 2X with PBS and lysed with RIPA lysis buffer. Immunoprecipitation was conducted as described for oligomeric analysis, and samples were resuspended in 2X SDS loading buffer containing DTT. Samples were boiled and analyzed by 10% SDS-PAGE, and band densitometry quantifications were performed as described for surface biotinylation.

Immunoprecipitation with prefusion conformation-specific antibody

To analyze mAb 5B3 binding prior to cell disruption, Vero cells in 60-mm dishes were transiently transfected using Lipofectamine and Plus per the manufarcturer's protocol with pCAGGS-HeV F or one of the TMD mutants. At 24 hr post-transfection, the cells were washed 2X with PBS, starved for 45 min, and metabolically labeled in 2 mL overnight label media (85% Cys-/Met- DMEM, 10% DMEM + 10% FBS, 5% FBS) containing Tran35S-label for 24 hr. Then, the cells were washed 3X with PBS and treated with mAb 5B3 at 1 ug/mL in 1X PBS + 1% bovine serum albumin for 1 hr at 4 ºC with rocking. Following the antibody incubation, the cells were lysed with RIPA lysis buffer and centrifuged at 136,500 x g for 15 min at 4 ºC. Control samples were treated with 8 µL anti-peptide antibody

for 1.5 hr after being lysed with RIPA lysis buffer and centrifuged. All samples were treated with 30 uL protein A-sepharose beads for 1 hr. Then, the samples were washed as described previously. After boiling the samples, they were separated by 10% SDS-PAGE, and band densitometry quantifications were performed as described for surface biotinylation.

To analyze mAb 5B3 binding following cell disruption, Vero cells in 6-well plates were transiently transfected using Lipofectamine and Plus per the manufacturer's protocol with pCAGGS-HeV F or one of the TMD mutants. At 24 hr post-transfection, the cells were starved, labeled, lysed, and centrifuged as described for oligomeric analysis. Then, the cells were treated with 1 µg/mL mAb 5B3 or 4 µL anti-peptide Ab for 3 hr. The rest of the immunoprecipitation was performed as described for oligomeric analysis. Then, the samples were boiled and separated using 10% SDS-PAGE, and band densitometry quantifications were performed as described for surface biotinylation.

HMPV phase separation project

Expression and purification of HMPV N^0-P

The CAN97-83 HMPV N^0-P construct with a 6X C-terminal His_6-tag was purchased from GenScript in the pET-29b(+) plasmid. It was cloned into the plasmid between the NdeI and KpnI cleavage sites. The construct was expressed in *E. coli* Rosetta 2(DE3) competent cells (Novagen) overnight at 18 °C in terrific broth containing kanamycin after induction at an optical density of 0.8 with 1 mM isopropyl-β-d-thiogalactopyranoside. Cells were lysed with 20 mM Tris, 500 mM NaCl, 10 mM imidazole, pH 7 containing cOmplete EDTA-free protease inhibitor cocktail (Sigma), 125 ug/mL lysozyme, and 250 units of Benzonase (Sigma). After incubating on ice for 20 min, the solution was sonicated three times at 60% intensity for 15 sec. The lysate was spun at 18,000 rpm for 45 min at 4 °C. The crude lysate rocked with HIS-select nickel affinity gel resin (Sigma) for 45 min at 4 °C. The resin was washed one time with lysis buffer and two times with 20 mM

Tris, 500 mM NaCl, pH 7. The protein was eluted with 20 mM Tris, 500 mM NaCl, 300 mM imidazole, pH 7. The eluate was concentrated and buffer exchanged into 25 mM HEPES, 150 mM KCl, pH 7.5 using a PD-10 desalting column with Sephadex G-25 resin (GE Healthcare). Alternatively, some N^0-P protein preparations were loaded onto a HiTrap Heparin HP column (Sigma) for further purification using an increasing NaCl gradient from 200 mM to 1M to remove nucleic acid from the sample prior to buffer exchange with the PD-10 column. After buffer exchange, the protein was concentrated, flash frozen, and stored at -80 °C.

Expression and purification of HMPV N-RNA

The CAN97-83 HMPV N construct with a 6X C-terminal His_6-tag was purchased from GenScript in the pET-29b(+) plasmid. It was cloned into the plasmid between the NdeI and KpnI cleavage sites. The construct was expressed in *E. coli* Rosetta 2(DE3) competent cells overnight at 18 °C in terrific broth containing kanamycin after induction at an optical density of 0.8 with 1 mM isopropyl-β-d-thiogalactopyranoside. Cells were lysed with 25 mM Tris, 1 M NaCl, pH 8 containing cOmplete EDTA-free protease inhibitor cocktail, 125 ug/mL lysozyme, and 250 units of Benzonase. After incubating on ice for 20 min, the solution was sonicated three times at 60% intensity for 15 sec. The lysate was spun at 18,000 rpm for 1 hr at 4 °C. The crude lysate was loaded onto a column containing pre-equilibrated HIS-select nickel affinity gel resin at 4°C. The resin was washed two times with lysis buffer. The protein was eluted with 25 mM Tris, 1 M NaCl, 400 mM imidazole, pH 8. The eluate was concentrated and the NaCl concentration of the sample was adjusted to 100 mM using 25 mM Tris, pH 8. Then, the sample was loaded onto a HiTrap Heparin HP column using an increasing NaCl gradient from 200 mM to 1M. Fractions containing the HMPV N protein were concentrated and buffer exchanged into 25 mM HEPES, 150 mM KCl, pH 7.5 using a PD-10 desalting column with Sephadex G-25 resin. The protein was then concentrated, flash frozen, and stored at -80 °C.

Expression and purification of HMPV P

The CAN97-83 HMPV P construct was cloned into the plasmid pET 302/NT-His between the cleavage sites EcoRI and XhoI. The construct was expressed in BL21(DE3) CodonPlus RIL cells (Agilent) overnight at 37 °C in terrific broth containing ampicillin after induction at an optical density of 1.4 with 1 mM isopropyl-β-d-thiogalactopyranoside. Cells were lysed with 20 mM Tris, 200 mM NaCl, pH 7.5 containing cOmplete EDTA-free protease inhibitor cocktail and 125 ug/mL lysozyme. After incubating on ice for 20 min, the solution was sonicated three times at 60% intensity for 15 sec. The lysate was spun at 18,000 rpm for 30 min at 4 °C. The crude lysate rocked with HIS-select nickel affinity gel resin (Sigma) for 45 min at 4 °C. The resin was washed one time with lysis buffer and two times with 20 mM Tris, 200 mM NaCl, 20 mM imidazole, pH 7.5. The protein was eluted with 20 mM Tris, 200 mM NaCl, 250 mM imidazole, pH 7.5. The eluate was loaded onto a HiTrap Q HP anion exchange chromatography column (Cytiva). The column was washed with 20 mM Tris, pH 7.5. Then, fractions were eluted with 20 mM Tris, 1 M NaCl, pH 7.5. The fractions containing HMPV P were concentrated and buffer exchanged into 25 mM HEPES, 150 mM KCl, pH 7.5 using a PD-10 desalting column with Sephadex G-25 resin.

To reduce nucleic acid binding, some HMPV P lysates were treated with Benzonase during the cell lysis step. Instead of anion exchange, the HIS-select purification was followed by heparin purification using a HiTrap Heparin HP column with an increasing NaCl gradient from 200 mM to 1M prior to buffer exchange with the PD-10 column. After buffer exchange, the protein was concentrated, flash frozen, and stored at -80°C.

Protein labeling

Prior to buffer exchange, immobilized metal affinity chromatography (IMAC) purified HMPV N^0-P was labeled with Alexa 488 TFP ester (ThermoFisher). The Alexa 488 TFP ester was prepared with DMSO to make a 10 mg/mL solution. The solution was added dropwise to the HMPV N^0-P protein sample. The sample rocked for 1 hr in the dark. A PD-10 column was used to buffer exchange the

sample into 25 mM HEPES, 150 mM KCl, pH 7.5. After buffer exchange, the protein was concentrated, flash frozen, and stored at -80°C. Anion exchange purified HMPV P was labeled in a similar manner using Alexa 594 NHS ester (ThermoFisher).

Droplet assay

A 20% dextran solution was prepared in 25 mM HEPES, 150 mM KCl, pH 7.5. The solution was filter sterilized prior to use. DTT was added to the dextran solution to give a final concentration of 1 mM. HMPV protein constructs were diluted in the 20% dextran, 1 mM DTT, 25 mM HEPES, 150 mM KCl, pH 7.5 solution in 1.5 mL Eppendorf tubes. This solution was used in samples for standard droplet imaging, fusion droplet imaging, and in turbidity assays. For the HMPV P samples tested at different KCl concentrations, similar buffers were prepared with KCl ranging from 0 mM to 500 mM. 1.5 µL of sample was plated on an 8-well printed microscopy slide and covered with a glass coverslip. For droplets imaged at later time points, the slides were stored in a humidified chamber

Microscopy imaging

HMPV samples were imaged using either DIC or epifluorescence on a Nikon Eclipse E600 with the 60X objective. Fusion time lapse images were acquired with MetaMorph software using DIC on a Zeiss Axiovert 200M with the 100X oil objective. Images were acquired at 0.3 sec or 0.5 sec intervals.

RNA

The fluorescent RNA decamer was purchased from Integrated DNA Technologies. It was terminated with OH at the 5’ end and 6-carboxyfluorescein at the 3’ end.

Turbidity assay

Protein solutions were mixed with filter sterilized 20% dextran, 1 mM DTT, 25 mM HEPES, 150 mM KCl, pH 7.5 in clear 96-well plates. The final concentration of the proteins was 40 µM. The absorbance of the solutions was measured on a

SpectraMax iD3 at 395 nm (87). Readings were taken at 5 min intervals for 8 hr or longer.

Chapter 3: Transmembrane Domain Dissociation is Required for Hendra F Protein Fusogenic Activity

Portions of this chapter were adapted and reprinted with permission from the American Society for Microbiology: Slaughter KB, Dutch RE. 2019. Transmembrane Domain Dissociation Is Required for Hendra Virus F Protein Fusogenic Activity. J Virol 93:e01069-19.

Introduction

The *Paramyxoviridae* family consists of negative-sense single-stranded RNA viruses enclosed within lipid membranes. Hendra (HeV) and Nipah (NiV) viruses, members of the Henipavirus genus, are highly pathogenic zoonotic viruses within the *Paramyxoviridae* family (101). Due to the high mortality rates associated with HeV and NiV infections and the lack of a human vaccine or effective treatment, they have been designated as biosafety level 4 pathogens (102). HeV and NiV were identified in Australia and Malaysia, respectively, in the 1990s following outbreaks of severe encephalitis and respiratory disease in humans (8, 102-104). Further investigation revealed that fruit bats of the *Pteropodidae* family were the natural reservoir for the viruses, and transmission to other organisms, including pigs and horses, contributed to the zoonotic spread to humans (105-107). The potential for future outbreaks of henipavirus infections and the emergence of similar zoonotic viruses warrants further research into the entry mechanisms of these pathogens.

Membrane fusion is an essential step in entry of enveloped viruses that relies on the coordination of specialized proteins at the viral membrane surface. HeV and NiV possess two surface glycoproteins: the attachment protein (G), which allows the virus to bind a target cell, and the fusion protein (F), which promotes merger of the viral membrane with the target membrane (108, 109). Both glycoproteins, F and G, are required for paramyxovirus membrane fusion, but it is still unclear how interactions between F and G and receptor binding promote triggering of F (18). The henipaviruses and other members of the *Paramyxoviridae*

family use a trimeric class I F protein to drive membrane fusion (20, 110, 111). Before the F protein can participate in fusion events, the inactive precursor (F_0) must be proteolytically cleaved within the host cell to form a fusion active disulfide-linked heterodimer (F_1+F_2) (FIG 3.1A). For HeV and NiV, the F protein traffics to the cell surface and is subsequently endocytosed to be cleaved by the protease cathepsin L before being recycled back to the surface (24-26). Following the cleavage event, the F protein is maintained at the surface in a metastable prefusion state until it is triggered to undergo the conformational changes needed to promote membrane fusion. These conformational changes from the prefusion to post-fusion form involve an essentially irreversible rearrangement of the F protein ectodomain that results in formation of a stable six-helix bundle (FIG 3.1B-F).

Studies of several viral fusion proteins have shown that the transmembrane domain (TMD) is critical for driving fusion events (29, 30, 33-39, 112, 113). For HeV, previous work has shown that TMD interactions within the F protein trimer help preserve the metastable prefusion conformation and play a role in fusion promotion (41, 114, 115). More specifically, these findings suggest that HeV F TMD interactions are needed to stabilize the heptad repeat B (HRB) domains that form the stalk of the protein prior to triggering (FIG 3.1B). Thus, the current model for HeV F fusion events suggests that dissociation of TMD trimeric interactions is required to initiate conformational changes that destabilize interactions between the HRB domains and eventually promote formation of the post-fusion six-helix bundle to drive membrane fusion (41).

Based on this model, we hypothesized that fusion could be blocked by introducing disulfide bonds to covalently link the TMDs of HeV F. Studies using substituted cysteine residues to generate disulfide bonds have previously been conducted to examine conformational changes in paramyxovirus surface glycoproteins. For measles virus (MeV), residues in the attachment protein stalk were replaced with cysteine to promote disulfide bond formation to identify four conserved residues required for folding into a fusion-conducive conformation (116). In addition, studies of the attachment proteins from canine distemper virus

and MeV showed that introduced disulfide bonds in the central region of the stalk blocked fusion, but fusion activity was restored under reducing conditions (117). For the Newcastle disease virus attachment protein, disulfide bonds were generated across the dimer interface in the globular domain to show changes in receptor binding and fusion promotion (118).

Introduced disulfide bonds have also been an important tool for studying paramyxovirus F proteins. Single cysteine substitutions were made in the membrane-proximal region of the heptad repeat B (HRB) domain of MeV F, generating disulfide-linked dimers, to study formation of the post-fusion six-helix bundle. Results showed that the constructs were able to promote efficient viral entry even though two HRB domains were locked together by a disulfide bond (119). Other studies have used double cysteine substitutions to further restrict conformational changes in the paramyxovirus F protein. For MeV F, introduced disulfide bonds that linked the globular head and stalk domain of different monomers within the F trimer blocked fusion activity, and fusion was partially restored by subsequently reducing the disulfide bridges. These findings suggested that fusion activity requires reversible interactions between the stalk and head domains of the F protein (120). For PIV5 F, double cysteine substitutions were used to introduce disulfide bonds in the membrane-proximal external region (MPER) which is N-terminal to the TMD. Results from this study showed that dissociation of the MPER region within the PIV5 F trimer is necessary to promote the conformational changes that drive fusion events (121). Additionally, work on HeV F used double cysteine substitutions to block conformational changes in the ectodomain to analyze effects on fusion. This study showed that introduced disulfide bonds in the ectodomain could inhibit fusion by stabilizing HeV F in the prefusion conformation (122).

Previous evidence and calculations for paramyxoviruses have shown that the TMDs of the F protein are potentially longer than a typical vertically inserted membrane-spanning helix (112). Due to the lack of structural data for membrane-spanning regions, the orientation of the paramyxovirus F protein TMDs within the

membrane remains unclear. We selected residues near the N-terminal region of the predicted HeV F TMD for substitution with double cysteine residues to determine if TMD dissociation is essential to drive conformational changes required for fusion events (FIG 3.1A). These TMD mutants were designed with the goal of introducing disulfide bonds that would link the three monomers of the F trimer in the TMD region to assess alterations in fusion activity, protein stability, and overall protein conformation.

Double cysteine substitutions in the HeV F TMD led to the formation of disulfide-linked trimers, and fusion was blocked for these mutants. Attempts to restore fusion for the mutants with a disulfide reducing agent were unsuccessful, suggesting that the introduced disulfide bonds were protected in the membrane. Further analysis showed that two of the mutants were expressed at the cell surface in the prefusion conformation at levels that would normally promote fusion. Our results suggest that these two mutants were properly folded and processed, supporting the conclusion that TMD dissociation is required for fusion promotion. This study is the first to show that HeV F fusogenic activity can be prohibited by blocking TMD dissociation. These findings provide important new information on paramyxovirus fusion and contribute to our current knowledge of HeV F TMD interactions in protein stability, conformation, and fusion promotion events.

Results

Double cysteine substitutions in the HeV F TMD promote disulfide bond formation

Our current model suggests that TMD dissociation is important for conformational changes in the ectodomain needed for fusion, so substitutions were made in the HeV F TMD to analyze the effects on protein folding, stability, and fusion promotion when the TMDs are locked together. HeV F associates as a homotrimer immediately following synthesis, so double cysteine substitutions were made to link the three monomers with disulfide bonds (T483C/V484C,

V484C/N485C, N485C/P486C). The mutation locations were selected based on the prediction that the residues were present in the N-terminal region of the HeV F TMD. HeV F is synthesized in the endoplasmic reticulum (ER) which has a thinner lipid bilayer than the plasma membrane (123). Our goal was to mutate residues in the TMD that could be exposed to the oxidizing environment of the ER to allow for disulfide bond formation before trafficking to the cell surface.

The oligomeric state of the HeV F TMD mutants was analyzed to determine if disulfide bonds successfully linked the monomers of the HeV F trimer. Vero cells were transiently transfected with plasmids encoding WT HeV F or one of the TMD mutants. Then, cells were starved, metabolically labeled, and samples immunoprecipitated using an anti-peptide antibody that binds to the cytoplasmic tail of HeV F. Boiled samples were separated on 3.5% polyacrylamide gels under non-reducing conditions to allow for visualization of different oligomeric forms of HeV F. T483C/V484C, V484C/N85C, and N485C/P486C migrated primarily in the trimeric form, whereas WT HeV F migrated primarily as a monomer (FIG 3.2A). This suggested that the double cysteine substitutions in HeV F resulted in disulfide bonds that covalently linked the monomers of the HeV F trimer. In contrast, WT HeV F migrated primarily in the monomeric form because the monomers of the trimer lack covalent interactions. To confirm that the trimeric form was a result of introduced disulfide bonds, samples were alternatively treated under reducing conditions. Results showed that the HeV F TMD mutants migrated in the monomeric form, similar to WT HeV F, under reducing conditions (FIG 3.2B). Taken together, these findings indicate that the monomers of T483C/V484C, V484C/N85C, and N485C/P486C were effectively cross-linked due to the introduction of disulfide bonds between the TMDs of the F trimer.

Fusogenic activity is blocked for the HeV F TMD mutants

Fusion assays were conducted to determine whether the mutants could promote fusion when TMD dissociation was inhibited. Vero cells were transiently transfected with plasmids encoding WT HeV G and WT HeV F or one of the TMD mutants. Cells transfected with WT HeV G alone or empty vector served as

negative controls. At 48 hr post-transfection, the cells were analyzed by microscopy for syncytia formation. As expected, cells transfected with a combination of WT HeV F and G showed the formation of small and large syncytia (FIG 3.3A). However, samples transfected with WT HeV G and one of the TMD mutants showed no syncytia formation, suggesting that the introduced disulfide bonds blocked normal fusion promotion (FIG 3.3A).

A quantitative luciferase reporter gene assay was used to confirm the syncytia assay results. Vero cells were transiently transfected with plasmids encoding luciferase under the control of a T7 promoter, WT HeV G, and WT HeV F or one of the TMD mutants. At 24 hr post-transfection, the Vero cells were overlaid with BSR cells containing the T7 polymerase. After a 3 hr incubation, the cells were lysed and analyzed for luminescence as a measure of cell-cell fusion. Results showed that the TMD mutants did not promote fusion above the levels observed for the negative control (HeV G alone). Together, these results indicate that introduced disulfide bonds in the HeV F TMD prohibit fusion activity.

Cell surface expression is variably reduced for the HeV F TMD mutants

Previous studies have shown that increased cell surface density of WT HeV F correlates with increased fusion activity (124). Cell surface expression analysis was performed to determine if the TMD mutants were trafficked to the surface at levels that would normally allow for fusion promotion. Vero cells were transiently transfected with WT HeV F or one of the TMD mutants, starved, and metabolically labeled. Then, the samples were biotinylated prior to lysis and immunoprecipitation so that the cell surface protein population could be isolated and compared to total protein levels via SDS-PAGE analysis. Results for total protein expression showed no significant differences for the TMD mutants compared to WT HeV F (FIG 3.4A, 3.4C), whereas protein cleavage was significantly reduced for the mutants (FIG 3.4D), indicating they may be processed and trafficked less efficiently. Analysis of cell surface protein expression and cleavage showed significantly reduced levels for N485C/P486C, suggesting that this mutant may be misfolded or have severe trafficking defects (FIG 3.4B, 3.4E). Similar to total protein cleavage results,

surface protein cleavage levels for the TMD mutants were significantly reduced, further indicating that they are trafficked and processed less efficiently than WT HeV F (FIG 4F). Although T483C/V484C and V484C/N485C cleavage was reduced, the amount of fusion active F_1 on the surface was above the level previously shown to be needed for HeV F fusion (124). Based on these results, T483C/V484C and V484C/N485C are likely unable to promote fusion because TMD dissociation is an essential step for initiating conformational changes during fusion events.

T483C/V484C and V484C/N485C are maintained over time at levels that normally allow for fusion

Since the HeV F TMD mutants showed moderate differences in total expression and variable differences in surface expression compared to WT HeV F, a time course immunoprecipitation experiment was performed to monitor stability of the F protein over time (FIG 3.5). Vero cells were transiently transfected with WT HeV F or one of the TMD mutants. Then, the cells were starved, metabolically labeled, and chased with regular media for different amounts of time, as indicated. Finally, cells were lysed and samples immunoprecipitated for SDS-PAGE analysis. At early time points, WT HeV F and the TMD mutants were predominantly found in the F_0 inactive form (FIG 3.5A). Over time, levels of the F_1 proteolytically active form increased, indicating that WT HeV F and the mutants were processed. Interestingly, quantification of expression levels at different time points showed that the mutants were highly expressed compared to WT HeV F at early time points (FIG 3.5B). At later times, T483C/V484C and V484C/N485C showed reductions in protein levels compared to WT HeV F, indicating that these mutants may have minor folding changes that target some of the protein for degradation. However, N485C/P486C showed a more severe reduction in protein level over time, suggesting that this mutant is likely targeted for degradation after synthesis due to improper folding. This result is consistent with the finding that N485C/P486C surface expression was significantly reduced (FIG 3.4). Overall, these results show that the location of introduced disulfide bonds in the HeV F

TMD can variably affect protein folding and stability over time. These findings suggest the minor changes observed for T483C/V484C and V484C/N485C protein stability are likely not the cause of fusion prohibition.

Introduced disulfide bonds in the HeV F TMD mutants are poorly accessible to reducing agent

Since fusion assays with the TMD mutants suggested that TMD dissociation is essential for fusion promotion, the mutants were analyzed to determine if fusion could be restored by reducing the introduced disulfide bonds. In theory, reduction of the disulfide bonds linking the TMDs would allow for dissociation of the TMDs to initiate the necessary conformational changes in the ectodomain for fusion activity. To test this, a luciferase reporter gene assay was conducted as described previously, except that the overlay media contained the cell-impermeant reducing agent tris(2-carboxyethyl)phosphine (TCEP). Following the 3 hr incubation with overlaid BSR cells in 6 mM TCEP-containing media, the samples were analyzed for luminescence. Interestingly, fusion increased for WT HeV F treated with TCEP, suggesting that reduction of intramolecular disulfide bonds may impact overall protein stability and enhance triggering (FIG 3.6A). However, results for the TMD mutants showed no significant change in fusion levels between treated and untreated samples, indicating that fusion was not restored in the presence of TCEP (FIG 3.6A).

Oligomeric analysis was performed to further understand the effects of TCEP on the introduced disulfide bonds in the TMD mutants. The samples were prepared as described in FIG 3.2, except a 3 hr incubation with 6 mM TCEP or untreated media was included after the metabolic label. Then, samples were immunoprecipitated and analyzed by SDS-PAGE. Interestingly, results of the analysis showed that TCEP was capable of reducing disulfide bonds within the WT F protein, as indicated by the shift in bands for the trimer, dimer, and monomer in treated samples (FIG 3.6B). This shift is consistent with loss of the extracellular F2 subunit when F_1+F_2 is reduced in the presence of TCEP. The TMD mutants also showed shifts consistent with loss of the F_2 subunit (FIG 3.6B, asterisks).

T483C/V484C showed some reduction from the trimeric to monomeric form, but a portion of the trimeric form was still present in the TCEP-treated samples. The trimeric form of V484C/N485C partially shifted to a trimer lacking F_2 in the TCEP-treated samples, but there was little change in the amount of monomer. The oligomeric forms of N485C/P486C remained relatively unchanged following TCEP treatment. This indicates that TCEP was poorly able to access the introduced disulfide bonds linking the TMDs of the mutant HeV F proteins, and accessibility decreased as the mutations went further into the TMD region. Altogether, this data suggests that the introduced disulfide bonds in the mutants are likely buried in cell membrane, making them, in some cases, inaccessible to the reducing agent.

T483C/V484C and V484C/N485C bind a prefusion conformation-specific antibody prior to cell disruption

Since T483C/V484C and V484C/N485C were present at the cell surface at levels that would allow for fusion, further studies were conducted to analyze the conformation of the mutant protein structures. A HeV F prefusion conformation-specific antibody, mAb 5B3, was used to compare WT HeV F to the TMD mutants (100, 122). Vero cells were transiently transfected with WT HeV F or one of the mutants. At 24 hr post-transfection, the cells were metabolically labeled overnight and treated with the prefusion antibody prior to cell lysis and immunoprecipitation. Control samples were treated with the HeV F anti-peptide antibody after cell lysis. Results showed that T483C/V484C and V484C/N485C were able to bind the prefusion conformation-specific antibody at moderately reduced levels compared to WT HeV F (FIG 3.7A, 3.7B). This result is consistent with the cell surface protein expression levels observed for T483C/V484C and V484C/N485C, suggesting that the TMD mutants trafficked to the surface are present in the prefusion form (FIG 3.4).

Prior work with the prefusion conformation-specific antibody has shown that WT HeV F is unable to bind the antibody when it is applied following cell lysis, likely due to disruption of the metastable prefusion conoformation of HeV F following lysis buffer treatment. Since the TMDs of T483C/V484C and V484C/N485C are

locked together by disulfide bonds, these mutants were tested to determine if the introduced disulfide bonds permanently lock the prefusion conformation of the ectodomain. The HeV F TMD mutants were tested with mAb 5B3 after cell lysis to analyze prefusion conformation-specific antibody binding, and results showed that treating the mutants with mAb 5B3 following cell disruption dramatically reduced levels of binding (FIG 3.7C). Together, these results suggest that T483C/V484C and V484C/N485C are synthesized in a prefusion conformation, but locking the TMDs together with disulfide bonds does not completely prevent unfolding of the ectodomain.

Discussion

The model for HeV fusion suggests that dissociation of the F protein TMDs is an essential step for initiating and completing conformational changes in the ectodomain required for membrane fusion (41). We tested this model by designing HeV F TMD mutants to introduce disulfide bonds that would link the TMDs and prevent trimeric dissociation. Results showed that the mutants were successfully synthesized as disulfide-linked trimers, but fusion was prohibited for the mutants, suggesting that TMD dissociation is critical for the conformational changes in HeV F needed for fusion. Whereas surface expression and stability of T483C/V484C and V484C/N485C were maintained at levels that would allow for fusion, our results showed that N485C/P486C surface expression was significantly reduced, suggesting that the position of these introduced disulfide bonds interfered with proper protein folding. Attempts to restore fusion for the TMD mutants were unsuccessful, indicating that the introduced disulfide bonds were poorly accessible to the reducing agent due to their position in the membrane. Additional analysis of the TMD mutants showed that T483C/V484C and V484C/N485C were maintained in a prefusion conformation prior to cell disruption. Together, these findings support the hypothesis that TMD dissociation is required for HeV fusogenic activity and that TMD interactions play a crucial role in F protein folding and stability.

Cleavage of the HeV F TMD mutants was significantly reduced compared to WT HeV F, which could contribute to the lack of fusion. Previous work from our lab showed that decreased WT HeV F expression leads to decreased fusion activity, but fusion was still detectable when normal WT HeV F surface expression was reduced by 80 percent (124). The amount of active F_1 protein at the surface for the mutants T483C/V484C and V484C/N485C was above that needed for fusion for the WT protein. However, our reporter gene assay results showed no fusion above background levels for the HeV F TMD mutants, supporting our conclusion that fusion is blocked.

Previous work with other paramyxoviruses has utilized introduced disulfide bonds to probe the effects of limiting mobility within the F protein. For PIV5, introduced disulfide bonds that linked the monomers within the MPER, N-terminal to the predicted TMD, blocked fusion activity (121). This was consistent with the inhibition of fusion observed for the HeV F TMD mutants. Treatment of the PIV5 F MPER mutant with TCEP restored fusion activity. However, similar treatment of the HeV F TMD mutants with TCEP did not restore fusion. This suggests that the disulfide bonds of the HeV F TMD mutants in this story were protected in the membrane, whereas the MPER disulfide bonds in the PIV5 F mutant were exposed at the cell surface (121).

Additional work related to PIV5 F has addressed the role of the TMD in fusion. Investigations showed that single cysteine substitutions near the N-terminus of the TMD led to disulfide bond formation in the absence of an oxidative cross-linker, similar to the disulfide bond formation we observed in the HeV F TMD mutants (112). Further analysis of this region of PIV5 F using alanine-scanning mutagenesis indicated that two residues, L486 and I488, were required for efficient fusion activity. Different amino acids were substituted at these sites to test the effects of amino acid side chains on fusion activity. Interestingly, substitution with cysteine led to a minor reduction in fusion activity compared to the severe reductions observed with other substitutions. This finding is consistent with the idea that disulfide bond formation, rather than the presence of substituted cysteine

residues, drove the prohibition of fusion activity for the HeV F TMD mutants. In addition, an alanine substitution was previously made at residue 486 in HeV F, resulting in minimal changes in fusion activity compared to WT, further suggesting that disulfide bond formation, rather than the cysteine substitutions, played a key role in blocking fusion activity for the HeV F TMD mutants (Barrett, Popa, unpublished data).

Single cysteine substitutions were also used in a study to examine conformational changes in MeV F. They generated disulfide-linked mutants that were predicted to be unable to fully close the six-helix bundle (119). The single substitutions were made near the membrane-spanning region in the HRB domain. Despite this restriction on F protein flexibility, the mutants were able to efficiently open and stabilize fusion pores for viral entry, suggesting that these fusion events occur independently of complete six-helix bundle assembly (119). This work indicates that these single cysteine substitutions allow for greater flexibility than double cysteine substitutions in the membrane-proximal region of the F protein and provide evidence to support the idea that flexibility of interactions in the HRB and TMD are required for efficient fusion activity.

When TCEP was used in an attempt to restore fusion activity in our study, results showed that fusion was enhanced for WT HeV F. This increase may be due to the reduction of other disulfide bonds within the ectodomain of HeV F that are required for prefusion stability. Work on Newcastle disease virus identified free thiols in the surface-expressed F protein, a result of thiol/disulfide-exchange, and blocking these groups with a thiol-specific biotin inhibited fusion (125). Thiol/disulfide-exchange also plays a role in the entry of other enveloped viruses such as human immunodeficiency virus type I (126). These findings suggest that reduction of specific disulfide bonds in the F protein of paramyxoviruses may affect the efficiency of fusion activity. For HeV F, reducing disulfide bonds in the ectodomain by adding TCEP may cause the protein to trigger and promote fusion more readily than untreated HeV F. The HeV F TMD mutants showed small

increases in fusion following TCEP treatment. However, these changes in fusion activity were not significant when compared to the untreated mutants.

The paired cysteine substitutions we made in HeV F were located near the N-terminus of the TMD, but our results suggested that the introduced disulfide bonds were buried within the plasma membrane. The F protein is synthesized in the ER which consists of a slightly thinner lipid bilayer than the plasma membrane (123). This difference in membrane thickness may be important for exposing the N-terminal region of the HeV F TMD to the oxidizing environment of the ER to allow for disulfide bond formation immediately following synthesis. Once the mutant HeV F proteins are trafficked through the secretory pathway to the thicker plasma membrane, the disulfide bonds in the TMD may be shielded by the lipid environment from extracellular factors that could be introduced to disrupt the bonds.

Membrane thickness is largely determined by lipid composition, and a number of membrane lipids have been identified as important players in viral infectivity (127-133). Additionally, several studies of non-viral proteins have shown that cholesterol and sphingolipids play a role in promoting TMD helix interactions (134-136). Work with the paramyxovirus MeV has shown that the F protein is enriched in lipid rafts, and this partitioning is important for MeV assembly at the plasma membrane (132). Studies of NiV have shown evidence of F protein clustering in the plasma membrane, suggesting that membrane domains may be needed for proper surface glycoprotein organization for assembly and fusion (137). For Newcastle disease virus, lipid rafts have been shown to participate in forming and maintaining F protein and attachment protein complexes in the plasma membrane (138). Beyond paramyxoviruses, lipid rafts domains have been implicated in the assembly and spread of filoviruses, retroviruses, and orthomyxoviruses (139). It is possible that lipid rafts also play a role in HeV assembly and TMD helix interactions. Additionally, partitioning of the F protein into rafts could increase the number of TMD residues accommodated by the membrane. Therefore, HeV F localization to lipid rafts could explain why the

introduced disulfide bonds are initially formed at the ER but are protected from reducing agents at the plasma membrane. Future studies will analyze the importance of lipid composition for stability of the prefusion conformation and promotion of fusion events.

Here, we showed that disulfide bonds can be introduced to covalently link the TMDs of the HeV F trimer. Blocking TMD dissociation with introduced disulfide bonds prohibits fusion events, but further studies are needed to address the conformational changes that can occur in HeV F when the TMDs are locked. Our studies suggest that mutant HeV F proteins with linked TMDs are in some cases capable of maintaining a prefusion conformation. If cells expressing these constructs are disrupted, then the mutant HeV F proteins refold into a conformation that is no longer recognizable by a prefusion specific antibody. Additional analysis is needed to understand if the disulfide-linked HeV F mutants are capable of refolding into protein intermediates that are suggested to occur after an initial triggering event and prior to formation of the six-helix bundle. Our findings reported here and future studies will contribute to understanding HeV F dynamics required for fusion events and mechanisms of enveloped virus entry.

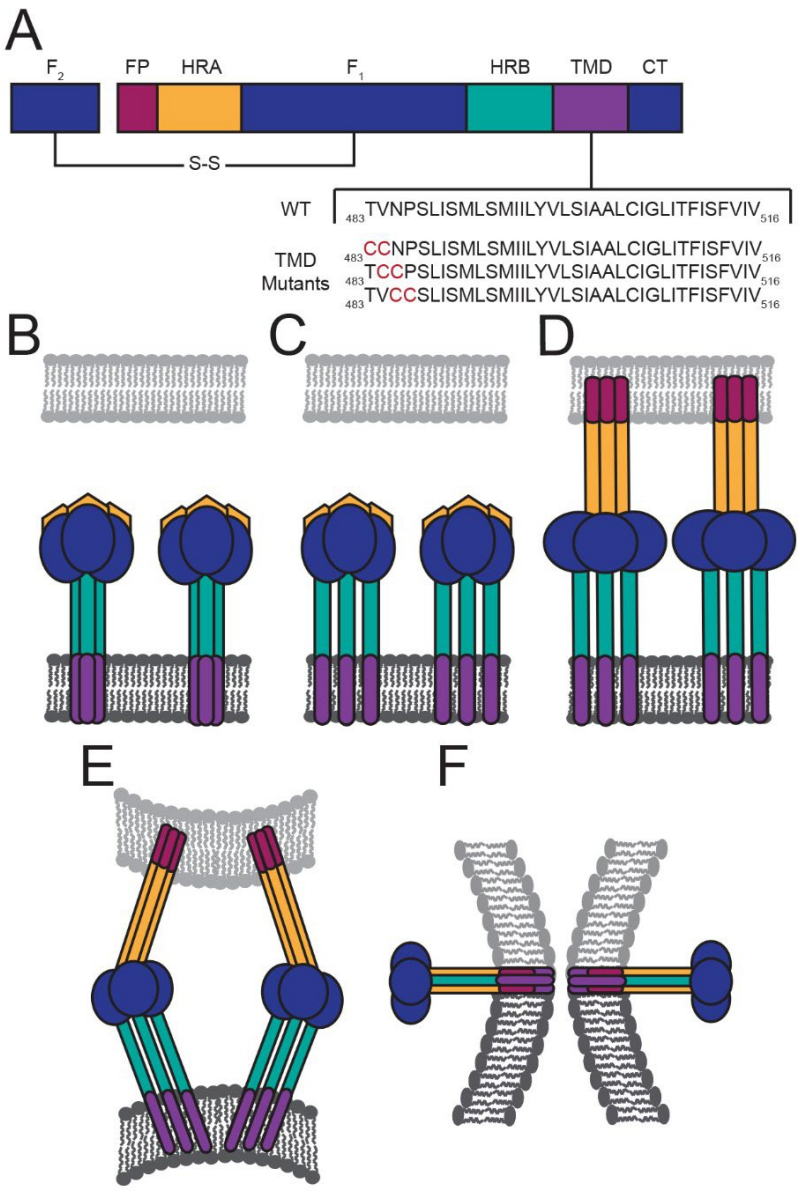

Figure 3.1. HeV F protein schematic and fusion model. (A) Diagram of the fusion-active, disulfide (S-S)-linked F protein with the HeV F TMD sequence below. Domain structure includes the fusion peptide (FP), heptad repeat A (HRA), HRB, TMD, and the cytoplasmic tail (CT). In the fusion model, the TMDs of the metastable prefusion F interact as a trimer (B). Then triggering of F leads to dissociation of the TMDs and the HRB domains (C). Changes in TMD interactions promote extension of the HRA domains and insertion of the FP into the target membrane (D). (E and F) Further refolding of F leads to formation of the postfusion six-helix bundle conformation.

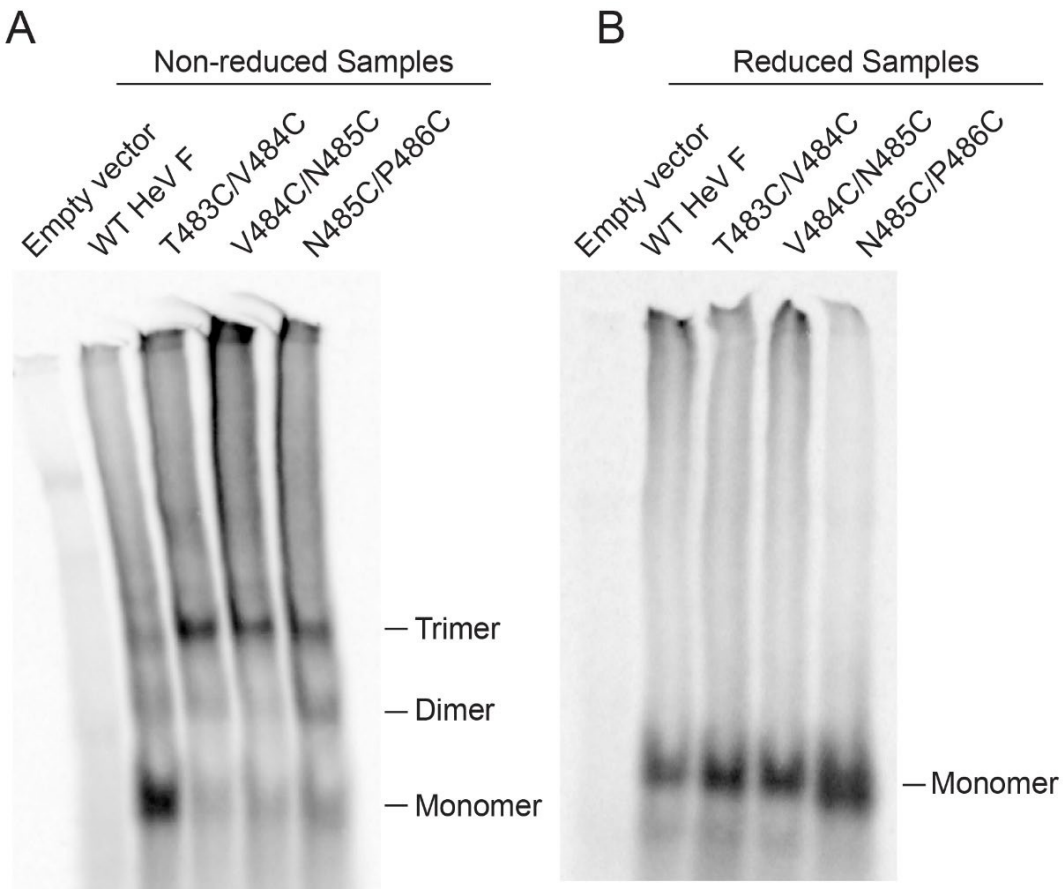

Figure 3.2. Double cysteine substitutions in the HeV F TMD promote disulfide bond formation. Vero cells were transfected with WT HeV F or one of the TMD mutants. At 24 h posttransfection, the cells were metabolically labeled for 3 h, and samples were immunoprecipitated. WT HeV F and the mutants were treated with nonreducing loading buffer (A) or reducing loading buffer (B) and separated using 3.5% SDS-PAGE.

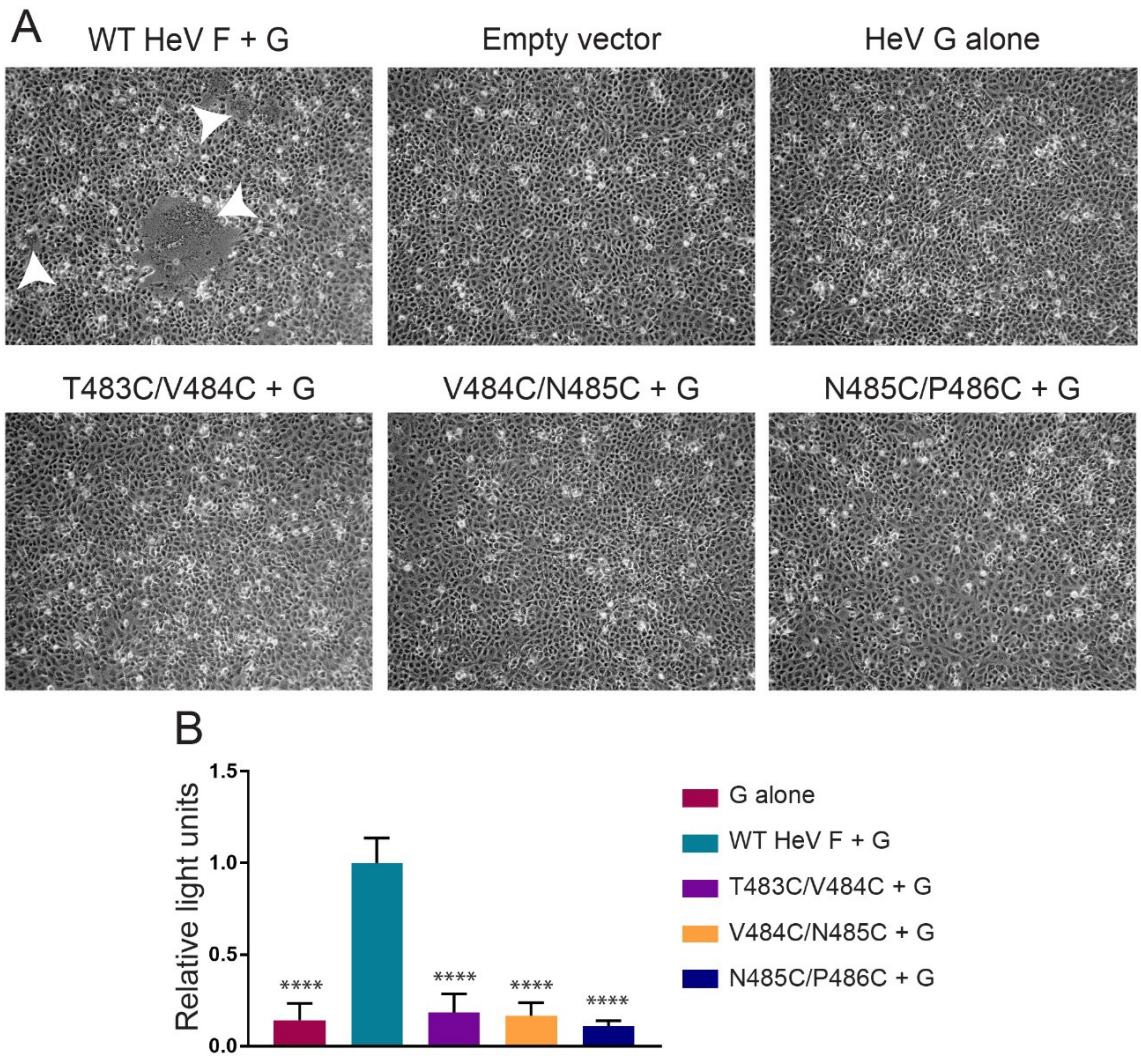

Figure 3.3. Fusogenic activity is blocked for the HeV F TMD mutants. (A) Vero cells were transfected with the attachment protein WT HeV G and WT HeV F or one of the TMD mutants. Syncytium formation was analyzed at 48 h posttransfection. Images were taken with a Zeiss Axiovert 100 microscope. White arrowheads indicate syncytia. Images are representative. (B) Vero cells were transfected with luciferase, WT HeV G, and WT HeV F DNA or one of the TMD mutants. At 24 h posttransfection, the Vero cells were overlaid with BSR cells. After a 3-h incubation period, the cells were lysed and prepared for luminosity analysis to quantify fusion. Results were normalized to samples transfected with WT HeV F and G. All data are presented as the means ± standard deviations for three independent experiments. Statistical analysis was performed using a two-way

analysis of variance with a Bonferroni correction. Asterisks indicate statistical significance compared to values for the WT HeV F (****, $P < 0.0001$).

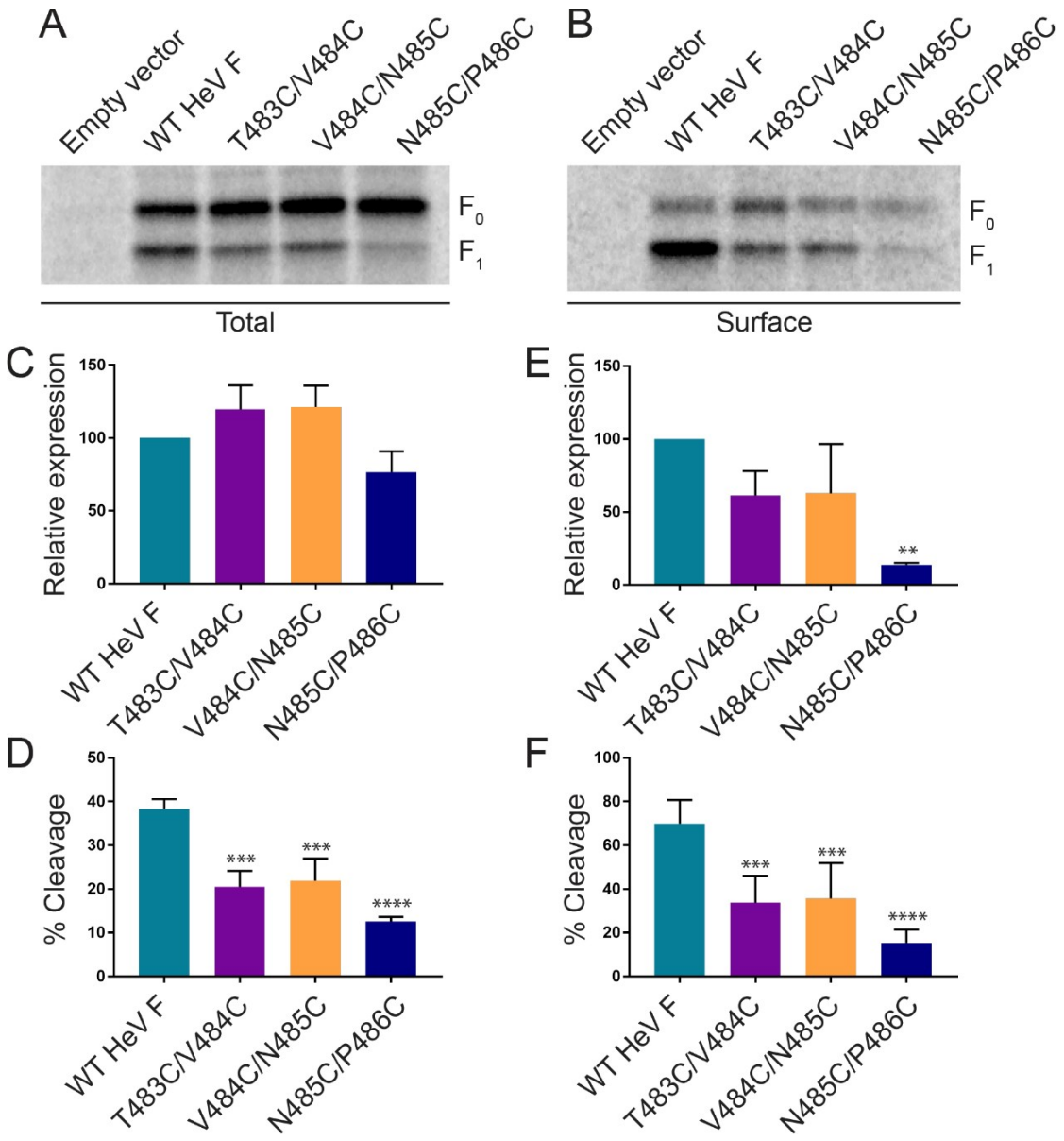

Figure 3.4. Cell surface expression is variably reduced for the HeV F TMD mutants. Total (A) and surface (B) expression levels were analyzed using a biotinylation method. Vero cells were transfected with WT HeV F or one of the TMD mutants. At 24 h posttransfection, the cells were metabolically labeled for 4 h, followed by biotinylation of the surface proteins and immunoprecipitation. The samples were analyzed by 15% SDS-PAGE. Total expression (F_0+ F_1) and cleavage [$F_1/(F_0+F_1)$] (C and D), as well as surface expression and cleavage (E and F) were quantified by densitometry and normalized to levels for WT HeV F. All

data are represented as the means ± standard deviations for three independent experiments. Statistical analyses were performed using a two-way analysis of variance with a Bonferroni correction. Asterisks indicate statistical significance compared to values for the WT HeV F (**, $P < 0.01$; ***, $P < 0.001$; ****, $P < 0.0001$).

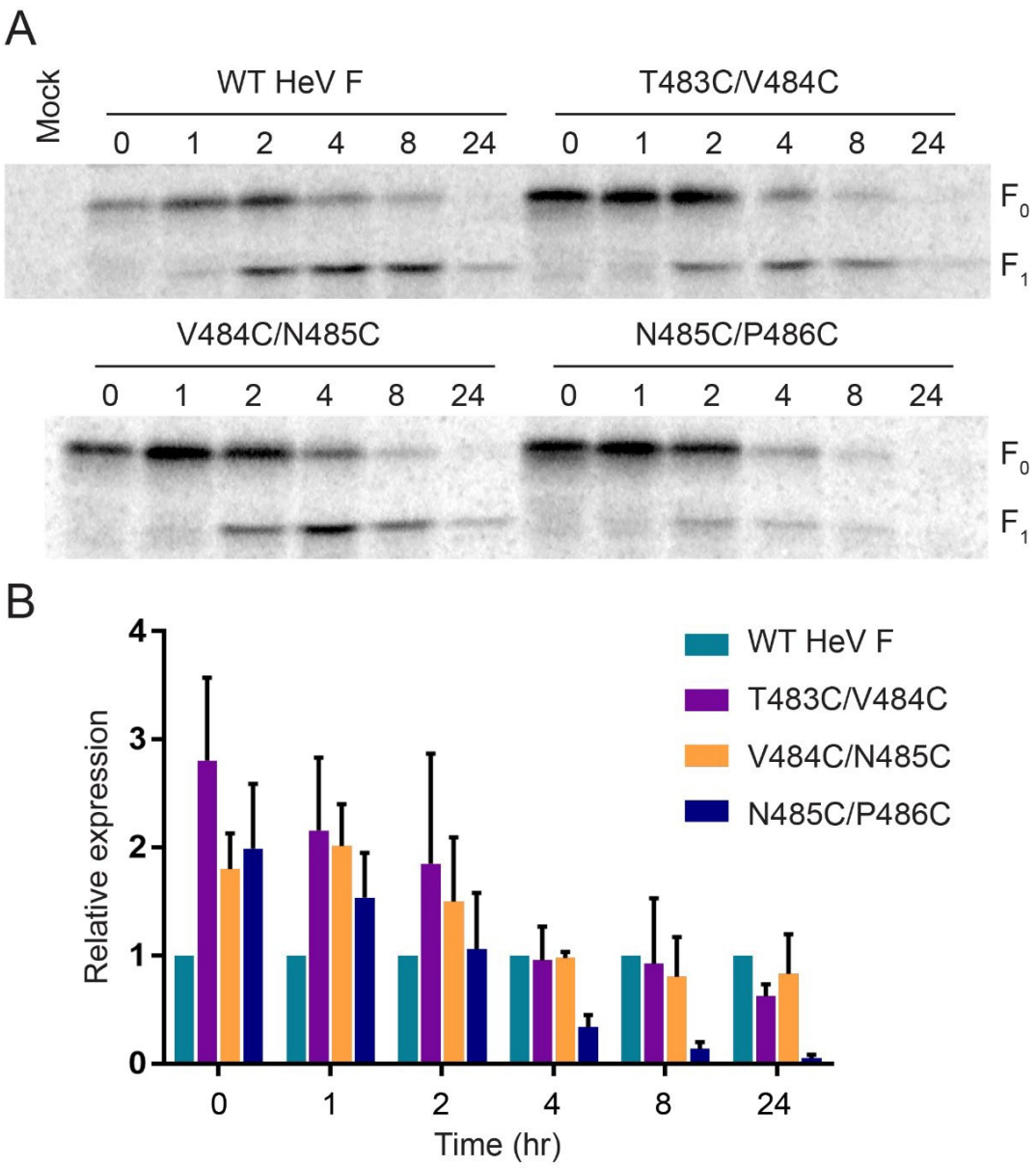

Figure 3.5. T483C/V484C and V484C/N485C are present over time at levels that normally allow for fusion. (A) Vero cells were transfected with WT HeV F or one of the TMD mutants. At 24 h posttransfection, the cells were metabolically labeled for 30 min. Following different chase time points, the samples were immunoprecipitated and analyzed by 10% SDS-PAGE. (B) Expression was quantified by densitometry and normalized to the value for WT HeV F at each time point. All data are represented as the means ± standard deviations for three independent experiments.

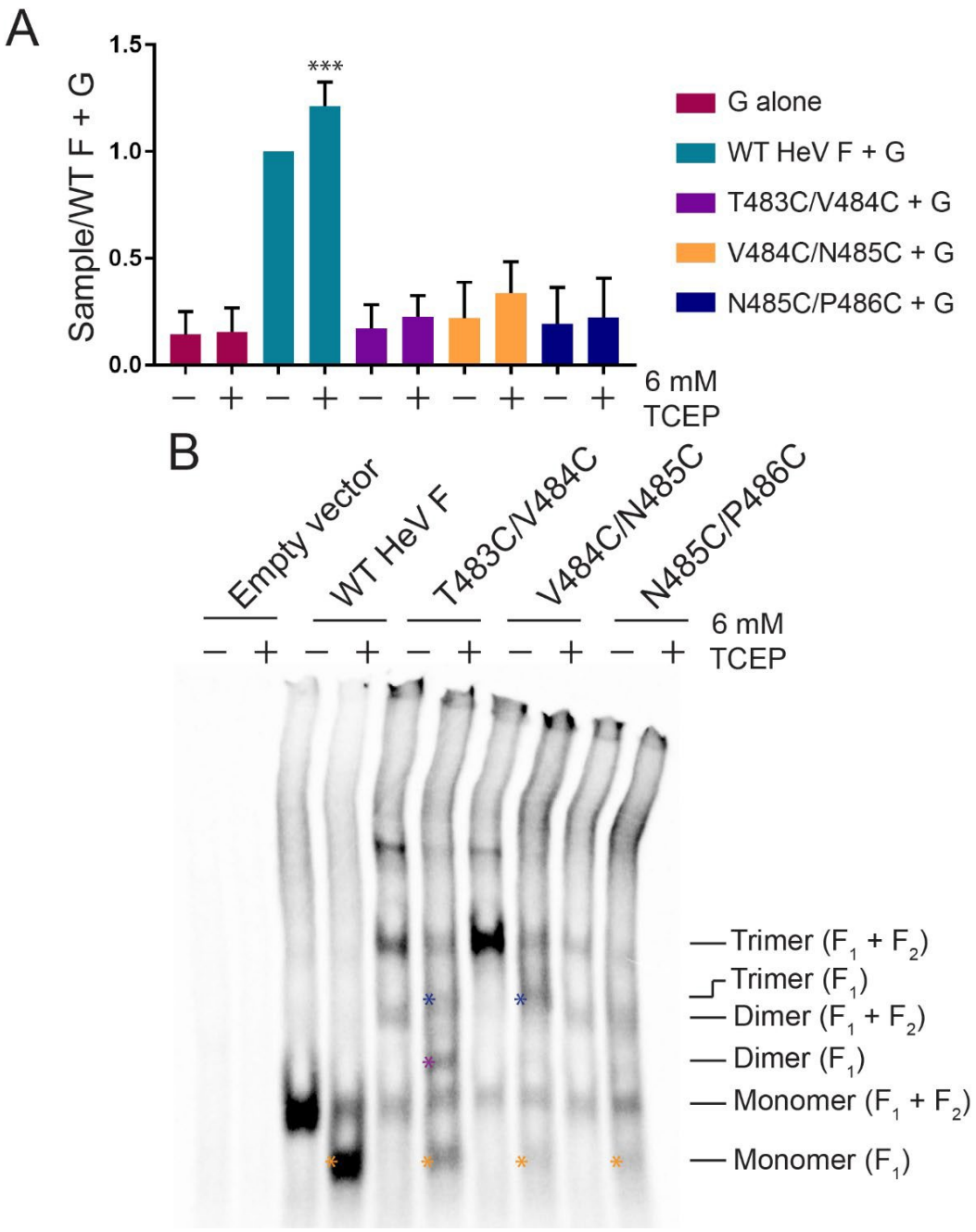

Figure 3.6. The introduced disulfide bonds in the HeV F TMD mutants are poorly accessible to reducing agent. (A) The samples were prepared as described in the legend of Fig. 3B, except the overlay medium consisted of BSRs in DMEM plus 10% FBS ± 6 mM TCEP. Results were normalized to levels of the samples transfected with WT HeV F and G (untreated). All data are presented as the means ± standard deviations for three independent experiments. Statistical analysis was performed using two-way analysis of variance with a Bonferroni

correction. Asterisks indicate statistical significance compared to the level of the WT HeV F+G (untreated) (***, $P < 0.005$). (B) The samples were prepared as described in the legend of Fig. 2A, except that the samples were treated with DMEM plus 10% FBS ± 6 mM TCEP for 3 h following the metabolic label. Blue asterisks indicate trimer (F_1), purple asterisk indicates dimer (F_1), and orange asterisks indicate monomer (F_1).

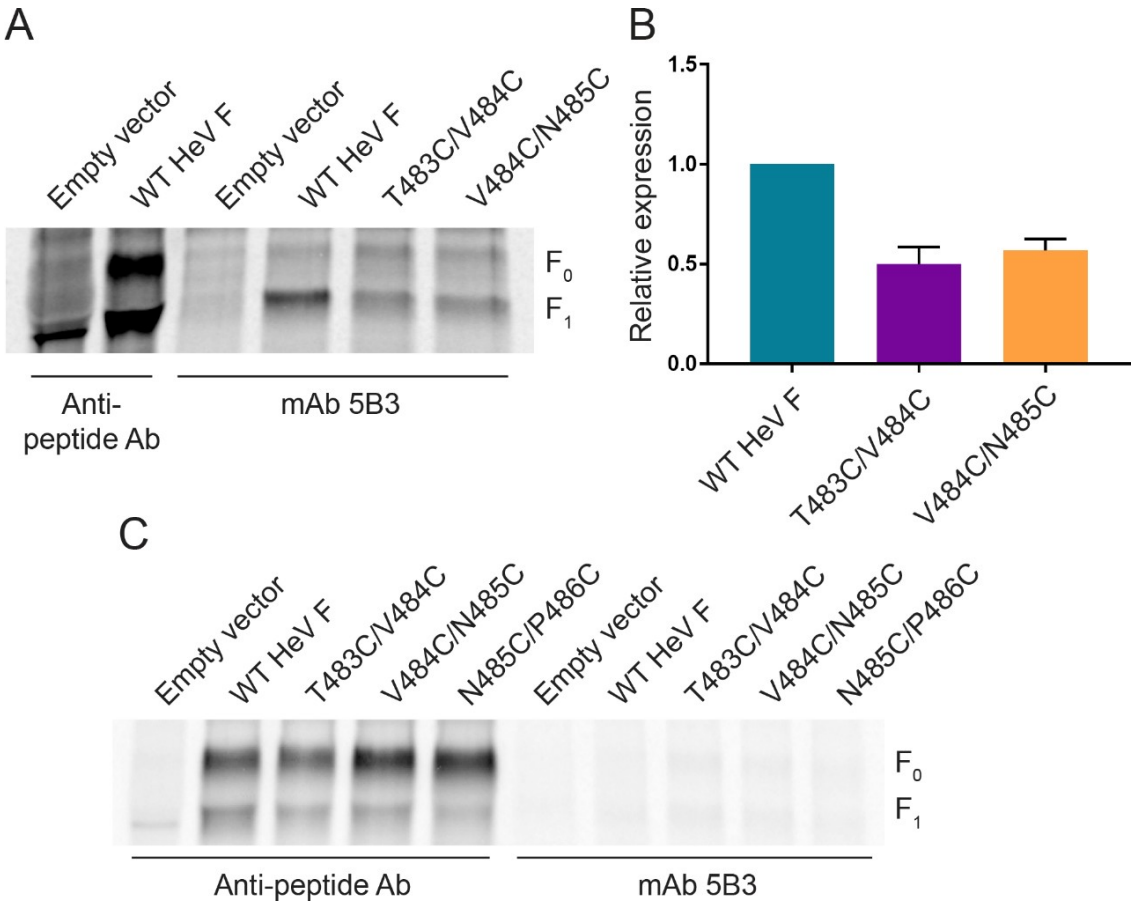

Figure 3.7. T483C/V484C and V484C/N485C bind a prefusion conformation-specific antibody prior to cell disruption. (A) Vero cells were transfected with WT HeV F or one of the TMD mutants. At 24 h posttransfection, the cells were metabolically labeled for 24 h. Then, the cells were treated with HeV F MAb 5B3 antibody for 1 h, followed by lysis and pulldown. Control samples were lysed after the overnight label and treated with HeV F anti-peptide Ab for immunoprecipitation. The samples were analyzed by 10% SDS-PAGE. (B) 5B3 binding was quantified by densitometry and normalized to the level of WT HeV F. All data are represented as the means ± standard deviations for three independent experiments. (C) Vero cells were transfected with WT HeV F or one of the TMD mutants. At 24 h posttransfection, the cells were metabolically labeled for 3 h. Then, the samples were immunoprecipitated with anti-peptide Ab or MAb 5B3 and analyzed by 10% SDS-PAGE.

Chapter 4: Human Metapneumovirus Replication Proteins Phase Separate to Form Liquid-like Inclusion Bodies

Introduction

Human metapneumovirus (HMPV), which was discovered in 2001, is a leading cause of severe respiratory tract infections in infants, the elderly, and immunocompromised individuals (140). Five to twenty percent of hospitalizations from respiratory infections in young children are due to HMPV (141, 142). Symptoms of HMPV infection are similar to respiratory syncytial virus (RSV) and include fever, cough, rhinorrhea, croup, bronchiolitis, pneumonia, and asthma exacerbation (143). HMPV and RSV are members of the *Pneumoviridae* family which was created in 2016 and classified within the *Mononegavirales* order (42). Currently, no vaccines or antiviral treatments are approved to treat HMPV infections, so most patients are managed with supportive care (143). The recent discovery of HMPV highlights the need to understand the basic mechanisms of its infectious life cycle. Specifically, analyzing the process of HMPV replication may be crucial for identifying new targets for antiviral development.

Along with the pneumoviruses HMPV and RSV, other disease-causing pathogens within the *Mononegavirales* order include Ebola virus, measles virus (MeV), and rabies virus (RABV), which have negative-sense, single-stranded RNA genomes. Though these viruses are classified within different families, they have all been reported to form membrane-less cytoplasmic structures within infected cells known as inclusion bodies (IBs) (58, 59, 61, 64). For some negative-sense, single-stranded viruses, including HMPV, IBs have been shown to house active viral replication and transcription (56, 57, 66-73). These processes involve several viral proteins, such as the large polymerase (L), phosphoprotein (P), and nucleoprotein (N). Further analysis of these structures has shown that RSV, MeV, RABV, and vesicular stomatitis virus (VSV) IBs possess the properties of liquid organelles formed via liquid-liquid phase separation (LLPS) (66, 85-88). LLPS is a biophysical process by which a homogenous fluid separates into two distinct liquid

phases (81). Phase separation plays a role in the formation of a variety of membrane-less cellular compartments, such as processing bodies (P-bodies), stress granules, and nucleoli, to concentrate specific proteins and nucleic acids, particularly RNA (83). Properties that define these structures as liquid organelles include the ability to undergo fusion and fission, rapid diffusion of internal contents, and a spherical shape due to surface tension (144). Though LLPS has been shown to play a role in the formation of IBs for some viruses, the physical mechanisms and materials that mediate this process in the viral life cycle are still poorly understood.

For RSV, HMPV, MeV, and RABV, the minimum viral components required to reconstitute IB-like structures in cells are the N protein, which encapsidates the RNA genome, and the P protein, which acts as a cofactor to mediate interactions between the nucleoprotein and polymerase (65, 66, 75, 86). VSV also requires the presence of the L protein with the N and P proteins to form IBs (85).These findings suggest that interactions between the N and P proteins regulate phase separation to form IBs as a structural platform for viral replication and transcription. Most studies thus far have focused on cellular experiments to investigate viral IB liquid dynamics, but recent publications on MeV and RSV have shown the importance of utilizing purified protein systems to analyze interactions between the N and P proteins *in vitro* (87, 88) . For MeV, the purified P protein and monomeric N protein failed to phase separate independently but formed liquid droplets when mixed, similar to the requirements for IB formation observed in cells. Interestingly, when RNA was added to MeV N/P liquid droplets, it incorporated into the droplets and led to the formation of nucleocapsid-like particles that were detected by electron microscopy (87). *In vitro* experiments with RSV proteins showed that RNA-bound N protein rings and P protein form phase separated liquid droplets when combined in solution (88). These findings support the model that viral IBs form via LLPS, and this mechanism is highly dependent upon interactions between the N and P proteins. This process may enhance viral replication transcription for RSV.

This is the first report to analyze phase separation for HMPV IBs. The HMPV life cycle begins with the virus attaching and fusing to a target cell to release its nucleocapsid into the cytoplasm with the associated replication proteins. The nucleocapsid structure protects the genome from host nucleases and acts as a template for the L protein. The genome is used to generate viral mRNA transcripts that are translated by the host cell ribosomal machinery. The genome is also replicated to make antigenome copies that can then be used to generate more negative-sense genome to package into new virions. The P protein acts as an adaptor to regulate interactions between the polymerase and RNA template during transcription and replication. It functions as a tetrameric protein, in which the monomers interact through a central oligomerization domain (84, 145). The oligomerization domain is flanked by large intrinsically disordered regions (IDRs) that give HMPV P the ability to interact with a variety of binding partners (84). For instance, the C-terminus of the P protein interacts with RNA-bound N protein to chaperone attachment to the polymerase. Additionally, HMPV P maintains a monomeric pool of unbound N protein (N^0) through an interaction involving the HMPV P N-terminus with the C-terminal domain of the N protein (47). The monomeric N^0 protein can then be used for nucleocapsid assembly at sites of replication where the polymerase synthesizes nascent RNA (47). HMPV P also recruits the antitermination factor M2-1 to the polymerase during transcription to bind nascent viral mRNA (99). Beyond transcription and replication, HMPV P has been shown to play a role in direct cell-to-cell spread of infection by interacting with actin, or an actin-binding protein, to reorganize the host cell cytoskeleton (76).

During HMPV infection, incoming and newly synthesized nucleocapsids concentrate together in the cytoplasm in an actin-dependent manner (56, 74). Eventually, the coalescence of these structures induces the formation of IBs where viral RNA, viral mRNA, P protein, and N protein are detected (56). Inhibition of actin polymerization was shown to significantly reduce HMPV viral transcription and replication, suggesting that IB coalescence enhances the efficiency of these processes (56). Recent work from our lab has shown that HMPV IBs are dynamic structures that undergo fusion and fission in cells (Cifuentes-Muñoz, unpublished

data). In addition, fluorescence recovery after photobleaching (FRAP) analysis has shown that the internal contents of HMPV IBs have diffusion rates consistent with other membrane-less compartments (El Najjar, unpublished data). Together, these results support the characterization of HMPV IBs as liquid organelles formed by LLPS.

Here we utilize a purified protein system to analyze LLPS of HMPV proteins *in vitro* to support the characterization of HMPV IBs as liquid organelles and to determine the interactions required for phase separation. We report that HMPV N and P undergo phase separation and colocalize within liquid droplets when they are mixed in solution. In contrast to MeV and RSV, the HMPV P protein undergoes phase separation in the absence of other protein binding partners *in vitro*. RNA localizes to HMPV P liquid droplets, providing the first evidence that HMPV P interacts directly with RNA. A heparin purified N^0-P construct, consisting of full-length N protein linked to the first 40 amino acids of P, also phase separated independently. However, combining N^0-P with RNA led to the formation of solid aggregates, suggesting that the addition of RNA promotes a liquid-to-solid transition. WT RNA-bound N protein rings formed aggregates in solution but incorporated into liquid droplets in the presence of P protein. These findings suggest that HMPV P acts as a scaffold protein to support multivalent interactions with HMPV N to promote phase separation of IBs.

Results

HMPV P phase separates independently *in vitro*

Since the HMPV N and P proteins are the minimum requirements needed to form IB-like structures in eukaryotic cells, recombinant versions of the proteins were expressed in *E. coli* and purified for *in vitro* analysis. Full-length, His_6-tagged HMPV P was purified by immobilized metal affinity chromatography (IMAC) followed by anion exchange chromatography. Purified HMPV P was then tested in the presence of the crowding agent dextran to assess its ability to undergo LLPS.

LLPS is typically driven by scaffold proteins with specific features that promote multivalent interactions with other proteins or RNA (80, 146, 147). HMPV P, which includes long IDRs and alternating charged regions, fits the criteria of an LLPS scaffold protein (84). Unlike the reports for MeV and RSV, purified HMPV P formed liquid droplets independently that were visualized using differential interference contrast (DIC) microscopy (FIG 4.1A). Time lapse imaging of the HMPV P droplets showed that they underwent fusion, consistent with the idea that they possess a liquid nature (FIG 4.1B). A turbidity assay was also used to analyze purified HMPV P phase separation. The absorbance of the purified HMPV P protein solution was measured at 395 nm at different time points to detect LLPS. The measurements showed a peak for the absorbance above 0.12 between two and four hours, supporting the microscopy imaging results that HMPV P phase separates in the absence of other protein binding partners (FIG 4.1C).

Interactions with nucleic acid modulate HMPV P phase separation dynamics

Using the protein purification protocol described above, we noticed that the A260/280 ratio was around 1.08, suggesting that the HMPV P protein sample was interacting with nucleic acid. Since nucleic acids are known to play a role in LLPS, we utilized an alternative purification protocol to determine if removing the nucleic acid would influence HMPV P liquid droplet formation. The alternative protocol included treatment with Benzonase nuclease and a IMAC purification step followed by a heparin affinity column purification. This method was successful in removing some of the nucleic acid as indicated by the decreased A260/280 ratio of 0.85. Interestingly, DIC microscopy analysis showed that the recombinant HMPV P protein purified by our alternative protocol formed liquid droplets more robustly than the original protein sample (FIG 4.2A). In addition, time lapse imaging analysis showed that the liquid droplets were capable of fusing (FIG 4.2B). Turbidity assay results for the heparin purified HMPV P protein were similar to previous samples, with a peak above 0.12 between two and four hours (FIG 4.2C). These results suggest that the presence of increased levels of nucleic acid modulate HMPV P phase separation dynamics.

Charge interactions are known to influence phase separation and nucleic acid binding, so both versions of purified HMPV P (anion exchange purified and heparin purified) were analyzed for liquid droplet formation using buffers with different concentrations of potassium chloride (KCl) ranging from 0 to 500 mM. For the anion exchange purified HMPV P, liquid droplets were easily detected between 150 and 250 mM KCl. However, droplet formation was inhibited at concentrations below or above that range (FIG 4.3A). For the heparin purified HMPV P, the largest droplets formed at 150 mM KCl (maximum droplet size >50 μm). However, unlike the anion exchange purified sample, liquid droplets formed for all the KCl buffers tested (FIG 4.3A). This result suggests that HMPV P protein samples containing higher levels of nucleic acid are more sensitive to changes in charge, thus leading to the disruption of liquid droplet formation *in vitro*.

The differences we observed for anion exchanged purified and heparin purified HMPV P led us to hypothesize that the multifunctional HMPV P protein also possesses the ability to bind RNA. Given that 35 percent of the HMPV P sequence consists of charged amino acids, it is not surprising that contaminating RNA from *E. coli* may bind to HMPV P during the expression and purification process (84). Based on our idea that HMPV P serves as a scaffold protein to drive phase separation and recruit other viral components to IBs, we tested purified HMPV P with a fluorescently tagged RNA oligomer to determine if RNA would localize to the liquid droplets. Fluorescence imaging showed that the RNA oligomer was incorporated into HMPV P liquid droplets, suggesting that the P protein may play a role in binding to viral RNA within IBs to facilitate replication and transcription (FIG 4.3B).

HMPV P recruits N^0-P to liquid droplets

WT HMPV N spontaneously oligomerizes and binds to nonspecific RNAs during standard purification procedures. Thus, we generated a recombinant N^0-P construct that includes full-length N (1-394) fused to a P peptide (1-40) to maintain N in a monomeric, RNA-free form for purified protein analysis (FIG 4.4A) (47). Like our approach with HMPV P, the N^0-P construct was purified by two different

methods to assess the effects of nucleic acid contaminants on our *in vitro* LLPS system. The first procedure included an IMAC purification, and the alternative procedure included both IMAC and heparin purification steps. Though the N^0-P protein purified by IMAC alone contained few protein contaminants, we were able to successfully reduce the nucleic acid level with the addition of a heparin purification step, as indicated by the A260/280 ratio of 0.6.

The N^0-P construct purified by IMAC alone formed gel-like droplets that were visualized by DIC microscopy (FIG 4.4B). Unlike the HMPV P liquid droplets, the gel-like HMPV N^0-P droplets remained partially undissolved in high salt concentrations (data not shown). Over time, these gel-like droplets aggregated together but did not undergo fusion (FIG 4.4B). In agreement with our microscopy results, turbidity assays performed with the IMAC purified N^0-P protein gave high absorbance readings that peaked above 0.6, further indicating that the gel-like droplets were aggregating in solution (FIG 4.5C). The subsequent drop in absorbance suggests that the gel-like droplets settled to the bottom of the 96-well plate.

The N^0-P construct was tested with anion exchange purified HMPV P using a droplet assay to determine if the P protein could influence N^0-P dynamics in solution. Our DIC and fluorescence microscopy analyses showed that mixing the two constructs together led to enhanced LLPS as indicated by the presence of larger and more numerous droplets than we previously observed for HMPV P alone. The results showed that N^0-P and P were incorporated into the same liquid droplets, as indicated by the colocalization of the fluorescent signals used to label the proteins (FIG 4.5A). In addition, the phase separated droplets underwent fusion events (FIG 4.5B). A turbidity assay was utilized to determine if combining N^0-P with P affected the absorbance of the solution. The results showed that compared to N^0-P alone, the combination of N^0-P and P led to lower absorbance readings that peaked around 0.3 at two hours (FIG 4.5C). Together, these findings support that HMPV P facilitates interactions with N^0-P to recruit the protein into liquid

droplets, and interactions between the proteins prevent the N^0-P construct from transitioning to a gel-like state.

The N^0-P construct that was alternatively purified by IMAC and heparin was also analyzed using our *in vitro* system. Unlike the N^0-P protein purified by IMAC alone, the heparin purified N^0-P formed liquid droplets in the absence of other protein binding partners (FIG 4.6A). Time lapse imaging of the heparin purified N^0-P droplets showed that they could fuse to form larger droplets (FIG 4.6B). Since the removal of contaminating nucleic acids had a dramatic effect on N^0-P LLPS dynamics, we tested the heparin purified N^0-P with a fluorescent RNA oligomer to determine if the addition of nucleic acid would influence droplet formation. Fluorescence microscopy imaging showed that the RNA oligomer disrupted N^0-P liquid droplet formation, leading to the formation of non-fusing aggregates (FIG 4.6C). These results suggest that RNA interactions inhibit N^0-P LLPS dynamics, causing the liquid droplets to transition to a gel-like or solid-like state.

HMPV P recruits N-RNA rings to liquid droplets

In addition to the monomeric N^0-P construct, WT N-RNA rings were purified for LLPS analysis in the presence or absence of HMPV P. DIC imaging of N-RNA rings in the droplet assay showed the formation of aggregates, suggesting that this protein-RNA complex does not phase separate independently (FIG 4.7A). Combining the purified N-RNA rings with heparin purified HMPV P resulted in the N-RNA complex being incorporated into liquid droplets (FIG 4.7B). The N-RNA/P droplets (maximum droplet size = 6 μm) were generally smaller than the P alone droplets (maximum droplet size = 11 μm), suggesting that this combination influences phase separation dynamics. The influence of HMPV P on N-RNA for liquid droplet formation was reflected in the turbidity assay results which showed a lower peak for absorbance around 0.2 at two hours, compared to the absorbance for N-RNA alone (FIG 4.7D).

HMPV P and N-RNA were tested in our *in vitro* system at different ratios to determine the conditions that were required for N-RNA to be recruited to liquid droplets. Though N-RNA aggregates were still present at 4:1 and 2:1 ratios of N-

RNA/P, liquid droplets were easily detected at a 1:1 ratio. The number and size of the liquid droplets increased in samples with a higher proportion of HMPV P (1:2 and 1:4) (FIG 4.7C). These results suggest that a minimum threshold for the P protein concentration must be met before N-RNA is induced to phase separate into droplets. Liquid droplets containing HMPV P and N-RNA were also shown to incorporate a fluorescent RNA oligomer (FIG 4.7E). These findings highlight that HMPV P, N, and RNA form complex multivalent interactions to promote phase separation and to support the structure of IBs required to enhance replication and transcription.

Discussion

IB formation has been reported for many negative-strand viruses across different families in the *Mononegavirales* order (148). An increasing wealth of evidence supports that these structures function as viral factories by concentrating the machinery and materials required for replication and transcription. Cellular studies of IBs have shown that these structures are membrane-less and dynamic, which led to the characterization of IBs as liquid organelles. Though liquid organelles have been recognized in the cell for many decades, scientists have only recently linked the formation of these structures to the biophysical process of LLPS. Understanding the role of LLPS in IB formation may be critical for discovering new targets for antiviral development. Until now, no reports have been published to identify HMPV IBs as phase separated liquid organelles. To analyze the viral protein interactions driving this process, an *in vitro* system was utilized to test recombinant versions of HMPV purified proteins.

We focused on purifying full-length P, N-RNA rings, and the monomeric N^0-P construct for *in vitro* analysis. Though the process of IB formation likely involves many similarities for different negative-strand viruses, our analysis of HMPV proteins led to the discovery of unique features that highlight differences among these viral systems. We found that HMPV P phase separates independently *in vitro*, supporting our hypothesis that the P protein is a scaffold which recruits other

client proteins to liquid droplets to drive LLPS. Interestingly, our data also showed that HMPV P incorporates RNA into liquid droplets. This suggests that the P protein, which is known to bind several proteins involved in the replication process, may also directly interact with RNA to facilitate phase separation and to enhance viral replication. In addition to incorporating RNA, purified HMPV P also recruited monomeric N^0-P and oligomeric N-RNA rings to liquid droplets, further supporting our model in which P serves as a scaffold for LLPS. This is the first report to highlight a negative-strand virus P protein as the independent driver of phase separation. Additionally, this work provides the first evidence for a previously undescribed role of HMPV P for interacting directly with RNA. Together, these findings provide important information for understanding the formation of HMPV IBs that may be applicable to other negative-strand viruses.

Our previous studies of HMPV IBs showed that these structures contain viral positive-sense RNA and genomic RNA along with the N and P proteins. However, other viral proteins, such as the fusion protein and matrix protein, are generally excluded from IBs (56). The contents of HMPV IBs suggested that these structures were likely involved in housing viral replication and transcription, whereas assembly steps appeared to occur outside of IBs. We highlighted that the cellular actin network plays a role in bringing small IBs together to form larger membrane-less structures. In addition, we confirmed that IB formation and coalescence is critical for promoting efficient replication and transcription (56). Other work from our lab has focused on late events in the HMPV life cycle to understand assembly and spread. Interestingly, the HMPV P protein was shown to extensively colocalize with actin and promote the formation of cellular extensions for direct cell-to-cell spread of infection (76). A recent report from our group utilizing three-dimensional human airway tissues to study HMPV infection supported these findings related to viral replication and spread. HMPV-infected human airway epithelial (HAE) cells showed the presence of IBs containing N protein, P protein, and viral genomic RNA (149). Additionally, the HMPV-infected HAE cells were shown to form actin-based filamentous extensions (149). These results suggested that IB and extension formation are physiologically relevant

processes used by HMPV to promote infection. HMPV extensions may provide a route for transporting IB components to new cells to expedite the infection process. The liquid-like nature of IBs may be critical for moving infectious materials through narrow cell-to-cell extensions.

We hypothesized that the intrinsically disordered regions of HMPV P allow it to interact with a variety of proteins to promote IB formation. Recently, a structure was published for the HMPV polymerase/P protein complex (92). The cryo-electron microscopy structure showed that the P protein tetramer interacts extensively with the N-terminal region of the polymerase. The central oligomerization domain of HMPV P is anchored to the polymerase, and the N-terminal regions of P undergo a disorder-to-order transition upon binding to N^0 (47). HMPV P may facilitate delivery of N^0 to the RNA exit tunnel to encapsidate nascent RNA. The C-terminal regions of P are asymmetrically oriented on the polymerase to promote interactions with N-RNA, likely to dislodge the RNA and deliver it to the entrance of the polymerase RNA tunnel (47, 92). The non-equivalent positions of the HMPV P C-terminal regions within the tetramer highlight the importance of IDRs, which allow a protein to adopt a variety of conformations (150). Like HMPV P, RSV P is also a tetrameric protein with a central oligomerization domain flanked by long IDRs (151-154). A structure of the RSV polymerase/P protein complex was published around the same time as the HMPV structure. The RSV structure showed that each protomer of the P protein tetramer adopts a different conformation in association with the polymerase (155). Similar to HMPV, these results highlight the dynamic nature of the P protein which is heavily influenced by the presence of large IDRs. Though some structural aspects of P proteins differ among negative-strand RNA viruses, IDRs are a common P protein feature across families (84, 90, 95, 145, 153, 154, 156, 157).

Features of HMPV P and other negative-strand virus P proteins, including long IDRs, repetitive blocks of alternating charge, and phosphorylation sites, fit the molecular signature of proteins that phase separate under physiological conditions (83, 84). The propensity for HMPV P to mediate multivalent interactions and phase

separate independently *in vitro* suggests that it functions as a scaffold to regulate LLPS for IB formation during infection (80). In contrast to our *in vitro* results, the HMPV N and P proteins must be coexpressed in cells to generate IB-like structures (65). Without HMPV N, the P protein shows diffuse cytoplasmic localization. This difference between the cellular and *in vitro* systems suggests that host factors present in the cytoplasm may block HMPV P interactions required to induce LLPS. However, coexpression of HMPV P and N likely creates more opportunities for multivalent protein-protein and protein-RNA interactions to concentrate enough IB components to drive phase separation. LLPS is a highly sensitive process that depends on a number of factors such as protein/RNA concentration, salt content, pH, and temperature (83). Thus, one or more of these factors in cells may prevent HMPV P from phase separating when expressed on its own. Our findings highlight notable contrasts between cellular and *in vitro* studies of HMPV IBs, suggesting that *in vitro* work must be carefully analyzed before applying conclusions to live virus systems. Though cellular and *in vitro* IB studies are both crucial for understanding HMPV replication, further analysis is needed to bridge the gap between these bodies of work.

Reports on MeV and RSV IBs have utilized a similar *in vitro* system to analyze phase separation dynamics of purified proteins (87, 88). MeV IBs were first characterized as liquid organelles by analyzing the structures in infected or transfected cells (86). Analysis of MeV IBs during infection showed that the structures are initially spherical, but they become large and irregularly shaped at later time points of infection. In transfected cells, MeV N and P are sufficient to mediate IB-like structure formation, with the C-terminal domains of both proteins being critical for phase separation. However, MeV P expression alone induced the formation of perinuclear puncta, which were rarely spherical and very large, in 35 percent of transfected cells. This suggests that MeV P may promote multivalent interactions under specific cellular conditions to form these structures (86). MeV *in vitro* studies showed that a combination of the N and P proteins was required to induce droplet formation. The minimum N and P domains needed for droplets to form were also reported: full-length N protein bound to a 50 amino acid N-terminal

P peptide (P_{50}) and $P_{304-507}$, which includes the tetramerization domain, intrinsically disordered P_{loop}, and C-terminal three-helix bundle (XD) (87). Contrasting LLPS results observed for MeV and our HMPV system may be due to differences in the P protein structures. For instance, MeV P is 213 amino acids longer than HMPV P and includes the folded XD domain after the unfolded P_{loop}.

A recent report on RSV used both cellular and *in vitro* analysis to characterize RSV IBs as liquid organelles formed via LLPS. Deletion of the N-terminal IDR of RSV P did not impact IB-like structure formation in cells, but the oligomerization domain and C-terminal IDR were required (88). This was supported by *in vitro* results which showed that the N-terminal domain was dispensable, but the C-terminal domain and oligomerization domain were required for liquid droplet formation with N-RNA. They also showed that a higher ratio of RSV P to N-RNA was needed to detect liquid droplet formation, whereas we observed that HMVP N-RNA/P droplets were easily detected at a 1:1 ratio (88). Compared to HMPV P, RSV P is 53 amino acids shorter, though the domain organization is similar for both. The differences observed for these viral systems highlight that LLPS is highly dependent on multivalent interactions mediated by the P protein, and these interactions are influenced by the unique composition of the P protein. Additional analysis of specific HMPV N and P protein domains will be beneficial for determining which domains are critical for phase separation and IB formation.

The RSV and MeV reports also analyzed the importance of interactions between the N protein and RNA for LLPS. An RNA-binding mutant of MeV N still formed IB-like structures with P protein in cells, suggesting that N/RNA interactions are not required for IB formation (86). The minimal MeV LLPS *in vitro* system was also used to show that RNA diffuses into MeV N/P liquid droplets, triggering the formation of nucleocapsid-like particles (87). The rate of particle assembly was significantly increased compared to non-phase separating conditions. These findings suggest that RNA is not required for N/P droplet formation, but IBs serve to enhance the efficiency of nucleocapsid assembly during infection. Incorporation

of RNA into HMPV P droplets in our system highlights that HMPV may utilize IB formation in a similar manner to facilitate nucleocapsid assembly. A monomeric, RNA-free RSV N protein mutant was unable to form IB-like structures with WT P protein in cells, suggesting that RSV N must oligomerize and bind RNA to mediate IB formation (88). However, our *in vitro* results with HMPV N^0-P suggested that oligomerization and RNA interactions are not required for phase separation. An *in vitro* analysis of HMPV and RSV N RNA-binding mutants would be useful for further analyzing the role of RNA interactions and oligomerization in LLPS. Though the structures of RSV N and HMPV N are quite similar, small differences may have a dramatic impact on the weak multivalent interactions with HMPV P that drive LLPS.

In conclusion, we showed that HMPV P acts as a scaffold for *in vitro* phase separation to recruit monomeric N protein, oligomerized N protein, and RNA to liquid droplets. These results support our cellular analysis of HMPV IBs, in which we have described IBs as dynamic, membrane-less structures that coalesce throughout infection. These findings support the hypothesis that many negative-strand viruses of the *Mononegavirales* order have evolved mechanisms to utilize LLPS for IB formation to promote efficient replication and transcription. Our results support that the large IDRs of HMPV P allow for the protein to phase separate independently and recruit other proteins to liquid droplets. Research from our lab has shown that HMPV P is phosphorylated in cells (Thompson, unpublished data). Phosphorylation and other post-translational modifications have been shown to play a role in phase separation. Thus, additional *in vitro* and cellular studies of HMPV P will be important for elucidating the effects of phosphorylation and dephosphorylation events. Work on HMPV should also continue to define the domains of the N and P proteins required for phase separation. Finally, further work on HMPV P to understand how it recruits RNA to liquid droplets will be critical for characterizing its role in LLPS. Overall, the findings presented here build on the foundation for understanding the formation of IBs and the mechanisms that regulate LLPS for negative-strand virus proteins.

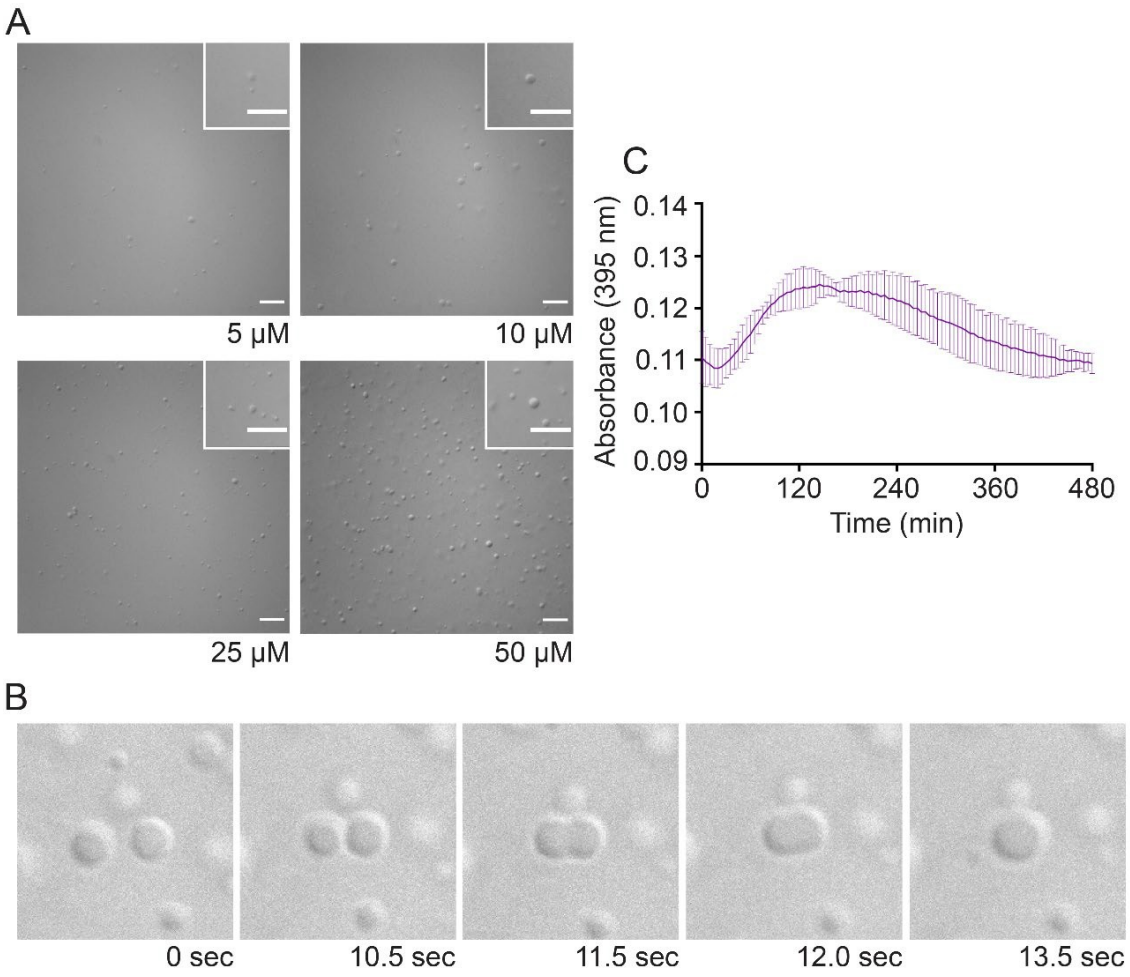

Figure 4.1 Anion exchange purified HMPV P phase separates independently *in vitro*. (A) Anion exchanged purified HMPV P was tested at concentrations ranging from 5 μM to 50 μM in a droplet assay (maximum droplet size = 3.4 μm). DIC microscopy imaging of droplets was performed with a 60X objective on a Nikon Eclipse E600. The scale bar is 10 μm. (D) Time lapse imaging of anion exchange purified HMPV P (80 μM) droplet fusion was acquired using a 100X oil objective on a Zeiss Axiovert 200M microscope. (C) Anion exchange purified HMPV P (40 μM) was mixed with turbidity assay buffer in a clear 96-well plate. The solution was analyzed using a SpectraMax iD3 to measure the absorbance at 395 nm at 5 min intervals with mixing.

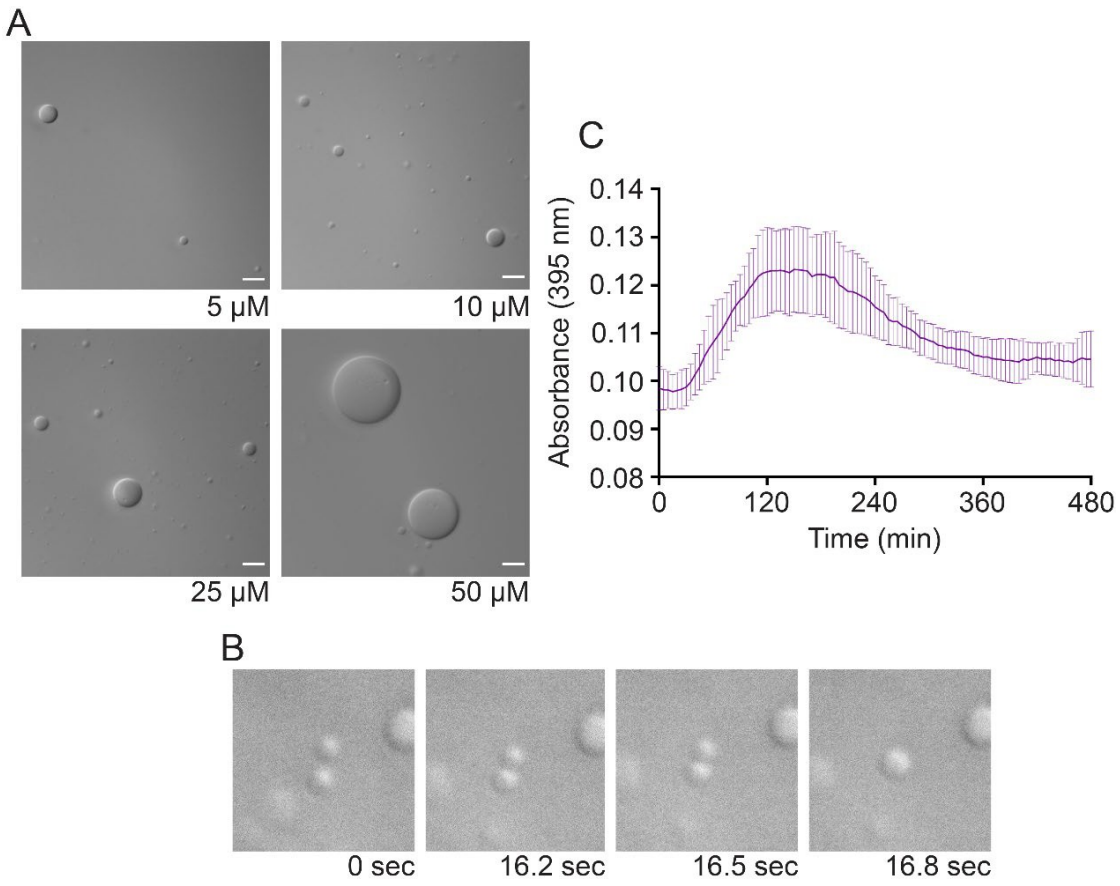

Figure 4.2. Heparin purified HMPV P phase separates independently *in vitro*. (A) Heparin purified HMPV P was tested at concentrations ranging from 5 μM to 50 μM in a droplet assay (maximum droplet size >50 μm). DIC microscopy imaging of droplets was performed with a 60X objective on a Nikon Eclipse E600. The scale bar is 10 μm. (B) Time lapse imaging of heparin purified HMPV P (150 uM) droplet fusion was acquired using a 100X oil objective on a Zeiss Axiovert 200M microscope. (C) Heparin purified HMPV P (40 μM) was mixed with turbidity assay buffer in a clear 96-well plate. The solution was analyzed using a SpectraMax iD3 to measure the absorbance at 395 nm at 5 min intervals with mixing.

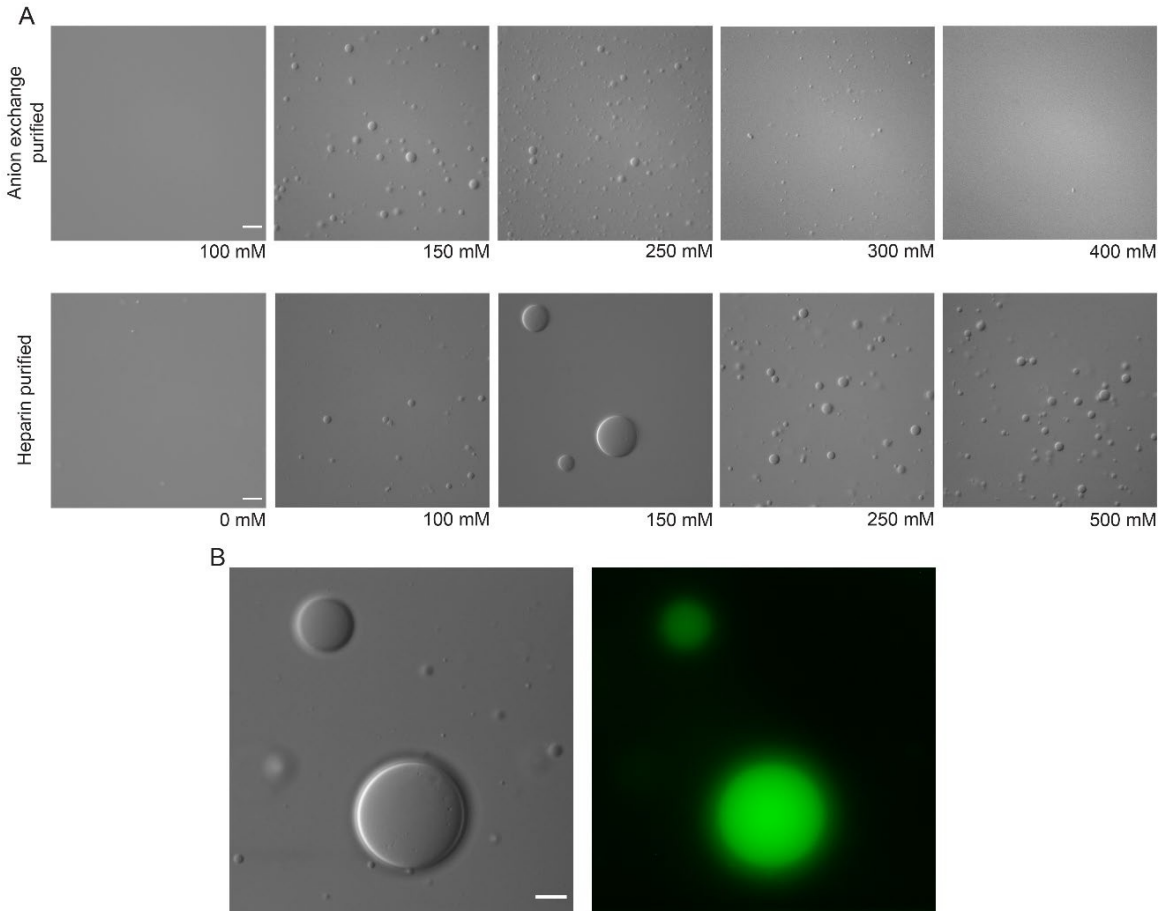

Figure 4.3. Interactions with nucleic acid modulate HMPV P phase separation dynamics. (A) Anion exchange purified HMPV P (15 μM) and heparin purified HMPV P (15 μM) were tested in a droplet assay using buffers with different concentrations of KCl ranging from 0 mM to 500 mM. DIC microscopy imaging of droplets was performed with a 60X objective on a Nikon Eclipse E600. The scale bar is 10 μm. (B) Heparin purified HMPV P (15 μM) was tested in a droplet assay with an RNA decamer tagged with 6-carboxyfluorescein on the 3' end (5 μM). The DIC and fluorescence images were acquired with a 60X objective on a Nikon Eclipse E600. The scale bar is 10 μm.

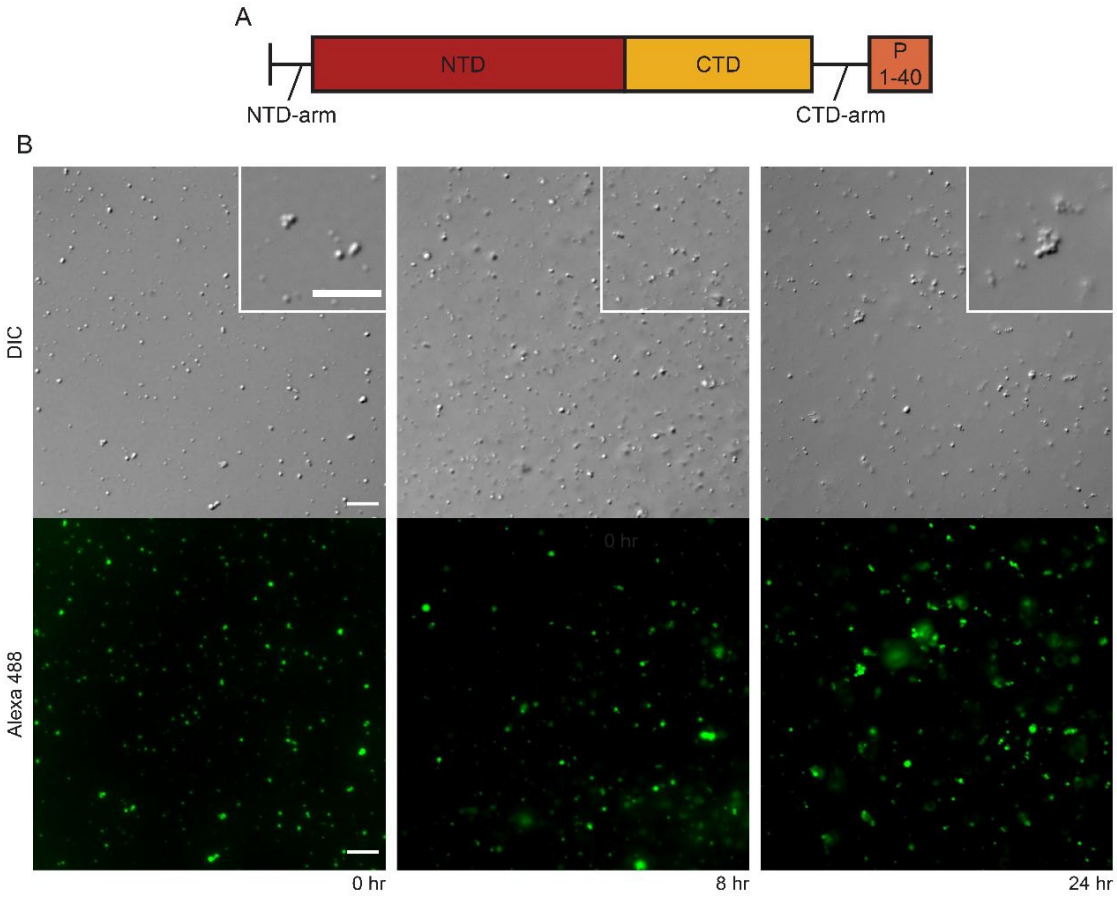

Figure 4.4 IMAC purified N^0-P forms gel-like droplets that aggregate over time. (A) Schematic of the N^0-P construct which includes full-length HMPV N fused to the first 40 amino acids of HMPV P. (B). IMAC purified HMPV N^0-P (15 μM) labeled with Alexa 488 TFP ester was tested in a droplet assay. DIC and fluorescence images were acquired at different time points using a 60X objective on a Nikon Eclipse E600. The scale bars are 10 μm.

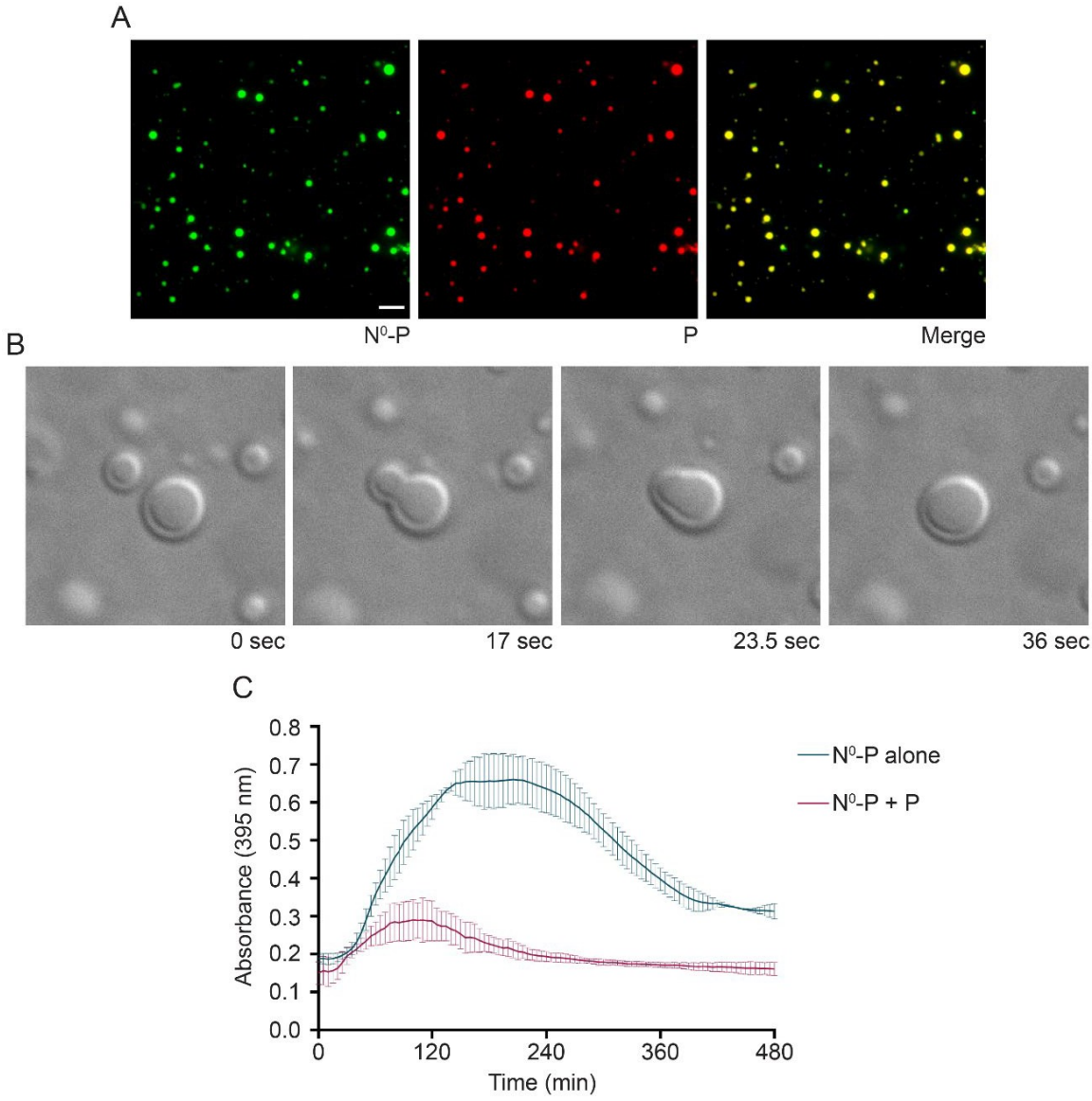

Figure 4.5. HMPV P recruits N^0-P to liquid droplets. (A) IMAC purified HMPV N^0-P (15 μM) labeled with Alexa 488 TFP ester was mixed with anion exchange purified HMPV P (15 μM) labeled with Alexa 594 NHS ester in a droplet assay. Fluorescence images were acquired using a 60X objective on a Nikon Eclipse E600. The scale bar is 10 μm. (B) IMAC purified HMPV N^0-P (50 μM) was mixed with anion exchange purified HMPV P (50 μM). Time lapse imaging of N^0-P/P droplet fusion was acquired using a 100X oil objective on a Zeiss Axiovert 200M microscope. (C) IMAC purified HMPV N^0-P (40 μM) was tested alone or with anion exchange purified HMPV P (40 μM) in a turbidity assay. The protein solutions were

plated in a clear 96-well plate with turbidity assay buffer, and the absorbance was measured at 395 nm by a SpectraMax iD3 at 5 min intervals with mixing.

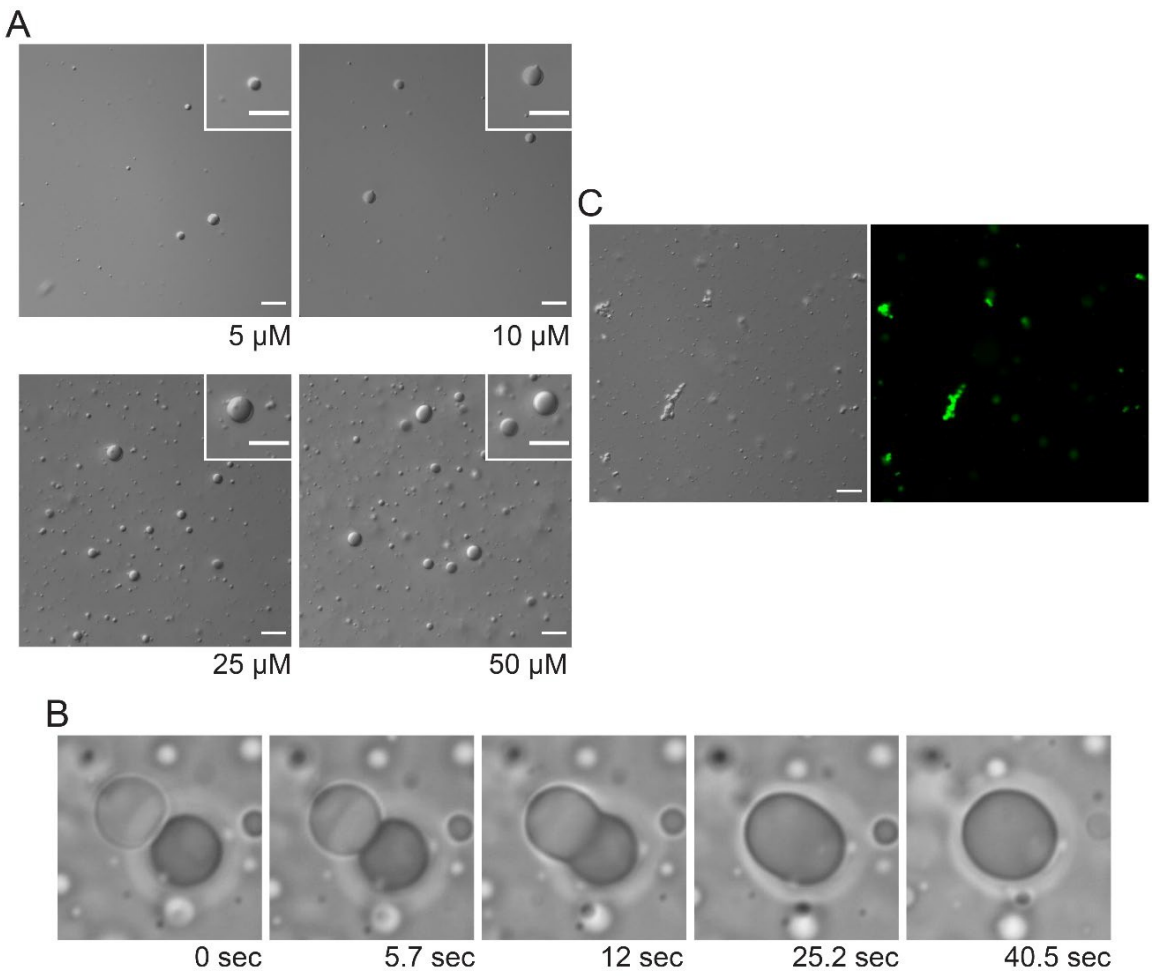

Figure 4.6. Heparin purified HMPV N^0-P phase separates independently *in vitro.* (A) Heparin purified HMPV N^0-P was tested at concentrations ranging from 5 μM to 50 μM in a droplet assay. DIC microscopy imaging of droplets was performed with a 60X objective on a Nikon Eclipse E600. The scale bar is 10 μm. (B) Time lapse imaging of heparin purified HMPV N^0-P (80 μM) droplet fusion was acquired using a 100X oil objective on a Zeiss Axiovert 200M microscope. (C) Heparin purified HMPV N^0-P (15 μM) was tested in a droplet assay with an RNA decamer tagged with 6-carboxyfluorescein on the 3' end (5 μM). The DIC and fluorescence images were acquired with a 60X objective on a Nikon Eclipse E600. The scale bar is 10 μm.

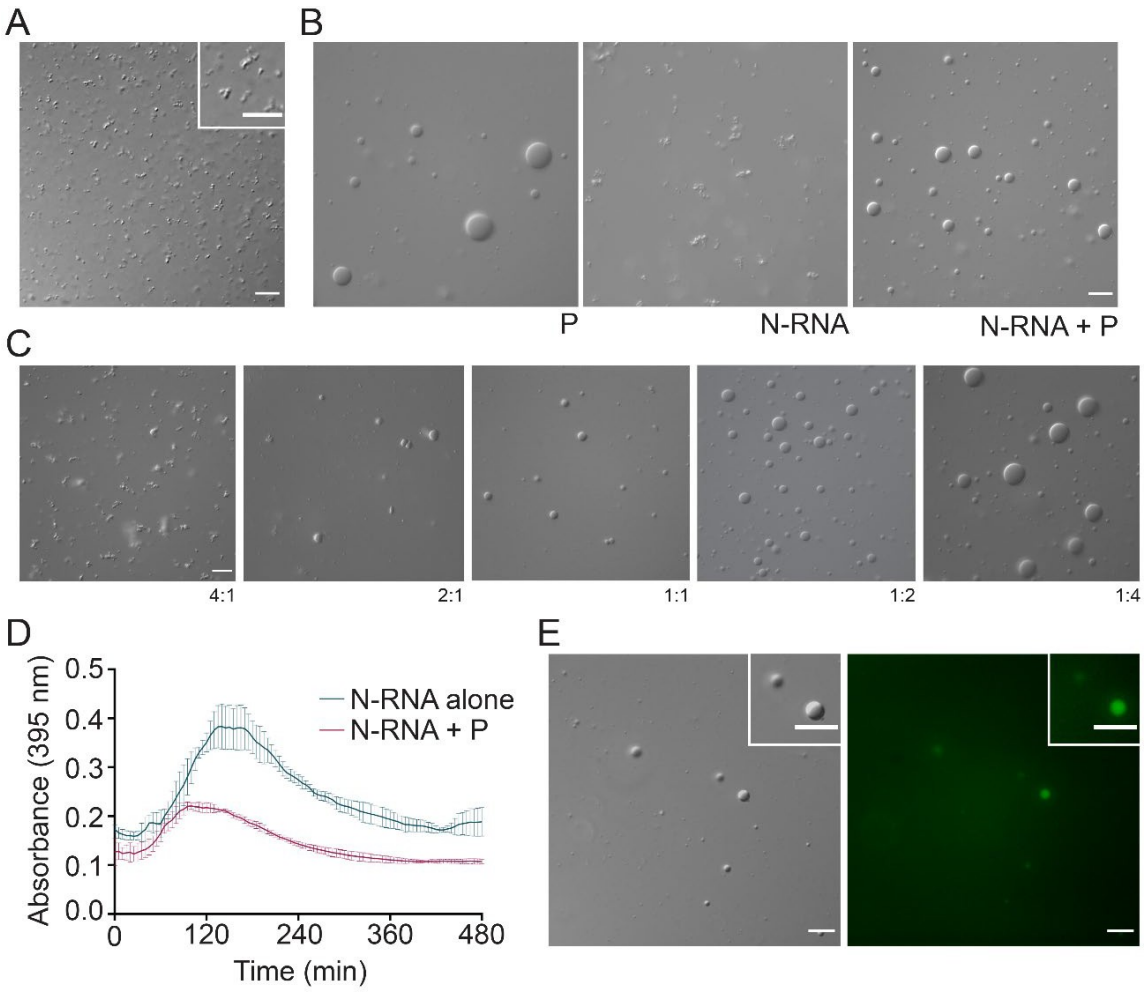

Figure 4.7. HMPV P recruits N-RNA rings to liquid droplets. (A) HMPV N-RNA (25 μM) was tested in a droplet assay. DIC microscopy imaging of droplets was performed with a 60X objective on a Nikon Eclipse E600. The scale bar is 10 μm. (B) HMPV N-RNA (15 μM) was mixed with heparin purified HMPV P (15 μM) in a droplet assay. DIC images were acquired using a 60X objective on a Nikon Eclipse E600. The scale bar is 10 μm. (C) HMPV N-RNA and heparin purified HMPV P were tested in a droplet assay at different ratios (4:1 = 20 μM N-RNA: 5 μM P; 2:1 = 10 μM N-RNA: 5 μM P; 1:1 = 5 μM N-RNA: 5 μM P; 1:2 = 5 μM N-RNA: 10 μM P; 1:4 = 5 μM N-RNA: 20 μM P). DIC microscopy imaging of droplets was performed as described above. (D) HMPV N-RNA (40 μM) was tested alone or with heparin purified HMPV P (40 μM) in a turbidity assay. The protein solutions were plated in a clear 96-well plate with turbidity assay buffer, and the absorbance was measured at 395 nm by a SpectraMax iD3 at 5 min intervals with mixing. (E)

HMPV N-RNA (15 μM), heparin purified HMPV P (15 μM), and an RNA decamer tagged with 6-carboxyfluorescein on the 3’ end (5 μM) were mixed and tested in a droplet assay. DIC and fluorescence microscopy imaging of droplets was performed as described above. The scale bar is 10 μm.

Chapter 5: Discussion and Future Directions

Overview

The work presented here builds on our current understanding of viral fusion events, replication, and inclusion body (IB) formation for viruses within the *Mononegavirales* order. Specifically, these findings elucidate previously unknown aspects of the viral life cycle for paramyxoviruses and pneumoviruses. Many studies on viral entry have focused on the membrane glycoprotein that promotes fusion with a target cell membrane. Cellular protein experiments and structural analysis of viral particles and proteins have provided a platform for determining the conformational changes in the glycoprotein that regulate the fusion event. Our group has focused its work on the transmembrane domain (TMD) of the Hendra virus (HeV) fusion protein (F) to determine how interactions in this region regulate fusion dynamics. We found that the TMDs of the HeV F trimer must dissociate to allow for conformational changes within the protein that lead to membrane fusion (Chapter 3). After analyzing this early step in the viral life cycle, we addressed questions regarding subsequent steps in the cycle that occur in the host cell cytoplasm. Many negative-strand viruses produce cytoplasmic IBs for replication and transcription, but numerous questions remain unanswered regarding how IBs form and function. We built on our previous work with human metapneumovirus (HMPV) to analyze the mechanisms regulating IB formation to understand how they promote replication and transcription. We discovered that the HMPV phosphoprotein (P) plays a critical role in mediating IB formation via the process of liquid-liquid phase separation (LLPS) (Chapter 4). These studies on HeV and HMPV shed light on the complex protein interactions that govern fusion protein triggering, IB coalescence, and replication/transcription events. In addition, they illuminate new questions that must be answered to identify novel targets for therapeutic development.

HeV entry

Determining HeV F TMD interactions

Analysis of the HeV F TMD sequence is important for understanding the interactions that contribute to trimerization as well as dissociation once the F protein is triggered. One sequence motif that has been shown to enhance TMD interactions in different proteins is GXXXG. The HeV F TMD includes an AXXXG motif, and mutation of the glycine residue decreased cell surface expression, suggesting that prefusion HeV F stability was reduced (40). Sedimentation equilibrium analysis was also used to determine the effects of mutating this TMD glycine residue. The results showed that mutating the glycine to alanine led to a moderate increase in TMD interactions, whereas mutating glycine to leucine or isoleucine led to even stronger TMD association (40). This suggested that the G508 residue was not the only factor driving TMD interactions in HeV F, since other residues must be responsible for maintaining the F protein trimer. Further work addressed the presence of polar residues in the TMD because cooperative interaction of polar residues has been associated with transmembrane helix packing. Mutation of HeV F TMD polar residues to alanine showed that protein folding was impacted and stability was reduced, suggesting that these polar residues are required for proper TMD interactions (40).

In addition to stabilizing the prefusion conformation, some HeV F TMD residues are important for endocytic recycling. This process is crucial so that the precursor F_0 can be cleaved to form the disulfide-linked heterodimer F_1+F_2, which can actively participate in fusion events. Compared to other TMDs, the HeV F TMD contains many noncharged polar residues (158). Two polar amino acids, S490 and Y498, in the HeV F TMD were shown to be important for proper HeV F trafficking. S490, which sits close to the ectodomain of HeV F in the N-terminal region of the TMD, is important for HeV F endocytosis. Specifically, the serine hydroxyl group is required for proper trafficking. Hydrogen bonds between this hydroxyl group and other side chains likely influence this process. Y498 is required for efficiently recycling HeV F to the surface after processing, and the aromatic ring, rather than

the hydroxyl group, promotes the interactions which allow for this event (28). The S490 and Y498 residues are also found in the TMD of the Nipah virus (NiV) F protein, suggesting that they are crucial for NiV F endocytosis and recycling events as well (28). This work further expanded our understanding of the importance of TMD interactions for critical HeV F functions.

The sequence of the HeV F TMD was compared to other paramyxovirus F protein TMD sequences to analyze similarities that could govern TMD interactions. Evaluation of 140 sequences led to the identification of a β-branched heptad repeat. Specifically, the HeV F TMD was shown to possess a heptad repeat leucine-isoleucine zipper, a motif which promotes oligomerization in a hydrophobic environment (114). Mutation of the leucine-isoleucine zipper reduced stability of the HeV F prefusion conformation. This suggests that TMD interactions promoted by the leucine-isoleucine zipper are required to maintain the metastable prefusion structure. In addition, results from this study suggested that TMD interactions play a significant role in the triggering process (114). The leucine-isoleucine zipper identified in the parainfluenza virus 5 (PIV5) F TMD was also mutated to determine the effects on F protein expression, stability, and fusion (159). Unlike HeV F, the mutations in the PIV5 F TMD only had modest effects on protein expression and stability. However, the PIV5 F TMD leucine-isoleucine zipper was critically important for fusogenic activity (159). Together, the work on HeV F and PIV5 F support the findings described in Chapter 3, which emphasize the significance of modulating TMD interactions to drive fusion. Overall, these findings highlight the dynamic TMD interactions which impact the F protein as it folds, traffics, undergoes processing, and triggers.

Targeting the viral F protein TMD

Though structural studies of HeV F and other F proteins have provided crucial conformational data, cellular expression studies are particularly important for further understanding the non-static conformational changes involved in F protein triggering. The work presented in Chapter 3 supports previous studies which showed that the TMD of HeV F has functional importance beyond anchoring

the protein in the viral membrane (41, 114). Specifically, the HeV F TMD interactions are required to stabilize the prefusion form prior to triggering, and changes in TMD interactions helps drive conformational refolding required for fusion. In addition, work on enveloped virus F proteins has shown that substituting the TMD region of one F protein into another can be detrimental for fusion activity, further suggesting that TMD interactions play a specific role in promoting fusion (160). Disrupting or prematurely triggering F proteins presents a potential therapeutic target that could be applicable to numerous enveloped viruses. Additional work was performed by our group to elucidate the role of TMD interactions in HeV F conformational stability. Exogenous transmembrane constructs mimicking the TMD of HeV F were expressed to determine if they could disrupt TMD interactions in wild type (WT) HeV F (161). Results showed that the transmembrane protein constructs reduced HeV F expression and fusion activity. This concept was also applied to the paramyxovirus PIV5 to see if homologous transmembrane constructs could block viral infection. Pretreatment of the virus with the PIV5 TMD construct led to reduced viral infection in cells (161). This suggests that TMD constructs or other peptides may be useful for targeting F proteins to cause them to misfold or prematurely trigger. Further studies on enveloped virus F proteins will be important for developing new therapies like this.

The role of the TMD in HeV F conformational changes

Work focused on TMD interactions and targeting the TMD has suggested that this region of the HeV F protein is critical for numerous functions, including fusogenic activity. To understand the factors that contribute to fusion events, we considered the TMD interactions that might promote conformational changes in the rest of the protein. The HeV F HRB forms a trimeric coiled coil, but isolated HRB peptides do not associate together (162). This suggests that HeV F TMD interactions are required to maintain the conformation of the HRB coiled coil prior to triggering. Interactions in the ectodomain may also help to preserve the spring-like HRB coiled coil. Our model, which is supported by data in Chapter 3, suggests that triggering of HeV F involves dissociation of the TMDs. TMD dissociation likely

modulates interactions within the HRB coiled coil, leading to further refolding of the ectodomain. Dissociation of the TMDs is suggested to begin with the C-terminal region where β-branched residues destabilize the alpha-helix (41). This localized dissociation may then initiate separation of N-terminal TMD regions and subsequently destabilize the HRB coiled coil.

In Chapter 3, we analyzed HeV F TMD mutants which were chemically linked by disulfide bonds to prohibit dissociation of the TMD trimer. The double cysteine substitutions were made at the N-terminal region of the TMD to promote disulfide bond formation within the oxidizing environment of the endoplasmic reticulum. Our results suggest that TMD dissociation was not necessary for proper folding or trafficking of HeV F. However, fusion activity was completely abolished for the mutants, suggesting that TMD dissociation is required for refolding of HeV F. These findings support that TMD dissociation, which likely initiates at the C-terminal residues, must subsequently occur in the N-terminal TMD to allow for fusion. Since the N-terminal TMD region is connected to the HRB domain, dissociation of the N-terminal TMD residues may be the critical event which immediately precedes destabilization of the HRB coiled coil. Further studies will address the role of the N-terminal TMD residues in HeV F stability, trafficking, and fusogenic activity.

The disulfide-linked HeV F TMD mutants were also tested with a prefusion conformation-specific antibody, and results showed that cell lysis led to decreased binding of the antibody, similar to WT HeV F which is triggered during cell disruption. This suggests that the mutants were not locked in the prefusion conformation and underwent some conformational changes. However, the conformations adopted by the mutants due to cell lysis are unclear. Cell lysis may alter interactions in the ectodomain, and the changes may be sufficient to destabilize the HRB coiled coil without the need for TMD dissociation. Future work should analyze the mutants to determine which conformational intermediates are able to form when the TMDs are locked together. These studies will be important

for elucidating the conformational changes that can occur in HeV F prior to TMD dissociation.

Phase separation for viral replication

Phase separation of liquid organelles: Function and dysfunction

Identification of IBs and other membrane-less compartments as phase separated condensates has generated many studies to understand how these structures are regulated. Researchers are particularly interested in the functions that emerge from organizing molecules into phase separated regions. For instance, reports have shown that disruption of condensates does not usually impact cell viability (80). However, the ubiquity of condensates in cells suggests that they serve an important functional role (80, 83, 163, 164). For HMPV, disruption of actin polymerization inhibited IB coalescence, leading to decreased viral expression. However, expression was not completely abolished (56). In the viral life cycle, any decrease in efficiency can be detrimental for the virus as it combats the host cell immune system to produce new viral progeny. This idea suggests that condensate formation may provide subtle enhancements in the frequency of biochemical reactions which together benefit the overall function of the cell or the invading pathogen.

Researchers have also been interested in LLPS and condensates due to their role in neurodegenerative disease. Several proteins that are known to phase separate have been shown to form pathological brain inclusions, leading to various forms of neurodegeneration. One example is TDP-43, a stress granule protein involved in mRNA processes such as splicing, transport, and translation regulation. TDP-43 brain inclusions have been linked to a number of diseases including Alzheimer's, amyotrophic lateral sclerosis (ALS), and chronic traumatic encephalopathy (165). Stress granules are known to form under certain conditions and dissociate when the stressor is removed. TDP-43 and other stress granule proteins can have pathological effects when mutations prevent disassembly of the

condensates. When liquid organelles lose dynamicity and transition to a solid-like state, they are generally unable to facilitate normal biochemical processes for the cell. Continued research into LLPS of liquid organelles is critical to understand how changes in protein-protein and protein-RNA interactions can drive condensates to transition to an aggregated, solid-like state. This work may also impact our knowledge of viral IB formation, since HMPV P modulates interactions with N-RNA, which aggregates in solution, to incorporate it into liquid droplets. Determining the mechanisms that drive phase transitions in liquid organelles and pathological inclusions will provide critical knowledge for understanding the links between LLPS and biomolecular condensates.

Maturation of IBs during infection

Though pathological inclusions transition to a solid-like state, it is normal for condensates to mature over time due to their metastable nature (165). Thermodynamically, larger droplets are more stable than smaller droplets, so smaller droplets spontaneously dissolve as proteins diffuse into larger droplets. This event, which is known as coarsening, is different from fusion events which involve two smaller droplets coming together to form a larger droplet (165). As coarsening occurs over time, droplets become less dynamic and mature to a gel-like state. This process is thought to be driven in part by proteins with intrinsically disordered regions (IDRs). Compared to pathological aggregates, which undergo a rapid transition to a solid-like state, this maturation process is much slower and can be reversed (165). A physical explanation for droplet maturation is interesting in the context of viral IBs.

The liquid nature of IBs was initially described for rabies virus (RABV) Negri bodies (66). RABV Negri bodies have been shown to incorporate a variety of proteins including the P protein, nucleoprotein (N), polymerase, and matrix protein (72, 166). In addition, the host proteins Hsp70 and focal adhesion kinase (FAK) localize to Negri bodies (167, 168). Interestingly, FAK was shown to directly interact with RABV P, and disruption of this interaction inhibited viral RNA replication and viral protein expression (168). The Hsp70 chaperone directly

interacts with RABV N and is suggested to be involved in viral transcription or translation (167). These findings highlight the complex composition of Negri bodies and their role in promoting efficient viral multiplication. Negri body formation was characterized over time during RABV infection, and results showed that the spherical structures grew over time and sometimes evolved into irregular shapes (66). The later stage, nonspherical Negri bodies were often associated with membranes. Observations of changes in the number, size, and shape of RABV Negri bodies suggests that these liquid organelles undergo a maturation process throughout infection. Characterizing the mechanisms that regulate Negri body maturation will be important for illuminating their role in the viral life cycle.

Maturation of measles virus (MeV) IBs has also been observed during infection (86). Until 12 hours post infection, MeV-infected cells showed the presence of small spherical structures in the cytoplasm. At later time points, larger IBs were observed, and some were irregularly shaped. The nonspherical structures were often located near the nucleus (86). The irregular shape of later stage IBs suggests that they transition to a less dynamic state over time. Like RABV, the loss of spherical shape may be partly due an association with host cell membrane components at later points of infection. Many positive-sense RNA viruses are known to associate with membranes to generate replication complexes (169). Thus, some negative-strand RNA viruses may also utilize membrane components within IBs to enhance replication or another step of the viral life cycle.

HMPV and RSV infections show differences in the maturation IBs. As HMPV infection progresses, the quantity of IBs was shown to modestly increase, with only a few IBs generally found in each cell at late infection time points (56). IBs tend to increase in size throughout infection, suggesting that they undergo fusion events and mature as more protein diffuses into the structures. Even at late time points, HMPV IBs typically retain a spherical shape, in contrast to the irregular structures observed for MeV and RABV. For RSV, IBs contain substructures known as IB-associated granules (IBAGs) (67). Newly synthesized viral mRNA and the M2-1 protein localize to IBAGs, whereas the N, L, and P proteins as well as

viral genomic RNA are excluded from these structures. These structures were shown to develop within IBs by 12 hours post infection, suggesting that they form as a result of IB maturation over time. IBAG formation within IBs was shown to be dependent upon viral mRNA synthesis (67). The findings for RSV IBs suggest that newly transcribed viral mRNAs are stored within IBAGs prior to release into the cytoplasm. However, further studies are needed to understand the function of IBAGs and the mechanisms that regulate maturation of these IB substructures. Thus far, IBAGs have not been observed for any other negative-strand RNA viruses.

In vitro analysis of HMPV proteins showed that heparin purified HMPV P liquid droplets often contained round, dimple-like regions (FIG 5.1). In addition, these dimple-like regions were also observed for liquid droplets containing HMPV N-RNA and P (FIG 5.1). Additional analysis is needed to determine if the formation of these regions is functionally important to liquid droplet formation. However, it is interesting to speculate that HMPV proteins may induce interactions for LLPS that lead to the formation of IB substructures, similar to the IBAGs observed for RSV. Though the initial characterization of HMPV IB formation did not show the presence of IB substructures, high resolution microscopy techniques may be beneficial for identifying previously unrecognized features of IBs for different viruses.

Liquid organelle maturation is also interesting in the context of the monomeric HMPV N^0-P construct that was purified for *in vitro* studies. As described in Chapter 4, immobilized metal affinity chromatography (IMAC) purified HMPV N^0-P formed gel-like droplets which did not undergo fusion. However, adding a heparin purification step allowed for N^0-P to phase separate in the absence of other binding partners. This suggests that nucleic acid contaminants in the IMAC purified HMPV N^0-P solution impact LLPS dynamics. Higher levels of nucleic acid may increase the rate at which N^0-P droplets transition from a liquid to gel-like state. This is an interesting result since some viral IBs appear to become more gel-like at late stages of infection (86). As the level of RNA increases within IBs during replication and transcription, the RNA may drive the transition of IBs from liquid-

like to gel-like, leading to slower exchange of materials with the cytoplasm. However, this maturation to a gel-like state likely involves modulation of numerous factors in addition to RNA concentration.

The role of RNA-binding in phase separation

Different varieties of RNA-protein granules are a common example of liquid organelles found in the cell. The presence of viral genomic RNA and viral mRNA in IBs suggests that they possess similarities with other RNA-protein granules. In Chapter 4, we reported that HMPV P recruited monomeric, RNA-free N protein and oligomeric N-RNA rings to liquid droplets. This suggests that RNA interactions with N protein are not required for phase separation with HMPV P. MeV work showed that IB-like structures formed in cells when an N protein RNA-binding mutant was cotransfected with MeV P (84). Additionally, recombinant MeV N protein purified as a monomer phase separated with MeV P *in vitro* (87). However, RSV studies suggested that N protein oligomerization and RNA-binding were required for IB-like structure formation with RSV P in cells (88). These varying results warrant further work into the role of RNA-binding in viral protein phase separation.

In addition to our monomeric N^0-P construct, we also purified a potential HMPV N RNA-binding mutant, based on an RNA-free mutant described for RSV (170). The RSV mutant N K170A/R185A was purified as a monomer and was shown to lack the ability to bind RNA, based on the low A260/280 ratio of the purified protein. After sequence comparison with RSV N, we designed HMPV N K171A/R186A as a potential RNA-binding mutant to test in our purified protein system. The construct was prepared using an IMAC purification step followed by a heparin purification step. When HMPV N K171A/R186A was tested independently in the droplet assay, it formed aggregates similar to N-RNA and IMAC purified N^0-P (FIG 5.2). Interestingly, HMPV N K171A/R186A was recruited to liquid droplets when it was mixed with anion exchange purified HMPV P (FIG 5.2). This further supports that N RNA-binding is not required for phase separation of HMPV proteins. However, further experiments are needed to confirm that the N K171A/R186A mutations effectively block RNA-binding. Additionally, the HMPV

N^0-P and N K171A/R186A constructs should be expressed in cells alone or with HMPV P to determine if IB-like structures form. These cellular results would be beneficial in conjunction with the *in vitro* purified protein data for explaining phase separation mechanisms.

Along with the HMPV N K171A/R186A mutant, future studies will analyze other HMPV N constructs that possess mutations in the RNA-binding cleft. We are particularly interested in analyzing these mutants since RNA plays a significant role in phase separation (164, 171). The published structure of the HMPV N RNA-binding cleft was analyzed to select specific residues to mutate: K171A, R185A, R186A, R189A, and R341A (47). These mutants will be tested in the *in vitro* system and in cellular studies to determine their effects on viral replication and phase separation. A minigenome assay will be used to determine if these mutations block or inhibit replication. Immunofluorescence experiments will be utilized to assess whether the mutants form IB-like structures with HMPV P. For the mutants that do form IB-like structures, fluorescence recovery after photobleaching (FRAP) analysis will be performed to analyze the internal contents of the compartments. The FRAP results will be compared to the recovery observed for IB-like structures formed by WT HMPV N and P.

The COVID-19 pandemic has generated an enormous amount of research focused on understanding the infectious mechanisms of the severe acute respiratory syndrome coronavirus 2 (SARS-CoV-2), and some studies have highlighted the role of phase separation in the SARS-CoV-2 life cycle. SARS-CoV-2 is a positive-strand RNA virus with a large genome of approximately 30 kilobases. It uses a multifunctional nucleoprotein (N) to package the genome into new virions. Unlike the negative-strand viruses described throughout this dissertation, SARS-CoV-2 does not have a separate P protein to act as a cofactor for the polymerase. Instead, the SARS-CoV 2 N protein contains three IDRs and is thought to facilitate viral RNA synthesis at early stages of infection. Several reports, many of which are still preprints, have reported that SARS-CoV-2 N forms condensates with viral RNA (172-176). This suggests that SARS-CoV-2 and other

coronaviruses may utilize LLPS to enhance viral replication and packaging. These findings support that viruses outside of the negative-strand RNA virus classification may have also evolved mechanisms to generate condensates to compartmentalize specific reactions.

Post-translational modification of the P protein

IDRs within proteins are particularly susceptible to post-translational modifications because they lack secondary structure (177). In general, post-translational modifications often act as switches to turn proteins on or off to regulate cellular events. Post-translational modification of intrinsically disordered proteins in liquid organelles provides another method by which cells can influence the formation and dissolution of these structures. One type of post-translational modification is phosphorylation of serine, threonine, and tyrosine residues. The addition of a negatively charged phosphoryl group to an uncharged amino acid may either promote or inhibit the formation of phase separated compartments (177).

MeV P is phosphorylated at several sites, including S86 and S151 which are located in IDRs. These two sites are phosphorylated by casein kinase 2, and the phosphorylation status of the residues changes when MeV P binds to N (178, 179). Mutating the serine residues or inhibiting casein kinase II led to a decrease in the size of IB-like compartments formed in cells, suggesting that phosphorylation of MeV P affects structural aspects of IB formation (86). Additionally, the vesicular stomatitis virus P protein has been shown to undergo phosphorylation events by cellular kinases, leading to changes in transcriptional activity (180). In a SARS-CoV-2 preprint, phosphorylation of the multifunctional N protein led to the formation of liquid-like droplets with RNA, whereas unmodified N protein formed gel-like droplets with RNA (181). This study hypothesized that unmodified SARS-CoV-2 N is required for nucleocapsid assembly, whereas phosphorylated N protein phase separates for viral genome processing. The HMPV P protein was analyzed by mass spectrometry to show that it is phosphorylated at residues 106, 148, 157, 158, 168, 171, and 271 (92). Further studies of HMPV P phosphorylation will be

important for understanding the role of these post-translational modifications in replication and IB regulation.

Identifying IB-resident proteins

Although some viral and host factors within IBs have been discovered, further identification of IB components may help elucidate the mechanisms that govern IB formation and maturation. However, purification of IBs from infected cells presents challenges since IBs have a liquid nature and lack a physical barrier. Recent work described the purification of liquid-like granules containing FUS, a DNA- and RNA-binding protein implicated in ALS (182). FUS contains a low complexity domain that allows it to form multivalent interactions to mediate LLPS (183). Since HMPV and other negative-strand RNA viruses form liquid organelles similar to FUS, this purification procedure may be beneficial for analyzing the internal contents of IBs to identify protein interactions that mediate LLPS. Viral IBs appear to mature throughout infection, so IBs would need to be purified at different time points and analyzed separately to fully understand the landscape of these structures. Purified IBs would be subjected to mass spectrometry and proteomic analysis to identify proteins that reside in IBs. These studies would provide critical information for understanding which proteins are recruited to IBs at different times during infection. Additional analysis would be needed to determine the protein-protein interactions that lead to IB recruitment. The different aspects of liquid organelles described here highlight some of the interesting research questions which must be addressed to benefit our fight against negative-strand RNA viruses that cause human disease.

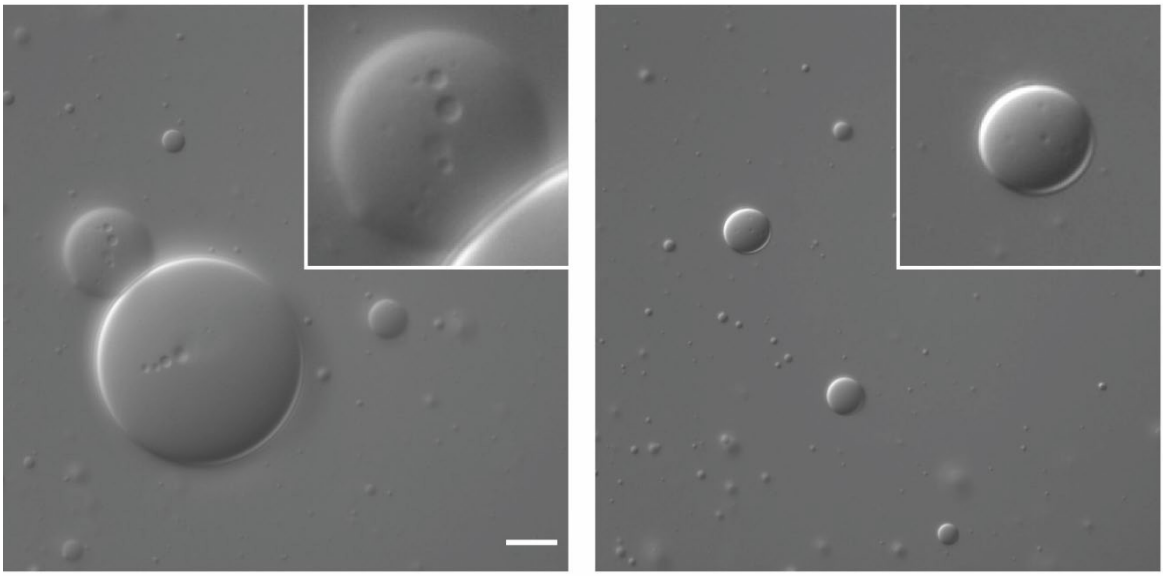

Figure 5.1. HMPV P and N-RNA/P liquid droplets contain round, dimple-like regions. Heparin purified HMPV P (15 μM) was tested alone or with HMPV N-RNA (15 μM) in a droplet assay. DIC microscopy images were acquired with a 60X objective on a Nikon Eclipse E600. The scale bar is 10 μm.

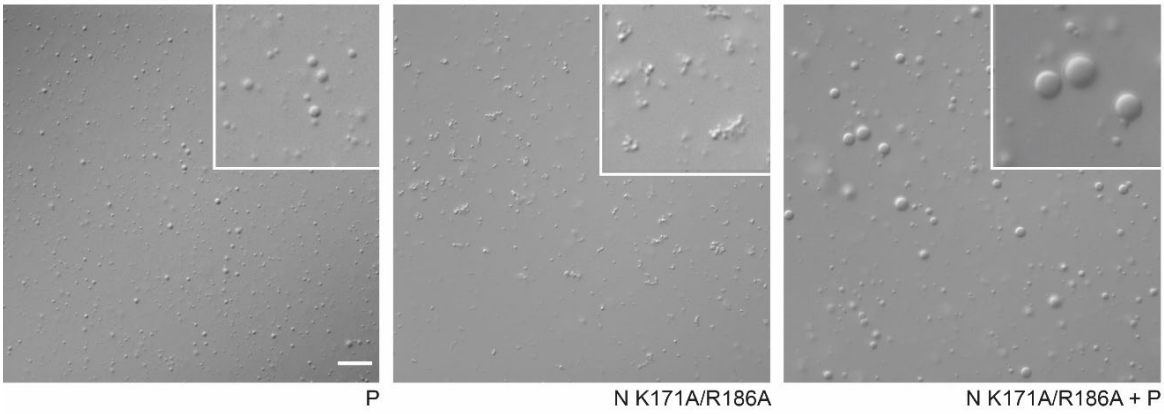

Figure 5.2. HMPV P recruits N K171A/R186A to liquid droplets. HMPV N K171A/R186A (15 μM) was mixed with anion exchange purified HMPV P (15 μM) in a droplet assay. DIC images were acquired using a 60X objective on a Nikon Eclipse E600. The scale bar is 10 μm.

APPENDIX

List of abbreviations

ALS	Amyotrophic lateral sclerosis
CedPV	Cedar virus
CT	C-terminal cytoplasmic tail
CTD	C-terminal domain
ER	Endoplasmic reticulum
F	Fusion protein
FAK	Focal adhesion kinase
FP	Fusion peptide
FRAP	Fluorescence recovery after photobleaching
G	Attachment protein
HeV	Hendra virus
HMPV	Human metapneumovirus
HRA/HRB	Heptad repeat A/B
IB	Inclusion body
IBAG	Inclusion body-associated granule
IDR	Intrinsically disordered region
IMAC	Immobilized metal affinity chromatography
L	Large polymerase protein
LLPS	Liquid-liquid phase separation
MeV	Measles virus

M	Matrix protein
M2-1/M2-2	Matrix-2 proteins
N^0	Monomeric RNA-free nucleoprotein
NiV	Nipah virus
N-RNA	RNA-bound nucleoprotein rings
NTD	N-terminal domain
P	Phosphoprotein
P-bodies	Processing bodies
PIV5	Parainfluenza virus 5
RABV	Rabies virus
RSV	Respiratory syncytial virus
SARS-CoV-2	Severe acute respiratory syndrome coronavirus 2
SH	Small hydrophobic protein
TMD	Transmembrane domain
VSV	Vesicular stomatitis virus
WT	Wild type

REFERENCES

1. Amarasinghe GK, Aréchiga Ceballos NG, Banyard AC, Basler CF, Bavari S, Bennett AJ, Blasdell KR, Briese T, Bukreyev A, Caì Y, Calisher CH, Campos Lawson C, Chandran K, Chapman CA, Chiu CY, Choi KS, Collins PL, Dietzgen RG, Dolja VV, Dolnik O, Domier LL, Dürrwald R, Dye JM, Easton AJ, Ebihara H, Echevarría JE, Fooks AR, Formenty PBH, Fouchier RAM, Freuling CM, Ghedin E, Goldberg TL, Hewson R, Horie M, Hyndman TH, Jiāng D, Kityo R, Kobinger GP, Kondō H, Koonin EV, Krupovic M, Kurath G, Lamb RA, Lee B, Leroy EM, Maes P, Maisner A, Marston DA, Mor SK, Müller T, et al. 2018. Taxonomy of the order Mononegavirales: update 2018. Arch Virol 163:2283-2294.
2. Latorre V, Mattenberger F, Geller R. 2018. Chaperoning the Mononegavirales: Current Knowledge and Future Directions. Viruses 10.
3. Halpin K, Mungall BA. 2007. Recent progress in henipavirus research. Comp Immunol Microbiol Infect Dis 30:287-307.
4. Chang A, Dutch RE. 2012. Paramyxovirus fusion and entry: multiple paths to a common end. Viruses 4:613-36.
5. Rima B, Balkema-Buschmann A, Dundon WG, Duprex P, Easton A, Fouchier R, Kurath G, Lamb R, Lee B, Rota P, Wang L, Ictv Report C. 2019. ICTV Virus Taxonomy Profile: Paramyxoviridae. J Gen Virol 100:1593-1594.
6. Wilson RL, Fuentes SM, Wang P, Taddeo EC, Klatt A, Henderson AJ, He B. 2006. Function of small hydrophobic proteins of paramyxovirus. J Virol 80:1700-9.
7. Hess IM, Massey PD, Walker B, Middleton DJ, Wright TM. 2011. Hendra virus: what do we know? N S W Public Health Bull 22:118-22.
8. Murray K, Selleck P, Hooper P, Hyatt A, Gould A, Gleeson L, Westbury H, Hiley L, Selvey L, Rodwell B, et al. 1995. A morbillivirus that caused fatal disease in horses and humans. Science 268:94-7.
9. Mahalingam S, Herrero LJ, Playford EG, Spann K, Herring B, Rolph MS, Middleton D, McCall B, Field H, Wang LF. 2012. Hendra virus: an emerging paramyxovirus in Australia. Lancet Infect Dis 12:799-807.
10. Dawes BE, Freiberg AN. 2019. Henipavirus infection of the central nervous system. Pathog Dis 77.
11. Field HE. 2016. Hendra virus ecology and transmission. Curr Opin Virol 16:120-125.

12. Wang LF, Anderson DE. 2019. Viruses in bats and potential spillover to animals and humans. Curr Opin Virol 34:79-89.
13. Sharma V, Kaushik S, Kumar R, Yadav JP, Kaushik S. 2019. Emerging trends of Nipah virus: A review. Rev Med Virol 29:e2010.
14. Clayton BA. 2017. Nipah virus: transmission of a zoonotic paramyxovirus. Curr Opin Virol 22:97-104.
15. Marsh GA, de Jong C, Barr JA, Tachedjian M, Smith C, Middleton D, Yu M, Todd S, Foord AJ, Haring V, Payne J, Robinson R, Broz I, Crameri G, Field HE, Wang LF. 2012. Cedar virus: a novel Henipavirus isolated from Australian bats. PLoS Pathog 8:e1002836.
16. Robson F, Khan KS, Le TK, Paris C, Demirbag S, Barfuss P, Rocchi P, Ng WL. 2020. Coronavirus RNA Proofreading: Molecular Basis and Therapeutic Targeting. Mol Cell 79:710-727.
17. Wu D, Wu T, Liu Q, Yang Z. 2020. The SARS-CoV-2 outbreak: What we know. Int J Infect Dis 94:44-48.
18. Jardetzky TS, Lamb RA. 2014. Activation of paramyxovirus membrane fusion and virus entry. Curr Opin Virol 5:24-33.
19. Carter JR, Pager CT, Fowler SD, Dutch RE. 2005. Role of N-linked glycosylation of the Hendra virus fusion protein. J Virol 79:7922-5.
20. Smith EC, Popa A, Chang A, Masante C, Dutch RE. 2009. Viral entry mechanisms: the increasing diversity of paramyxovirus entry. Febs j 276:7217-27.
21. Richardson C, Hull D, Greer P, Hasel K, Berkovich A, Englund G, Bellini W, Rima B, Lazzarini R. 1986. The nucleotide sequence of the mRNA encoding the fusion protein of measles virus (Edmonston strain): a comparison of fusion proteins from several different paramyxoviruses. Virology 155:508-23.
22. Welch BD, Liu Y, Kors CA, Leser GP, Jardetzky TS, Lamb RA. 2012. Structure of the cleavage-activated prefusion form of the parainfluenza virus 5 fusion protein. Proc Natl Acad Sci U S A 109:16672-7.
23. Pager CT, Craft WW, Jr., Patch J, Dutch RE. 2006. A mature and fusogenic form of the Nipah virus fusion protein requires proteolytic processing by cathepsin L. Virology 346:251-7.
24. Pager CT, Dutch RE. 2005. Cathepsin L is involved in proteolytic processing of the Hendra virus fusion protein. J Virol 79:12714-20.

25. Pager CT, Wurth MA, Dutch RE. 2004. Subcellular localization and calcium and pH requirements for proteolytic processing of the Hendra virus fusion protein. J Virol 78:9154-63.
26. Meulendyke KA, Wurth MA, McCann RO, Dutch RE. 2005. Endocytosis plays a critical role in proteolytic processing of the Hendra virus fusion protein. J Virol 79:12643-9.
27. Vogt C, Eickmann M, Diederich S, Moll M, Maisner A. 2005. Endocytosis of the Nipah virus glycoproteins. J Virol 79:3865-72.
28. Popa A, Carter JR, Smith SE, Hellman L, Fried MG, Dutch RE. 2012. Residues in the hendra virus fusion protein transmembrane domain are critical for endocytic recycling. J Virol 86:3014-26.
29. Armstrong RT, Kushnir AS, White JM. 2000. The transmembrane domain of influenza hemagglutinin exhibits a stringent length requirement to support the hemifusion to fusion transition. J Cell Biol 151:425-37.
30. Kemble GW, Danieli T, White JM. 1994. Lipid-anchored influenza hemagglutinin promotes hemifusion, not complete fusion. Cell 76:383-91.
31. Markosyan RM, Cohen FS, Melikyan GB. 2000. The lipid-anchored ectodomain of influenza virus hemagglutinin (GPI-HA) is capable of inducing nonenlarging fusion pores. Mol Biol Cell 11:1143-52.
32. Nüssler F, Clague MJ, Herrmann A. 1997. Meta-stability of the hemifusion intermediate induced by glycosylphosphatidylinositol-anchored influenza hemagglutinin. Biophys J 73:2280-91.
33. Miyauchi K, Komano J, Yokomaku Y, Sugiura W, Yamamoto N, Matsuda Z. 2005. Role of the specific amino acid sequence of the membrane-spanning domain of human immunodeficiency virus type 1 in membrane fusion. J Virol 79:4720-9.
34. Owens RJ, Burke C, Rose JK. 1994. Mutations in the membrane-spanning domain of the human immunodeficiency virus envelope glycoprotein that affect fusion activity. J Virol 68:570-4.
35. Salzwedel K, Johnston PB, Roberts SJ, Dubay JW, Hunter E. 1993. Expression and characterization of glycophospholipid-anchored human immunodeficiency virus type 1 envelope glycoproteins. J Virol 67:5279-88.
36. Shang L, Yue L, Hunter E. 2008. Role of the membrane-spanning domain of human immunodeficiency virus type 1 envelope glycoprotein in cell-cell fusion and virus infection. J Virol 82:5417-28.

37. Shang L, Hunter E. 2010. Residues in the membrane-spanning domain core modulate conformation and fusogenicity of the HIV-1 envelope glycoprotein. Virology 404:158-67.
38. Weiss CD, White JM. 1993. Characterization of stable Chinese hamster ovary cells expressing wild-type, secreted, and glycosylphosphatidylinositol-anchored human immunodeficiency virus type 1 envelope glycoprotein. J Virol 67:7060-6.
39. Wilk T, Pfeiffer T, Bukovsky A, Moldenhauer G, Bosch V. 1996. Glycoprotein incorporation and HIV-1 infectivity despite exchange of the gp160 membrane-spanning domain. Virology 218:269-74.
40. Smith EC, Smith SE, Carter JR, Webb SR, Gibson KM, Hellman LM, Fried MG, Dutch RE. 2013. Trimeric transmembrane domain interactions in paramyxovirus fusion proteins: roles in protein folding, stability, and function. J Biol Chem 288:35726-35.
41. Smith EC, Culler MR, Hellman LM, Fried MG, Creamer TP, Dutch RE. 2012. Beyond anchoring: the expanding role of the hendra virus fusion protein transmembrane domain in protein folding, stability, and function. J Virol 86:3003-13.
42. Rima B, Collins P, Easton A, Fouchier R, Kurath G, Lamb RA, Lee B, Maisner A, Rota P, Wang L, Ictv Report C. 2017. ICTV Virus Taxonomy Profile: Pneumoviridae. J Gen Virol 98:2912-2913.
43. Cox RG, Mainou BA, Johnson M, Hastings AK, Schuster JE, Dermody TS, Williams JV. 2015. Human Metapneumovirus Is Capable of Entering Cells by Fusion with Endosomal Membranes. PLoS Pathog 11:e1005303.
44. Battles MB, McLellan JS. 2019. Respiratory syncytial virus entry and how to block it. Nat Rev Microbiol 17:233-245.
45. Herfst S, Mas V, Ver LS, Wierda RJ, Osterhaus AD, Fouchier RA, Melero JA. 2008. Low-pH-induced membrane fusion mediated by human metapneumovirus F protein is a rare, strain-dependent phenomenon. J Virol 82:8891-5.
46. Schowalter RM, Smith SE, Dutch RE. 2006. Characterization of human metapneumovirus F protein-promoted membrane fusion: critical roles for proteolytic processing and low pH. J Virol 80:10931-41.
47. Renner M, Bertinelli M, Leyrat C, Paesen GC, Saraiva de Oliveira LF, Huiskonen JT, Grimes JM. 2016. Nucleocapsid assembly in pneumoviruses is regulated by conformational switching of the N protein. Elife 5:e12627.

48. Griffiths C, Drews SJ, Marchant DJ. 2017. Respiratory Syncytial Virus: Infection, Detection, and New Options for Prevention and Treatment. Clin Microbiol Rev 30:277-319.
49. Shafagati N, Williams J. 2018. Human metapneumovirus - what we know now. F1000Res 7:135.
50. van den Hoogen BG, Bestebroer TM, Osterhaus AD, Fouchier RA. 2002. Analysis of the genomic sequence of a human metapneumovirus. Virology 295:119-32.
51. Bermingham A, Collins PL. 1999. The M2-2 protein of human respiratory syncytial virus is a regulatory factor involved in the balance between RNA replication and transcription. Proc Natl Acad Sci U S A 96:11259-64.
52. Panda S, Mohakud NK, Pena L, Kumar S. 2014. Human metapneumovirus: review of an important respiratory pathogen. Int J Infect Dis 25:45-52.
53. Leyrat C, Renner M, Harlos K, Huiskonen JT, Grimes JM. 2014. Structure and self-assembly of the calcium binding matrix protein of human metapneumovirus. Structure 22:136-48.
54. Vinci A, Lee PJ, Krilov LR. 2018. Human Metapneumovirus Infection. Pediatr Rev 39:623-624.
55. Schuster JE, Williams JV. 2014. Human Metapneumovirus. Microbiol Spectr 2.
56. Cifuentes-Muñoz N, Branttie J, Slaughter KB, Dutch RE. 2017. Human Metapneumovirus Induces Formation of Inclusion Bodies for Efficient Genome Replication and Transcription. J Virol 91.
57. Heinrich BS, Cureton DK, Rahmeh AA, Whelan SP. 2010. Protein expression redirects vesicular stomatitis virus RNA synthesis to cytoplasmic inclusions. PLoS Pathog 6:e1000958.
58. Kolesnikova L, Mühlberger E, Ryabchikova E, Becker S. 2000. Ultrastructural organization of recombinant Marburg virus nucleoprotein: comparison with Marburg virus inclusions. J Virol 74:3899-904.
59. Matsumoto S. 1962. Electron microscopy of nerve cells infected with street rabies virus. Virology 17:198-202.
60. Compans RW, Holmes KV, Dales S, Choppin PW. 1966. An electron microscopic study of moderate and virulent virus-cell interactions of the parainfluenza virus SV5. Virology 30:411-26.
61. Nakai T, Shand FL, Howatson AF. 1969. Development of measles virus in vitro. Virology 38:50-67.

62. Churchill AE. 1963. Intranuclear inclusions produced by bovine para-influenza. Nature 197:409.
63. Narang HK. 1982. Ultrastructural study of long-term canine distemper virus infection in tissue culture cells. Infect Immun 36:310-9.
64. Norrby E, Marusyk H, Orvell C. 1970. Morphogenesis of respiratory syncytial virus in a green monkey kidney cell line (Vero). J Virol 6:237-42.
65. Derdowski A, Peters TR, Glover N, Qian R, Utley TJ, Burnett A, Williams JV, Spearman P, Crowe JE. 2008. Human metapneumovirus nucleoprotein and phosphoprotein interact and provide the minimal requirements for inclusion body formation. J Gen Virol 89:2698-2708.
66. Nikolic J, Le Bars R, Lama Z, Scrima N, Lagaudrière-Gesbert C, Gaudin Y, Blondel D. 2017. Negri bodies are viral factories with properties of liquid organelles. Nat Commun 8:58.
67. Rincheval V, Lelek M, Gault E, Bouillier C, Sitterlin D, Blouquit-Laye S, Galloux M, Zimmer C, Eleouet JF, Rameix-Welti MA. 2017. Functional organization of cytoplasmic inclusion bodies in cells infected by respiratory syncytial virus. Nat Commun 8:563.
68. Nanbo A, Watanabe S, Halfmann P, Kawaoka Y. 2013. The spatio-temporal distribution dynamics of Ebola virus proteins and RNA in infected cells. Sci Rep 3:1206.
69. Ma D, George CX, Nomburg JL, Pfaller CK, Cattaneo R, Samuel CE. 2018. Upon Infection, Cellular WD Repeat-Containing Protein 5 (WDR5) Localizes to Cytoplasmic Inclusion Bodies and Enhances Measles Virus Replication. J Virol 92.
70. Zhang S, Jiang Y, Cheng Q, Zhong Y, Qin Y, Chen M. 2017. Inclusion Body Fusion of Human Parainfluenza Virus Type 3 Regulated by Acetylated α-Tubulin Enhances Viral Replication. J Virol 91.
71. Carlos TS, Young DF, Schneider M, Simas JP, Randall RE. 2009. Parainfluenza virus 5 genomes are located in viral cytoplasmic bodies whilst the virus dismantles the interferon-induced antiviral state of cells. J Gen Virol 90:2147-56.
72. Lahaye X, Vidy A, Pomier C, Obiang L, Harper F, Gaudin Y, Blondel D. 2009. Functional characterization of Negri bodies (NBs) in rabies virus-infected cells: Evidence that NBs are sites of viral transcription and replication. J Virol 83:7948-58.

73. Hoenen T, Shabman RS, Groseth A, Herwig A, Weber M, Schudt G, Dolnik O, Basler CF, Becker S, Feldmann H. 2012. Inclusion bodies are a site of ebolavirus replication. J Virol 86:11779-88.
74. Cifuentes-Muñoz N, Ellis Dutch R. 2019. To assemble or not to assemble: The changing rules of pneumovirus transmission. Virus Res 265:68-73.
75. García J, García-Barreno B, Vivo A, Melero JA. 1993. Cytoplasmic inclusions of respiratory syncytial virus-infected cells: formation of inclusion bodies in transfected cells that coexpress the nucleoprotein, the phosphoprotein, and the 22K protein. Virology 195:243-7.
76. El Najjar F, Cifuentes-Muñoz N, Chen J, Zhu H, Buchholz UJ, Moncman CL, Dutch RE. 2016. Human metapneumovirus Induces Reorganization of the Actin Cytoskeleton for Direct Cell-to-Cell Spread. PLoS Pathog 12:e1005922.
77. Cifuentes-Muñoz N, Dutch RE, Cattaneo R. 2018. Direct cell-to-cell transmission of respiratory viruses: The fast lanes. PLoS Pathog 14:e1007015.
78. Jobe F, Simpson J, Hawes P, Guzman E, Bailey D. 2020. Respiratory syncytial virus sequesters NF-κB subunit p65 to cytoplasmic inclusion bodies to inhibit innate immune signalling. J Virol doi:10.1128/jvi.01380-20.
79. Mehedi M, McCarty T, Martin SE, Le Nouën C, Buehler E, Chen YC, Smelkinson M, Ganesan S, Fischer ER, Brock LG, Liang B, Munir S, Collins PL, Buchholz UJ. 2016. Actin-Related Protein 2 (ARP2) and Virus-Induced Filopodia Facilitate Human Respiratory Syncytial Virus Spread. PLoS Pathog 12:e1006062.
80. Banani SF, Lee HO, Hyman AA, Rosen MK. 2017. Biomolecular condensates: organizers of cellular biochemistry. Nat Rev Mol Cell Biol 18:285-298.
81. Hyman AA, Weber CA, Jülicher F. 2014. Liquid-liquid phase separation in biology. Annu Rev Cell Dev Biol 30:39-58.
82. Pederson T. 2011. The nucleolus. Cold Spring Harb Perspect Biol 3.
83. Alberti S, Gladfelter A, Mittag T. 2019. Considerations and Challenges in Studying Liquid-Liquid Phase Separation and Biomolecular Condensates. Cell 176:419-434.
84. Renner M, Paesen GC, Grison CM, Granier S, Grimes JM, Leyrat C. 2017. Structural dissection of human metapneumovirus phosphoprotein using small angle x-ray scattering. Sci Rep 7:14865.

85. Heinrich BS, Maliga Z, Stein DA, Hyman AA, Whelan SPJ. 2018. Phase Transitions Drive the Formation of Vesicular Stomatitis Virus Replication Compartments. mBio 9.
86. Zhou Y, Su JM, Samuel CE, Ma D. 2019. Measles Virus Forms Inclusion Bodies with Properties of Liquid Organelles. J Virol 93.
87. Guseva S, Milles S, Jensen MR, Salvi N, Kleman JP, Maurin D, Ruigrok RWH, Blackledge M. 2020. Measles virus nucleo- and phosphoproteins form liquid-like phase-separated compartments that promote nucleocapsid assembly. Sci Adv 6:eaaz7095.
88. Galloux M, Risso-Ballester J, Richard CA, Fix J, Rameix-Welti MA, Eléouët JF. 2020. Minimal Elements Required for the Formation of Respiratory Syncytial Virus Cytoplasmic Inclusion Bodies In Vivo and In Vitro. mBio 11.
89. Tokuriki N, Oldfield CJ, Uversky VN, Berezovsky IN, Tawfik DS. 2009. Do viral proteins possess unique biophysical features? Trends Biochem Sci 34:53-9.
90. Gerard FC, Ribeiro Ede A, Jr., Leyrat C, Ivanov I, Blondel D, Longhi S, Ruigrok RW, Jamin M. 2009. Modular organization of rabies virus phosphoprotein. J Mol Biol 388:978-96.
91. Guseva S, Milles S, Blackledge M, Ruigrok RWH. 2019. The Nucleoprotein and Phosphoprotein of Measles Virus. Front Microbiol 10:1832.
92. Pan J, Qian X, Lattmann S, El Sahili A, Yeo TH, Jia H, Cressey T, Ludeke B, Noton S, Kalocsay M, Fearns R, Lescar J. 2020. Structure of the human metapneumovirus polymerase phosphoprotein complex. Nature 577:275-279.
93. Yabukarski F, Lawrence P, Tarbouriech N, Bourhis JM, Delaforge E, Jensen MR, Ruigrok RW, Blackledge M, Volchkov V, Jamin M. 2014. Structure of Nipah virus unassembled nucleoprotein in complex with its viral chaperone. Nat Struct Mol Biol 21:754-9.
94. Leyrat C, Jensen MR, Ribeiro EA, Jr., Gérard FC, Ruigrok RW, Blackledge M, Jamin M. 2011. The N(0)-binding region of the vesicular stomatitis virus phosphoprotein is globally disordered but contains transient α-helices. Protein Sci 20:542-56.
95. Leung DW, Borek D, Luthra P, Binning JM, Anantpadma M, Liu G, Harvey IB, Su Z, Endlich-Frazier A, Pan J, Shabman RS, Chiu W, Davey RA, Otwinowski Z, Basler CF, Amarasinghe GK. 2015. An Intrinsically Disordered Peptide from Ebola

Virus VP35 Controls Viral RNA Synthesis by Modulating Nucleoprotein-RNA Interactions. Cell Rep 11:376-89.

96. Guryanov SG, Liljeroos L, Kasaragod P, Kajander T, Butcher SJ. 2015. Crystal Structure of the Measles Virus Nucleoprotein Core in Complex with an N-Terminal Region of Phosphoprotein. J Virol 90:2849-57.
97. Tran TL, Castagné N, Dubosclard V, Noinville S, Koch E, Moudjou M, Henry C, Bernard J, Yeo RP, Eléouët JF. 2009. The respiratory syncytial virus M2-1 protein forms tetramers and interacts with RNA and P in a competitive manner. J Virol 83:6363-74.
98. Blondot ML, Dubosclard V, Fix J, Lassoued S, Aumont-Nicaise M, Bontems F, Eléouët JF, Sizun C. 2012. Structure and functional analysis of the RNA- and viral phosphoprotein-binding domain of respiratory syncytial virus M2-1 protein. PLoS Pathog 8:e1002734.
99. Leyrat C, Renner M, Harlos K, Huiskonen JT, Grimes JM. 2014. Drastic changes in conformational dynamics of the antiterminator M2-1 regulate transcription efficiency in Pneumovirinae. Elife 3:e02674.
100. Chan YP, Lu M, Dutta S, Yan L, Barr J, Flora M, Feng YR, Xu K, Nikolov DB, Wang LF, Skiniotis G, Broder CC. 2012. Biochemical, conformational, and immunogenic analysis of soluble trimeric forms of henipavirus fusion glycoproteins. J Virol 86:11457-71.
101. Lee B, Ataman ZA. 2011. Modes of paramyxovirus fusion: a Henipavirus perspective. Trends Microbiol 19:389-99.
102. Eaton BT, Broder CC, Middleton D, Wang LF. 2006. Hendra and Nipah viruses: different and dangerous. Nat Rev Microbiol 4:23-35.
103. Harcourt BH, Tamin A, Ksiazek TG, Rollin PE, Anderson LJ, Bellini WJ, Rota PA. 2000. Molecular characterization of Nipah virus, a newly emergent paramyxovirus. Virology 271:334-49.
104. O'Sullivan JD, Allworth AM, Paterson DL, Snow TM, Boots R, Gleeson LJ, Gould AR, Hyatt AD, Bradfield J. 1997. Fatal encephalitis due to novel paramyxovirus transmitted from horses. Lancet 349:93-5.
105. Marsh GA, Wang LF. 2012. Hendra and Nipah viruses: why are they so deadly? Curr Opin Virol 2:242-7.
106. Chua KB, Bellini WJ, Rota PA, Harcourt BH, Tamin A, Lam SK, Ksiazek TG, Rollin PE, Zaki SR, Shieh W, Goldsmith CS, Gubler DJ, Roehrig JT, Eaton B, Gould AR,

Olson J, Field H, Daniels P, Ling AE, Peters CJ, Anderson LJ, Mahy BW. 2000. Nipah virus: a recently emergent deadly paramyxovirus. Science 288:1432-5.

107. Halpin K, Young PL, Field HE, Mackenzie JS. 2000. Isolation of Hendra virus from pteropid bats: a natural reservoir of Hendra virus. J Gen Virol 81:1927-1932.

108. Bossart KN, Wang LF, Eaton BT, Broder CC. 2001. Functional expression and membrane fusion tropism of the envelope glycoproteins of Hendra virus. Virology 290:121-35.

109. Bossart KN, Wang LF, Flora MN, Chua KB, Lam SK, Eaton BT, Broder CC. 2002. Membrane fusion tropism and heterotypic functional activities of the Nipah virus and Hendra virus envelope glycoproteins. J Virol 76:11186-98.

110. Dutch RE, Jardetzky TS, Lamb RA. 2000. Virus membrane fusion proteins: biological machines that undergo a metamorphosis. Biosci Rep 20:597-612.

111. Harrison SC. 2015. Viral membrane fusion. Virology 479-480:498-507.

112. Bissonnette ML, Donald JE, DeGrado WF, Jardetzky TS, Lamb RA. 2009. Functional analysis of the transmembrane domain in paramyxovirus F protein-mediated membrane fusion. J Mol Biol 386:14-36.

113. Fritz R, Blazevic J, Taucher C, Pangerl K, Heinz FX, Stiasny K. 2011. The unique transmembrane hairpin of flavivirus fusion protein E is essential for membrane fusion. J Virol 85:4377-85.

114. Webb S, Nagy T, Moseley H, Fried M, Dutch R. 2017. Hendra virus fusion protein transmembrane domain contributes to pre-fusion protein stability. J Biol Chem 292:5685-5694.

115. Webb SR, Smith SE, Fried MG, Dutch RE. 2018. Transmembrane Domains of Highly Pathogenic Viral Fusion Proteins Exhibit Trimeric Association In Vitro. mSphere 3.

116. Navaratnarajah CK, Kumar S, Generous A, Apte-Sengupta S, Mateo M, Cattaneo R. 2014. The measles virus hemagglutinin stalk: structures and functions of the central fusion activation and membrane-proximal segments. J Virol 88:6158-67.

117. Ader N, Brindley MA, Avila M, Origgi FC, Langedijk JP, Örvell C, Vandevelde M, Zurbriggen A, Plemper RK, Plattet P. 2012. Structural rearrangements of the central region of the morbillivirus attachment protein stalk domain trigger F protein refolding for membrane fusion. J Biol Chem 287:16324-34.

118. Mahon PJ, Mirza AM, Musich TA, Iorio RM. 2008. Engineered intermonomeric disulfide bonds in the globular domain of Newcastle disease virus hemagglutinin-

neuraminidase protein: implications for the mechanism of fusion promotion. J Virol 82:10386-96.

119. Brindley MA, Plattet P, Plemper RK. 2014. Efficient replication of a paramyxovirus independent of full zippering of the fusion protein six-helix bundle domain. Proc Natl Acad Sci U S A 111:E3795-804.

120. Lee JK, Prussia A, Snyder JP, Plemper RK. 2007. Reversible inhibition of the fusion activity of measles virus F protein by an engineered intersubunit disulfide bridge. J Virol 81:8821-6.

121. Zokarkar A, Connolly SA, Jardetzky TS, Lamb RA. 2012. Reversible inhibition of fusion activity of a paramyxovirus fusion protein by an engineered disulfide bond in the membrane-proximal external region. J Virol 86:12397-401.

122. Wong JJ, Paterson RG, Lamb RA, Jardetzky TS. 2016. Structure and stabilization of the Hendra virus F glycoprotein in its prefusion form. Proc Natl Acad Sci U S A 113:1056-61.

123. Yamamoto T. 1963. On the thickness of the unit membrane. J Cell Biol 17:413-21.

124. Smith EC, Dutch RE. 2010. Side chain packing below the fusion peptide strongly modulates triggering of the Hendra virus F protein. J Virol 84:10928-32.

125. Jain S, McGinnes LW, Morrison TG. 2007. Thiol/disulfide exchange is required for membrane fusion directed by the Newcastle disease virus fusion protein. J Virol 81:2328-39.

126. Stantchev TS, Paciga M, Lankford CR, Schwartzkopff F, Broder CC, Clouse KA. 2012. Cell-type specific requirements for thiol/disulfide exchange during HIV-1 entry and infection. Retrovirology 9:97.

127. Aizaki H, Morikawa K, Fukasawa M, Hara H, Inoue Y, Tani H, Saito K, Nishijima M, Hanada K, Matsuura Y, Lai MM, Miyamura T, Wakita T, Suzuki T. 2008. Critical role of virion-associated cholesterol and sphingolipid in hepatitis C virus infection. J Virol 82:5715-24.

128. Huang H, Li Y, Sadaoka T, Tang H, Yamamoto T, Yamanishi K, Mori Y. 2006. Human herpesvirus 6 envelope cholesterol is required for virus entry. J Gen Virol 87:277-285.

129. Miller ME, Adhikary S, Kolokoltsov AA, Davey RA. 2012. Ebolavirus requires acid sphingomyelinase activity and plasma membrane sphingomyelin for infection. J Virol 86:7473-83.

130. Sun X, Whittaker GR. 2003. Role for influenza virus envelope cholesterol in virus entry and infection. J Virol 77:12543-51.
131. van Til NP, Heutinck KM, van der Rijt R, Paulusma CC, van Wijland M, Markusic DM, Elferink RP, Seppen J. 2008. Alteration of viral lipid composition by expression of the phospholipid floppase ABCB4 reduces HIV vector infectivity. Retrovirology 5:14.
132. Vincent S, Gerlier D, Manié SN. 2000. Measles virus assembly within membrane rafts. J Virol 74:9911-5.
133. Adu-Gyamfi E, Johnson KA, Fraser ME, Scott JL, Soni SP, Jones KR, Digman MA, Gratton E, Tessier CR, Stahelin RV. 2015. Host Cell Plasma Membrane Phosphatidylserine Regulates the Assembly and Budding of Ebola Virus. J Virol 89:9440-53.
134. Cristian L, Lear JD, DeGrado WF. 2003. Use of thiol-disulfide equilibria to measure the energetics of assembly of transmembrane helices in phospholipid bilayers. Proc Natl Acad Sci U S A 100:14772-7.
135. de Almeida RF, Loura LM, Prieto M, Watts A, Fedorov A, Barrantes FJ. 2004. Cholesterol modulates the organization of the gammaM4 transmembrane domain of the muscle nicotinic acetylcholine receptor. Biophys J 86:2261-72.
136. Sparr E, Ash WL, Nazarov PV, Rijkers DT, Hemminga MA, Tieleman DP, Killian JA. 2005. Self-association of transmembrane alpha-helices in model membranes: importance of helix orientation and role of hydrophobic mismatch. J Biol Chem 280:39324-31.
137. Liu Q, Chen L, Aguilar HC, Chou KC. 2018. A stochastic assembly model for Nipah virus revealed by super-resolution microscopy. Nat Commun 9:3050.
138. Laliberte JP, McGinnes LW, Morrison TG. 2007. Incorporation of functional HN-F glycoprotein-containing complexes into newcastle disease virus is dependent on cholesterol and membrane lipid raft integrity. J Virol 81:10636-48.
139. Ono A, Freed EO. 2005. Role of lipid rafts in virus replication. Adv Virus Res 64:311-58.
140. van den Hoogen BG, de Jong JC, Groen J, Kuiken T, de Groot R, Fouchier RA, Osterhaus AD. 2001. A newly discovered human pneumovirus isolated from young children with respiratory tract disease. Nat Med 7:719-24.

141. Edwards KM, Zhu Y, Griffin MR, Weinberg GA, Hall CB, Szilagyi PG, Staat MA, Iwane M, Prill MM, Williams JV. 2013. Burden of human metapneumovirus infection in young children. N Engl J Med 368:633-43.
142. Williams JV, Harris PA, Tollefson SJ, Halburnt-Rush LL, Pingsterhaus JM, Edwards KM, Wright PF, Crowe JE, Jr. 2004. Human metapneumovirus and lower respiratory tract disease in otherwise healthy infants and children. N Engl J Med 350:443-50.
143. Schildgen V, van den Hoogen B, Fouchier R, Tripp RA, Alvarez R, Manoha C, Williams J, Schildgen O. 2011. Human Metapneumovirus: lessons learned over the first decade. Clin Microbiol Rev 24:734-54.
144. Brangwynne CP, Mitchison TJ, Hyman AA. 2011. Active liquid-like behavior of nucleoli determines their size and shape in Xenopus laevis oocytes. Proc Natl Acad Sci U S A 108:4334-9.
145. Leyrat C, Renner M, Harlos K, Grimes JM. 2013. Solution and crystallographic structures of the central region of the phosphoprotein from human metapneumovirus. PLoS One 8:e80371.
146. Shin Y, Brangwynne CP. 2017. Liquid phase condensation in cell physiology and disease. Science 357.
147. Wheeler RJ, Hyman AA. 2018. Controlling compartmentalization by non-membrane-bound organelles. Philos Trans R Soc Lond B Biol Sci 373.
148. Nevers Q, Albertini AA, Lagaudrière-Gesbert C, Gaudin Y. 2020. Negri bodies and other virus membrane-less replication compartments. Biochim Biophys Acta Mol Cell Res 1867:118831.
149. Kinder JT, Moncman CL, Barrett C, Jin H, Kallewaard N, Dutch RE. 2020. Respiratory Syncytial Virus and Human Metapneumovirus Infections in Three-Dimensional Human Airway Tissues Expose an Interesting Dichotomy in Viral Replication, Spread, and Inhibition by Neutralizing Antibodies. J Virol 94.
150. Babu MM. 2016. The contribution of intrinsically disordered regions to protein function, cellular complexity, and human disease. Biochem Soc Trans 44:1185-1200.
151. Castagné N, Barbier A, Bernard J, Rezaei H, Huet JC, Henry C, Costa BD, Eléouët JF. 2004. Biochemical characterization of the respiratory syncytial virus P-P and P-N protein complexes and localization of the P protein oligomerization domain. J Gen Virol 85:1643-1653.

152. Llorente MT, Taylor IA, López-Viñas E, Gomez-Puertas P, Calder LJ, García-Barreno B, Melero JA. 2008. Structural properties of the human respiratory syncytial virus P protein: evidence for an elongated homotetrameric molecule that is the smallest orthologue within the family of paramyxovirus polymerase cofactors. Proteins 72:946-58.
153. Pereira N, Cardone C, Lassoued S, Galloux M, Fix J, Assrir N, Lescop E, Bontems F, Eléouët JF, Sizun C. 2017. New Insights into Structural Disorder in Human Respiratory Syncytial Virus Phosphoprotein and Implications for Binding of Protein Partners. J Biol Chem 292:2120-2131.
154. Simabuco FM, Asara JM, Guerrero MC, Libermann TA, Zerbini LF, Ventura AM. 2011. Structural analysis of human respiratory syncytial virus p protein: identification of intrinsically disordered domains. Braz J Microbiol 42:340-5.
155. Gilman MSA, Liu C, Fung A, Behera I, Jordan P, Rigaux P, Ysebaert N, Tcherniuk S, Sourimant J, Eléouët JF, Sutto-Ortiz P, Decroly E, Roymans D, Jin Z, McLellan JS. 2019. Structure of the Respiratory Syncytial Virus Polymerase Complex. Cell 179:193-204.e14.
156. Longhi S, Oglesbee M. 2010. Structural disorder within the measles virus nucleoprotein and phosphoprotein. Protein Pept Lett 17:961-78.
157. Habchi J, Mamelli L, Darbon H, Longhi S. 2010. Structural disorder within Henipavirus nucleoprotein and phosphoprotein: from predictions to experimental assessment. PLoS One 5:e11684.
158. Landolt-Marticorena C, Williams KA, Deber CM, Reithmeier RA. 1993. Non-random distribution of amino acids in the transmembrane segments of human type I single span membrane proteins. J Mol Biol 229:602-8.
159. Branttie JM, Dutch RE. 2020. Parainfluenza virus 5 fusion protein maintains pre-fusion stability but not fusogenic activity following mutation of a transmembrane leucine/isoleucine domain. J Gen Virol 101:467-472.
160. Gravel KA, McGinnes LW, Reitter J, Morrison TG. 2011. The transmembrane domain sequence affects the structure and function of the Newcastle disease virus fusion protein. J Virol 85:3486-97.
161. Barrett CT, Webb SR, Dutch RE. 2019. A Hydrophobic Target: Using the Paramyxovirus Fusion Protein Transmembrane Domain To Modulate Fusion Protein Stability. J Virol 93.

162. Joshi SB, Dutch RE, Lamb RA. 1998. A core trimer of the paramyxovirus fusion protein: parallels to influenza virus hemagglutinin and HIV-1 gp41. Virology 248:20-34.
163. Goetz SK, Mahamid J. 2020. Visualizing Molecular Architectures of Cellular Condensates: Hints of Complex Coacervation Scenarios. Dev Cell 55:97-107.
164. Roden C, Gladfelter AS. 2020. RNA contributions to the form and function of biomolecular condensates. Nat Rev Mol Cell Biol doi:10.1038/s41580-020-0264-6.
165. Babinchak WM, Surewicz WK. 2020. Liquid-Liquid Phase Separation and Its Mechanistic Role in Pathological Protein Aggregation. J Mol Biol 432:1910-1925.
166. Pollin R, Granzow H, Köllner B, Conzelmann KK, Finke S. 2013. Membrane and inclusion body targeting of lyssavirus matrix proteins. Cell Microbiol 15:200-12.
167. Lahaye X, Vidy A, Fouquet B, Blondel D. 2012. Hsp70 protein positively regulates rabies virus infection. J Virol 86:4743-51.
168. Fouquet B, Nikolic J, Larrous F, Bourhy H, Wirblich C, Lagaudrière-Gesbert C, Blondel D. 2015. Focal adhesion kinase is involved in rabies virus infection through its interaction with viral phosphoprotein P. J Virol 89:1640-51.
169. Denison MR. 2008. Seeking membranes: positive-strand RNA virus replication complexes. PLoS Biol 6:e270.
170. Galloux M, Gabiane G, Sourimant J, Richard CA, England P, Moudjou M, Aumont-Nicaise M, Fix J, Rameix-Welti MA, Eléouët JF. 2015. Identification and characterization of the binding site of the respiratory syncytial virus phosphoprotein to RNA-free nucleoprotein. J Virol 89:3484-96.
171. Sanders DW, Kedersha N, Lee DSW, Strom AR, Drake V, Riback JA, Bracha D, Eeftens JM, Iwanicki A, Wang A, Wei MT, Whitney G, Lyons SM, Anderson P, Jacobs WM, Ivanov P, Brangwynne CP. 2020. Competing Protein-RNA Interaction Networks Control Multiphase Intracellular Organization. Cell 181:306-324.e28.
172. Jack A, Ferro LS, Trnka MJ, Wehri E, Nadgir A, Costa K, Schaletzky J, Yildiz A. 2020. SARS CoV-2 nucleocapsid protein forms condensates with viral genomic RNA. bioRxiv doi:10.1101/2020.09.14.295824.
173. Iserman C, Roden C, Boerneke M, Sealfon R, McLaughlin G, Jungreis I, Park C, Boppana A, Fritch E, Hou YJ, Theesfeld C, Troyanskaya OG, Baric RS, Sheahan TP, Weeks K, Gladfelter AS. 2020. Specific viral RNA drives the SARS CoV-2 nucleocapsid to phase separate. bioRxiv doi:10.1101/2020.06.11.147199.

174. Perdikari TM, Murthy AC, Ryan VH, Watters S, Naik MT, Fawzi NL. 2020. SARS-CoV-2 nucleocapsid protein undergoes liquid-liquid phase separation stimulated by RNA and partitions into phases of human ribonucleoproteins. bioRxiv doi:10.1101/2020.06.09.141101.
175. Lu S, Ye Q, Singh D, Villa E, Cleveland DW, Corbett KD. 2020. The SARS-CoV-2 Nucleocapsid phosphoprotein forms mutually exclusive condensates with RNA and the membrane-associated M protein. bioRxiv doi:10.1101/2020.07.30.228023.
176. Chen H, Cui Y, Han X, Hu W, Sun M, Zhang Y, Wang PH, Song G, Chen W, Lou J. 2020. Liquid-liquid phase separation by SARS-CoV-2 nucleocapsid protein and RNA. Cell Res doi:10.1038/s41422-020-00408-2:1-3.
177. Owen I, Shewmaker F. 2019. The Role of Post-Translational Modifications in the Phase Transitions of Intrinsically Disordered Proteins. Int J Mol Sci 20.
178. Das T, Schuster A, Schneider-Schaulies S, Banerjee AK. 1995. Involvement of cellular casein kinase II in the phosphorylation of measles virus P protein: identification of phosphorylation sites. Virology 211:218-26.
179. Sugai A, Sato H, Yoneda M, Kai C. 2012. Phosphorylation of measles virus phosphoprotein at S86 and/or S151 downregulates viral transcriptional activity. FEBS Lett 586:3900-7.
180. Takacs AM, Barik S, Das T, Banerjee AK. 1992. Phosphorylation of specific serine residues within the acidic domain of the phosphoprotein of vesicular stomatitis virus regulates transcription in vitro. J Virol 66:5842-8.
181. Carlson CR, Asfaha JB, Ghent CM, Howard CJ, Hartooni N, Morgan DO. 2020. Phosphorylation modulates liquid-liquid phase separation of the SARS-CoV-2 N protein. bioRxiv doi:10.1101/2020.06.28.176248.
182. Kamelgarn M, Chen J, Kuang L, Jin H, Kasarskis EJ, Zhu H. 2018. ALS mutations of FUS suppress protein translation and disrupt the regulation of nonsense-mediated decay. Proc Natl Acad Sci U S A 115:E11904-e11913.
183. Murthy AC, Dignon GL, Kan Y, Zerze GH, Parekh SH, Mittal J, Fawzi NL. 2019. Molecular interactions underlying liquid-liquid phase separation of the FUS low-complexity domain. Nat Struct Mol Biol 26:637-648.

VITA

Kerri Beth Boggs

Education

University of Kentucky: Lexington, Kentucky ..... 2016 – 2020
PhD student

Milligan University: Johnson City, Tennessee ..... 2012 – 2016
B.S. in Biology; B.S. in Chemistry

Professional Positions

Biology Adjunct Professor: Lexington, Kentucky 2020
Bluegrass Community and Technical College

Genetics Lab Instructor: Richmond, Kentucky..... 2019
Eastern Kentucky University

Biohchemistry Graduate Teaching Assistant: Lexington, KY..... 2017, 2019
University of Kentucky

Awards

Max Steckler Fellowship..... 2020

College of Medicine Fellowhsip for Excellence in Graduate Research..... 2018

American Society for Virology Student Travel Award..... 2018, 2019

Assoication of Emeriti Faculty Endowed Fellowship..... 2018

Infectious Disease Research Day Three Minute Thesis, First Place 2018

NSF Graduate Research Fellowship Program Honorable Mention 2018

Publications

Slaughter KB, Dutch RE. 2019. Transmembrane Domain Dissociation Is Required for Hendra Virus F Protein Fusogenic Activity. 93:e01069-19.

Cifuentes-Muñoz N, Branttie J, Slaughter KB, Dutch RE. 2017. Human Metapneumovirus Induces Formation of Inclusion Bodies for Efficient Genome Replication and Transcription. J Virol 91.

Presentations

Oral Presentation, “Transmembrane domain dissociation is required for Hendra F fusogenic activity,” American Society for Virology, July 2019.

Poster Presentation, “Effect of inhibiting protein conformational changes by introducing disulfide bonds in the TMDs of the Hendra virus fusion protein,” American Society for Virology, July 2018.

Oral Presentation, “Effect of inhibiting protein conformational changes by introducing disulfide bonds in the TMDs of the Hendra virus fusion protein,” Bluegrass Biophysics Symposium, May 2018.

Poster Presentation, “Effect of inhibiting protein conformational changes by introducing disulfide bonds in the TMDs of the Hendra virus fusion protein,” ASBMB, Apr 2018.